Advances in Meteorology

Propagation of Drought: From Meteorological Drought to Agricultural and Hydrological Drought

Guest Editors: Wen Wang, Maurits W. Ertsen, Mark D. Svoboda, and Mohsin Hafeez

Propagation of Drought: From Meteorological Drought to Agricultural and Hydrological Drought

Advances in Meteorology

Propagation of Drought: From Meteorological Drought to Agricultural and Hydrological Drought

Guest Editors: Wen Wang, Maurits W. Ertsen, Mark D. Svoboda, and Mohsin Hafeez

Editorial Board

Contents

Propagation of Drought: From Meteorological Drought to Agricultural and Hydrological Drought
Wen Wang, Maurits W. Ertsen, Mark D. Svoboda, and Mohsin Hafeez
Volume 2016, Article ID 6547209, 5 pages

Evolution of Hydrological Drought in Human Disturbed Areas: A Case Study in the Laohahe Catchment, Northern China
Yi Liu, Liliang Ren, Ye Zhu, Xiaoli Yang, Fei Yuan, Shanhu Jiang, and Mingwei Ma
Volume 2016, Article ID 5102568, 12 pages

Robust Response of Streamflow Drought to Different Timescales of Meteorological Drought in Xiangjiang River Basin of China
Lin Zhao, Jianjun Wu, and Jian Fang
Volume 2016, Article ID 1634787, 8 pages

Drought Assessment by a Short-/Long-Term Composited Drought Index in the Upper Huaihe River Basin, China
Meixiu Yu, Xiaolong Liu, Li Wei, Qiongfang Li,
Jianyun Zhang, and Guoqing Wang
Volume 2016, Article ID 7986568, 10 pages

Spatial-Temporal Variation of Aridity Index of China during 1960–2013
Huiping Huang, Yuping Han, Mingming Cao, Jinxi Song, and Heng Xiao
Volume 2016, Article ID 1536135, 10 pages

Possible Future Climate Change Impacts on the Hydrological Drought Events in the Weihe River Basin, China
Fei Yuan, Mingwei Ma, Liliang Ren, Hongren Shen, Yue Li, Shanhu Jiang, Xiaoli Yang, Chongxu Zhao, and Hao Kong
Volume 2016, Article ID 2905198, 14 pages

Drought Occurrence in Central European Mountainous Region (Tatra National Park, Slovakia) within the Period 1961–2010
Jaroslav Vido, Tsegaye Tadesse, Zbyšek Šustek, Radoslav Kandrík, Miriam Hanzelová, Jaroslav Škvarenina, Jana Škvareninová, and Michael Hayes
Volume 2015, Article ID 248728, 8 pages

Hindawi Publishing Corporation
Advances in Meteorology
Volume 2016, Article ID 6547209, 5 pages
http://dx.doi.org/10.1155/2016/6547209

Editorial

Propagation of Drought: From Meteorological Drought to Agricultural and Hydrological Drought

Wen Wang,[1] Maurits W. Ertsen,[2] Mark D. Svoboda,[3] and Mohsin Hafeez[4]

[1]*State Key Laboratory of Hydrology-Water Resources and Hydraulic Engineering, Hohai University, Nanjing 210098, China*
[2]*Department of Water Resources Management, Delft University of Technology, 2628 CN Delft, Netherlands*
[3]*National Drought Mitigation Center, University of Nebraska-Lincoln, 815 Hardin Hall, Lincoln, NE 68583-0988, USA*
[4]*Water Resources Modelling Unit, Bureau of Meteorology, Brisbane, QLD 4000, Australia*

Correspondence should be addressed to Wen Wang; w.wang@126.com

Received 4 January 2016; Accepted 11 January 2016

1. Drought in the World and China

Drought is a hazard that occurs everywhere in the world (both in dry and in wet areas). Despite the controversy regarding drought changes in the last decades [1–3], increases in drought intensity are clearly identified in some areas [4] and it is believed that although increased heating from global warming may not directly cause droughts, it is expected that when droughts occur, they are likely to set in quicker and be more intense [5].

Throughout its history, China has frequently suffered from drought disasters due to its monsoon climate and was regularly hit hard by droughts over the last decades. Although little evidence of an expansion of the area affected by droughts was found in China over the last 50 years [6], severe droughts in southwestern China in 2010 and the middle/lower Yangtze Basin and Huaihe River Basin in 2011 have drawn more attention from the research community as well as from the public and governments alike on the impacts and problems brought on by drought. Poor performance by China's emergency response management during recent major drought events highlights the necessity of improving both drought preparedness and emergency response skills.

To improve our skills for drought monitoring and forecasting as a means of reducing society's vulnerability to droughts and the risks they pose, it is important to distinguish between different types of drought, reveal how droughts propagate from one type to another, study the causes of drought, and know how drought affects various economic sectors (e.g., agriculture, energy production, and navigation) and ecosystems in diverse ways. Furthermore, it is vital that we continue to explore and better understand how aggregated human activities affect the process of drought propagation so as to better prepare for and adapt to future drought changes.

2. From Meteorological Drought to Agricultural/Hydrological Drought

Drought originates from a deficiency of precipitation over an extended period of time resulting in a water shortage for some activity, group, or environmental sector. It is the result of a complex interplay between (1) natural precipitation deficiencies, or excessive evapotranspiration over varying time periods and different areal extents, and (2) the demands of human and environmental water use that may be exacerbated by inefficiencies in water distribution, planning, and management [7]. To facilitate communication, management, and response, drought often is categorized into four general types [7]: (1) meteorological or climatological, (2) agricultural, (3) hydrological, and (4) socioeconomic. Drought can develop over short periods (weeks or months) or longer periods (seasons, years, or even decades). Different types of droughts have their own specific spatiotemporal characteristics [8, 9]. Although hydrological drought and agricultural drought start from meteorological droughts, hydrological and agricultural drought indicators cannot be straightforwardly derived from

meteorological drought indicators [10, 11]. Lack of precipitation combined with higher evaporation rates propagates through the hydrological cycle from a meteorological phenomenon/drought into soil moisture depletion to the point where crops or terrestrial ecosystems are impacted, and eventually into a hydrological phenomenon/drought [12, 13].

The development of droughts involves numerous interacting climate processes and various land-atmosphere feedback. In addition, different stores in catchments (providing persistence) lead to potentially complicated propagations of the climate signal into the water system [14]. To fight against drought and mitigate the impacts of major droughts, it is important to distinguish between different types of drought, to understand how drought evolves from one type to another, and to know how human activities influence the cause/linkages of droughts. The study on the topic of drought propagation has been quite a hot issue in the hydrology community over the last decade [8–10, 14–21]. It is found that there is a significant link between meteorological drought and hydrological drought, except for catchments where groundwater storage and snow processes are important [18]. Several common features of drought propagation have been revealed, such as [17]: (a) meteorological droughts evolve collectively into a prolonged hydrological drought (pooling); (b) meteorological droughts are attenuated when storage is high at the start of the event (attenuation); (c) a lag occurs between meteorological, soil moisture, and hydrological drought (lag); and (d) droughts get longer in duration in moving from meteorological to soil moisture to hydrological drought (lengthening).

However, there are still many more mechanisms behind drought propagation that need to be investigated, such as the interaction between surface water and groundwater during the process of drought development, the evapotranspiration of different plant communities in response to droughts, and human (anticipating and response) strategies manipulating these features. On the other hand, while drought mechanism research has certainly moved forward, more progress has been made in the realm of qualitative knowledge rather than quantitatively. Knowing more about the mechanisms quantitatively will provide a stronger basis for monitoring and forecasting hydrological and agricultural droughts.

3. The Roles of Human Intervention in Drought Propagation

Human interventions in the water cycle are about manipulating water flows by (groups of) users for different reasons and adapting water availability in time and space and changing the hydrological patterns in their surrounding landscape. Human activities, such as irrigation activities, dam and reservoir operations, and water diversion may significantly alter the propagation process from meteorological to hydrological droughts as well as affecting drought vulnerability [22–25]. Therefore, the impacts of drought could be mitigated by managing water demand through crop management, modifying water allocation rules during times of water scarcity, developing various water resources (such as groundwater recharge and salt water desalination), managing multiple water use, setting up water-trading mechanisms in advance of times of drought or scarcity, and physically redistributing available supplies during times of scarcity [26].

However, while drought is a climatic phenomenon with relatively predictable biophysical repercussions, social perceptions of and responses to drought from the individual through community and up to the state level are highly varied [27]. At the same time, interactions between natural water availability and societal water demand and management are complex, and drought mitigation strategies in some sectors (e.g., agricultural and energy sectors) may increase the vulnerability of other systems (especially ecosystems) [28]. Multiobjective optimization could be helpful for developing drought plans incorporating traditional short-term tactical measures (e.g., facility operation) and long-term or in-advance strategic mitigation measures for drought preparedness [29] while also balancing the drought risks among different sectors at the same time.

4. Drought Monitoring and Prediction

At present, droughts are commonly monitored using indices based on data from three primary sources, that is, ground observations such as the Standardized Precipitation Index (SPI) [30], satellite observations such as the global Drought Severity Index (DSI) [31], and Multivariate Standardized Drought Index (MSDI) [32], as well as model simulations [33–35].

Indicators based on any single source of drought information have their limitations. In order to fully characterize drought magnitude, spatial extent, and potential impacts, drought monitoring methods or indicators should be integrated, coupling multiple climate, water, vegetation, and soil parameters, as well as socioeconomic information retrieved from different sources [36]. Many efforts have been put into developing drought indicators jointly using ground-based, satellite-based, and model simulated data. One of the earliest examples of such a composite, or hybrid, approach is found in the operational US Drought Monitor (USDM) [37], which combines several inputs consisting of modelled data, satellite vegetation health indicators, climate-based indices (such as the SPI), impacts, and local expert input from the field. Other examples include the Aggregated Drought Index (ADI), which comprehensively considers all physical forms of drought through variables like precipitation, streamflow, evapotranspiration, reservoir storage, soil moisture content, and snow water content [38]; the Vegetation Drought Response Index (VegDRI) integrates satellite-based observations of vegetation conditions, climate data, and other biophysical information such as land cover/land use type, soil characteristics, and ecological setting [39]; the Combined Drought Indicator combines the Standardized Precipitation Index (SPI), the anomalies of soil moisture, and the anomalies of the fraction of Absorbed Photosynthetically Active Radiation (fAPAR) [40]. However, there is no significantly preferable or universally accepted multivariate drought index so far (nor is that likely to come) and it is difficult to prove

the superiority of the various multivariate drought indicators because there is no "ground truth" of drought observations for most places that can be used for an exact validation process [41].

Unlike a flood, a drought does not have an obvious start or end. While monitoring has been done for decades, forecasting drought is still in its infancy [42]. As meteorological drought is dominated by precipitation processes, its forecast is fundamentally an issue of medium-to-long range weather forecasting. Hydrological and agricultural droughts are driven by meteorological droughts; therefore their forecasts also heavily depend on weather forecasting. It is common to use atmospheric model outputs to drive hydrological models for making seasonal hydrological drought forecasts [43, 44] or estimating future droughts [45]. In knowing that the drought propagation process is complicated, especially when considering human managed interventions such as reservoir operations, diversions, water consumption, and agricultural activities, many more factors should be involved in hydrological and agricultural drought forecasting. Another major challenge for drought forecasting is due to the fact that forecasts are often unreliable on the seasonal timescale and lack specificity, reducing their usefulness for agriculture and other sectors [36].

5. Highlights in the Special Issue

In this special issue, a collection of six papers were chosen that cover topics addressing regional drought changes, drought assessment methods, and impacts of human activities and climate change on drought evolution.

H. Huang et al. investigated the spatial-temporal variation of the aridity index, which is defined as the ratio of potential evapotranspiration and precipitation, in China during 1960–2013, and found that the average annual aridity index showed a decreasing trend. J. Vido et al. found that the frequency of 24 droughts occurring in the Tatra National Park in Slovakia has a cyclical pattern with approximately a 30-year period. Furthermore, the precipitation shadow of the mountains influences the risk of drought occurrence. L. Zhao et al. found strong correlations between the Standardized Runoff Index (SRI) and Standardized Precipitation Evapotranspiration Index (SPEI) in the Xiangjiang River Basin in southern China, with a stronger correlation in the dry season compared to the wet season. M. Yu et al. proposed a multiscale Composited Drought Index (CDI) by integrating the self-calibrating Palmer Drought Severity Index (scPDSI), the 1- and 3-month Standardized Precipitation and Evapotranspiration Index (SPEI), Z index, and standardized Soil Moisture Index (SMI) using a principle component analysis method for improving the skill of drought monitoring. Y. Liu et al. presented a case study in a semiarid catchment in northern China addressing the impacts of human activities, which shows that human activities significantly amplified both drought duration and severity in that catchment. F. Yuan et al. develop a modelling system for projecting the potential climate change impacts on hydrological drought events in the Weihe River Basin in northern China and show that that basin can expect more severe droughts in the future.

6. Future Works on Drought Propagation Mechanisms

Significant progress has been made in the last decade centering around a better understanding of the mechanisms of drought propagation. Future advances are required in order to address the following aspects:

(1) Develop more long-term and reliable series of drought data, and quantitatively assess data uncertainty whether the data are observed through ground networks or satellites or especially through modelled or simulated approaches, so as to avoid any misinterpretation about changes in drought characteristics.

(2) Establish more comprehensive drought monitoring frameworks, which use multiple observation techniques and modelling tools conjunctively to reflect drought-related hydrological and biophysical variables at different spatial-temporal scales, in order to meet the specific needs of different sectors.

(3) Quantitatively describe the water conversion/drought relationship among different existing forms, that is, soil water, snow/ice water, plant water, groundwater, and river water, at multiple spatial and temporal scales in different catchments and geographical settings.

(4) Reveal the interrelationship between the natural hydrological system and the role of humans played in the process of drought development, considering the effects of different management practices dealing with water allocation, water use, land use/land cover planning, and so on, which are based on multidisciplinary inputs from history, archaeology, anthropology, sciences, and engineering.

(5) Develop strategies for reducing society's vulnerability to drought by improving the skills of drought response based on the knowledge of drought propagation.

Acknowledgments

The research work on drought by Wen Wang is financially supported by Natural Science Foundation of China project "Mechanism of Catchment Hydrological Responses to Meteorological Droughts" (no. 41371050).

Wen Wang
Maurits W. Ertsen
Mark D. Svoboda
Mohsin Hafeez

References

[1] J. Sheffield, E. F. Wood, and M. L. Roderick, "Little change in global drought over the past 60 years," *Nature*, vol. 491, no. 7424, pp. 435–438, 2012.

[2] A. G. Dai, "Increasing drought under global warming in observations and models," *Nature Climate Change*, vol. 3, no. 1, pp. 52–58, 2013.

[3] L. Damberg and A. AghaKouchak, "Global trends and patterns of drought from space," *Theoretical and Applied Climatology*, vol. 117, no. 3-4, pp. 441–448, 2014.

[4] I. Masih, S. Maskey, F. E. F. Mussá, and P. Trambauer, "A review of droughts on the African continent: a geospatial and long-term perspective," *Hydrology and Earth System Sciences*, vol. 18, no. 9, pp. 3635–3649, 2014.

[5] K. E. Trenberth, A. Dai, G. Van Der Schrier et al., "Global warming and changes in drought," *Nature Climate Change*, vol. 4, no. 1, pp. 17–22, 2014.

[6] W. Wang, Y. Zhu, R. Xu, and J. Liu, "Drought severity change in China during 1961–2012 indicated by SPI and SPEI," *Natural Hazards*, vol. 75, no. 3, pp. 2437–2451, 2014.

[7] American Meteorological Society (AMS), Drought, 2013, https://www2.ametsoc.org/ams/index.cfm/about-ams/ams-statements/statements-of-the-ams-in-force/drought/.

[8] E. Peters, G. Bier, H. A. J. van Lanen, and P. J. J. F. Torfs, "Propagation and spatial distribution of drought in a groundwater catchment," *Journal of Hydrology*, vol. 321, no. 1–4, pp. 257–275, 2006.

[9] L. M. Tallaksen, H. Hisdal, and H. A. J. V. Lanen, "Space-time modelling of catchment scale drought characteristics," *Journal of Hydrology*, vol. 375, no. 3-4, pp. 363–372, 2009.

[10] E. Peters, P. J. J. F. Torfs, H. A. J. Van Lanen, and G. Bier, "Propagation of drought through groundwater—a new approach using linear reservoir theory," *Hydrological Processes*, vol. 17, no. 15, pp. 3023–3040, 2003.

[11] N. Wanders, H. A. J. Van Lanen, and A. F. Van Loon, "Indicators for drought characterization on a global scale," WATCH Technical Report 24, 2010.

[12] D. A. Wilhite, Ed., *Drought: A Global Assessment*, Routledge, London, UK, 2000.

[13] L. M. Tallaksen and H. A. J. Van Lanen, Eds., *Hydrological Drought: Processes and Estimation Methods for Streamflow and Groundwater*, Elsevier, Amsterdam, Netherlands, 2004.

[14] A. F. Van Loon and G. Laaha, "Hydrological drought severity explained by climate and catchment characteristics," *Journal of Hydrology*, vol. 526, pp. 3–14, 2015.

[15] S. M. Vicente-Serrano and J. I. López-Moreno, "Hydrological response to different time scales of climatological drought: an evaluation of the Standardized Precipitation Index in a mountainous Mediterranean basin," *Hydrology and Earth System Sciences*, vol. 9, no. 5, pp. 523–533, 2005.

[16] A. F. Van Loon, H. A. J. Van Lanen, L. M. Tallaksen et al., "Propagation of drought through the hydrological cycle," WATCH Technical Report 32, 2011.

[17] A. F. Van Loon and H. A. J. Van Lanen, "A process-based typology of hydrological drought," *Hydrology and Earth System Sciences*, vol. 16, no. 7, pp. 1915–1946, 2012.

[18] K. Haslinger, D. Koffler, W. Schöner, and G. Laaha, "Exploring the link between meteorological drought and streamflow: effects of climate-catchment interaction," *Water Resources Research*, vol. 50, no. 3, pp. 2468–2487, 2014.

[19] J. Niu, J. Chen, and L. Sun, "Exploration of drought evolution using numerical simulations over the Xijiang (West River) basin in South China," *Journal of Hydrology*, vol. 526, pp. 68–77, 2015.

[20] S. Huang, Q. Huang, J. Chang, G. Leng, and L. Xing, "The response of agricultural drought to meteorological drought and the influencing factors: a case study in the Wei River Basin, China," *Agricultural Water Management*, vol. 159, pp. 45–54, 2015.

[21] L. J. Barker, J. Hannaford, A. Chiverton, and C. Svensson, "From meteorological to hydrological drought using standardised indicators," *Hydrology and Earth System Sciences*, vol. 12, no. 12, pp. 12827–12875, 2015.

[22] J. I. López-Moreno, S. M. Vicente-Serrano, S. Begueria, J. M. Garcia-Ruiz, M. M. Portela, and A. B. Almeida, "Dam effects on droughts magnitude and duration in a transboundary basin: the lower river tagus, pain and Portugal," *Water Resources Research*, vol. 45, no. 2, Article ID W02405, 2009.

[23] L. Wen, K. Rogers, J. Ling, and N. Saintilan, "The impacts of river regulation and water diversion on the hydrological drought characteristics in the Lower Murrumbidgee River, Australia," *Journal of Hydrology*, vol. 405, no. 3-4, pp. 382–391, 2011.

[24] C. M. G. Gómez and C. D. P. Blanco, "Do drought management plans reduce drought risk? A risk assessment model for a Mediterranean river basin," *Ecological Economics*, vol. 76, pp. 42–48, 2012.

[25] R. Zhang, X. Chen, Z. Zhang, and P. Shi, "Evolution of hydrological drought under the regulation of two reservoirs in the headwater basin of the Huaihe River, China," *Stochastic Environmental Research and Risk Assessment*, vol. 29, no. 2, pp. 487–499, 2014.

[26] A. C. Tyagi, "Developing management strategies for coping with drought," *Irrigation and Drainage*, vol. 63, no. 2, pp. 271–272, 2014.

[27] P. J. O'Farrell, P. M. L. Anderson, S. J. Milton, and W. R. J. Dean, "Human response and adaptation to drought in the arid zone: lessons from southern Africa," *South African Journal of Science*, vol. 105, no. 1-2, pp. 34–39, 2009.

[28] J. Christian-Smith, M. C. Levy, and P. H. Gleick, "Maladaptation to drought: a case report from California, USA," *Sustainability Science*, vol. 10, no. 3, pp. 491–501, 2015.

[29] X. Cai, R. Zeng, W. H. Kang, J. Song, and A. J. Valocchi, "Strategic planning for drought mitigation under climate change," *Journal of Water Resources Planning and Management*, vol. 141, no. 9, Article ID 04015004, 2015.

[30] T. B. McKee, N. J. Doesken, and K. John, "The relationship of drought frequency and duration to time scales," in *Proceedings of the 8th Conference on Applied Climatology*, American Meteorological Society, Anaheim, Calif, USA, January 1993.

[31] Q. Mu, M. Zhao, J. S. Kimball, N. G. McDowell, and S. W. Running, "A remotely sensed global terrestrial drought severity index," *Bulletin of the American Meteorological Society*, vol. 94, no. 1, pp. 83–98, 2013.

[32] Z. C. Hao and A. AghaKouchak, "Multivariate standardized drought index: a parametric multi-index model," *Advances in Water Resources*, vol. 57, pp. 12–18, 2013.

[33] B. Narasimhan and R. Srinivasan, "Development and evaluation of Soil Moisture Deficit Index (SMDI) and Evapotranspiration Deficit Index (ETDI) for agricultural drought monitoring," *Agricultural and Forest Meteorology*, vol. 133, no. 1–4, pp. 69–88, 2005.

[34] C. Cammalleri, F. Micale, and J. Vogt, "On the value of combining different modelled soil moisture products for European drought monitoring," *Journal of Hydrology*, vol. 525, pp. 547–558, 2015.

[35] M. C. Anderson, C. hain, J. Otkin et al., "An intercomparison of drought indicators based on thermal remote sensing and

NLDAS-2 simulations with U.S. drought monitor classifications," *Journal of Hydrometeorology*, vol. 14, no. 4, pp. 1035–1056, 2013.

[36] World Meteorological Organization, "Drought monitoring and early warning: concepts, progress and future challenges," WMO 1006, World Meteorological Organization, 2006.

[37] M. Svoboda, D. LeComte, M. Hayes et al., "The drought monitor," *Bulletin of the American Meteorological Society*, vol. 83, no. 8, pp. 1181–1190, 2002.

[38] J. A. Keyantash and J. A. Dracup, "An aggregate drought index: assessing drought severity based on fluctuations in the hydrologic cycle and surface water storage," *Water Resources Research*, vol. 40, no. 9, Article ID W09304, 2004.

[39] J. F. Brown, B. D. Wardlow, T. Tadesse, M. J. Hayes, and B. C. Reed, "The Vegetation Drought Response Index (VegDRI): a new integrated approach for monitoring drought stress in vegetation," *GIScience & Remote Sensing*, vol. 45, no. 1, pp. 16–46, 2008.

[40] G. Sepulcre-Canto, S. M. A. F. Horion, A. Singleton, H. Carrao, and J. Vogt, "Development of a Combined Drought Indicator to detect agricultural drought in Europe," *Natural Hazards and Earth System Science*, vol. 12, no. 11, pp. 3519–3531, 2012.

[41] Z. Hao and V. P. Singh, "Drought characterization from a multivariate perspective: a review," *Journal of Hydrology*, vol. 527, pp. 668–678, 2015.

[42] P. Patel, "Predicting the future of drought prediction," *IEEE Spectrum*, vol. 49, no. 9, pp. 18–22, 2012.

[43] X. Yuan, E. F. Wood, N. W. Chaney et al., "Probabilistic seasonal forecasting of African drought by dynamical models," *Journal of Hydrometeorology*, vol. 14, no. 6, pp. 1706–1720, 2013.

[44] A. Ceppi, G. Ravazzani, C. Corbari, R. Salerno, S. Meucci, and M. Mancini, "Real-time drought forecasting system for irrigation management," *Hydrology and Earth System Sciences*, vol. 18, no. 9, pp. 3353–3366, 2014.

[45] G. Forzieri, L. Feyen, R. Rojas, M. Flörke, F. Wimmer, and A. Bianchi, "Ensemble projections of future streamflow droughts in Europe," *Hydrology and Earth System Sciences*, vol. 18, no. 1, pp. 85–108, 2014.

Hindawi Publishing Corporation
Advances in Meteorology
Volume 2016, Article ID 5102568, 12 pages
http://dx.doi.org/10.1155/2016/5102568

Research Article

Evolution of Hydrological Drought in Human Disturbed Areas: A Case Study in the Laohahe Catchment, Northern China

Yi Liu,[1,2] Liliang Ren,[1,2] Ye Zhu,[1,2] Xiaoli Yang,[2] Fei Yuan,[2] Shanhu Jiang,[2] and Mingwei Ma[2]

[1] *State Key Laboratory of Hydrology-Water Resources and Hydraulic Engineering, Hohai University, Nanjing 210098, China*
[2] *College of Hydrology and Water Resources, Hohai University, Nanjing 210098, China*

Correspondence should be addressed to Liliang Ren; njrll9999@126.com

Received 29 May 2015; Accepted 25 November 2015

Academic Editor: Maurits W. Ertsen

A case study on the evolution of hydrological drought in nonstationary environments is conducted over the Laohahe catchment in northern China. Using hydrometeorological observations during 1964–2009, meteorological and hydrological droughts are firstly analyzed with the threshold level method. Then, a comprehensive analysis on the changes within the catchment is conducted on the basis of hydrological variables and socioeconomic indices, and the whole period is divided into two parts: the undisturbed period (1964–1979) and the disturbed period (1980–2009). A separating framework is further introduced to distinguish droughts induced by different causes, that is, the naturalized drought and human-induced drought. Results showed that human activities are more inclined to play a negative role in aggravating droughts. Drought duration and deficit volume in naturalized conditions are amplified two to four times and three to eight times, respectively, when human activities are involved. For the two dry decades 1980s and 2000s, human activities have caused several consecutive drought events with rather long durations (up to 29 months). These results reflect the considerable impacts of human activities on hydrological drought, which could provide some theoretical support for local drought mitigation and water resources management.

1. Introduction

Drought is a recurring natural phenomenon primarily induced by successive reduction of precipitation over a period of time [1–4]. Different from aridity which is a permanent feature of climate condition, drought is a consequence of climate variability reflecting temporal water deficiencies and can be observed in many regions rather than constrained to dry climate zones [5]. In view of the widespread impacts of droughts, including economic, agricultural, hydrological, and ecological losses and costs, much concern is given to droughts in recent years. Climate changes associated with global warming and other climate extremes have aggravated the damage of droughts, even in some areas such as southern Europe and West Africa; droughts with higher peaks and severity levels have been frequently observed during recent decades [6].

Drought can be classified into four types according to the variable that is used, that is, meteorological (precipitation), agricultural (soil moisture), hydrological (streamflow, water level, reservoir storage, and groundwater discharge), and socioeconomic droughts [7]. Among them, the hydrological drought is mostly related to our social activities, which can be defined as inadequate surface and subsurface water resources for established water uses of a given water resources management system [4].

The development scheme of hydrological drought is rather complex and is subject to the effects of climate and catchment control or a combination of the two factors. Among various climatic variables, precipitation and temperature are two key variables which largely determine the weather pattern and antecedent condition for the occurrence of hydrological drought. Meanwhile, since a sustained change in precipitation or temperature is commonly induced by variation in large-scale circulations, analyzing the relationship between hydrological drought and atmospheric circulation indices (e.g., the El Niño Southern Oscillation (ENSO) and high-pressure areas) is also a hot issue in recent drought researches [8]. Catchment control also plays an important

role in drought propagation and influences processes like pooling, attenuation, lag, and lengthening [9]. Some studies further investigated the individual roles of climate and catchment control in governing hydrological drought characteristics, and the conclusion is highly dependent on spatial scales. Globally, hydrological drought duration and deficit volume are more related to climate than to catchment control. However, for regional scale where climate is assumed to be relatively uniform, catchment characteristics like geology, area, slope, and groundwater system play an important role in governing hydrological drought duration and deficit volume [10].

In fact, the impacts on hydrological drought are not limited to the above-mentioned natural factors (i.e., climatic and catchment factors), and influences from human activities in forms of land cover change, reservoir regulation, agricultural irrigation, and water withdrawal from streams or river channels should not be ignored. From the perspective of hydrology science, human activities influence the process of hydrological cycle, for example, infiltration and evapotranspiration processes, and further alter flow regimes and their spatiotemporal distributions [11]. Accordingly, the process of hydrological drought would also be influenced. With this in mind, the traditional understanding of hydrological droughts should never be limited to the naturalized dry situation; drought caused by human activities has become a new challenging issue that needs to be noticed and discussed.

The focus of our study is to investigate the impact of human activities on hydrological drought. In this paper, we call drought induced by climate variability the "naturalized drought" and drought caused by human activities the "human-induced drought." As aforementioned, human activities potentially influence underlying surfaces, which further leads to a nonstationary response in hydrological variables (e.g., runoff). Here comes the question, will these changes influence the characteristics of hydrological droughts and what is the difference between naturalized and human-induced droughts? Based on the above questions, a comprehensive investigation on the evolution of hydrological droughts is conducted in the Laohahe catchment in northern China (this catchment is selected due to its representative runoff change pattern influenced by combined effects of climate change and human activities, which is quite common in China water-stressed regions), combined with a separating framework for distinguishing the naturalized and human-induced droughts.

2. Study Area and Data

The Laohahe catchment (41°N~42.75°N, 117.25°E~120°E) located in northern China is selected as an example considering its drastic runoff change pattern which is a common and typical phenomenon for water-stressed regions in northern China. The drainage area of the Laohahe catchment is 18,112 km^2, and its elevation ranges between 427 m and 2054 m with a general increasing trend from northeast to southwest. The climate belongs to the semiarid zone, according to the observation during the period 1964–2009; mean annual temperature, precipitation, and runoff

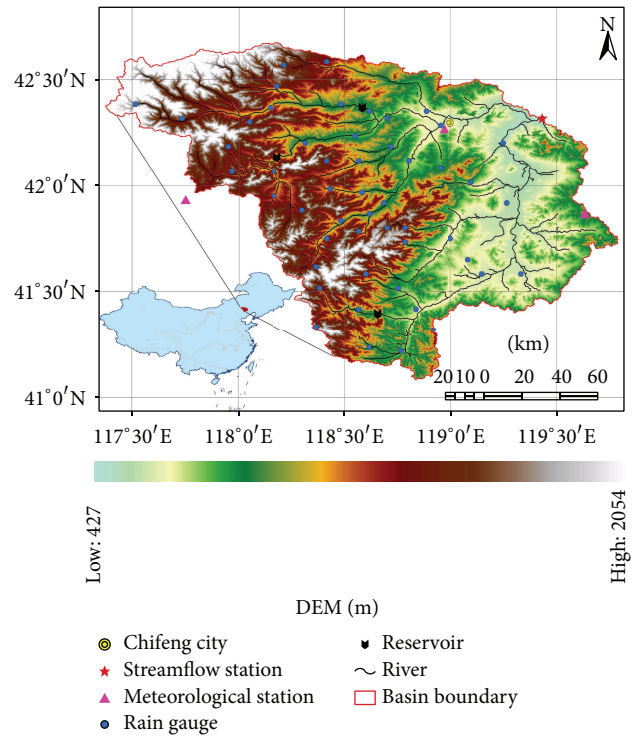

Figure 1: Location of the study area and the geographic distribution of hydrometeorological stations and reservoirs.

are 7.58°C, 418.3 mm, and 28.7 mm, respectively. Due to the temporally unevenly distributed precipitation (80% of annual precipitation concentrated between May and September) and temperature, the Laohahe catchment presents a strong seasonality in runoff. Normally, winter is cold and dry with relatively low streamflow observed, while in summer it is hot and wet with most peak flow occurring during this season.

The data used in this study includes materials for hydrological drought identification and input forcing for hydrological modeling. Daily precipitation of 52 rain gauges and streamflow records of the Xinglongpo hydrological station situated at the outlet of the Laohahe basin during 1964–2009 is provided by the Water Resources Department of the Inner Mongolia Autonomous Region. Streamflow data is further converted to catchment runoff by averaging the runoff amounts over the catchment area. Daily meteorological forcing (1964–2009) including maximum and minimum air temperature, wind speed, relative humidity, and sunshine duration of 3 national standard meteorological stations in and around the Laohahe catchment is downloaded from the China Meteorological Data Sharing Service System (http://data.cma.gov.cn/). Their geographic distributions are shown in Figure 1. Besides, locations of three large reservoirs (Erdaohezi, Dahushi, and Sanzuodian) within the Laohahe catchment are also given in Figure 1 considering their potential impacts on runoff.

Geographic information is obtained as follows: 3-arcsecond (about 90 m) digital elevation from the shuttle radar topography mission (SRTM) digital elevation model, soil types from the 5-minute FAO dataset [12], and land

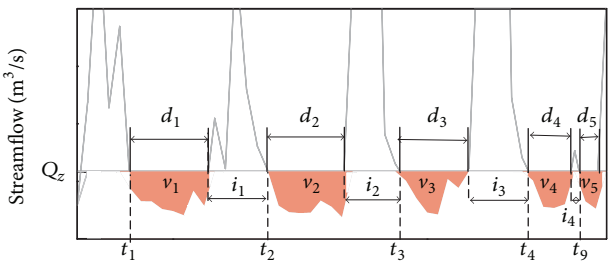

FIGURE 2: Illustration of threshold level method: time of occurrence, t_i, duration, d_i, deficit volume or severity, v_i, drought interval, i_k, and the threshold level, Q_z.

cover data provided by the Chinese Academy of Science. We also collect socioeconomic statistics of the Chifeng city from the local statistical bureau, including population, agricultural production, gross industrial product (GIP), and gross domestic product (GDP). In addition, the baseflow and baseflow index (BFI) are calculated by the Hydrological Utility Package (http://www.cnhup.com/) using the recursive digital filtering method (RDF, [13]). BFI itself is not a catchment characteristic but it integrates storage and release properties of a catchment [14] and has been shown to have a close relationship with hydrological drought duration [15, 16]. Therefore, we use this index to reflect varied catchment characteristics.

3. Methodology

3.1. Hydrological Drought Analysis. The threshold level method is so far the most commonly used approach in view of recent hydrological drought researches. Originating from the statistical theory of runs introduced by [17], this method is commonly used to analyze a sequential time series with a time resolution of one month or longer. Figure 2 gives the general illustration of this method. A sequence of drought events can be derived from a streamflow hydrograph when the flow falls below a certain threshold level, Q_z. Accordingly, drought characteristics including the time of occurrence, t_k, drought duration, d_k, deficit volume, v_k, and drought interval, i_k (the time period between two consecutive drought events) can be obtained.

The selection of threshold value Q_z is subjective but essential since it influences the number of events, drought duration, and deficit volume. For perennial streams like our studied catchment, threshold levels between the 70-percentile flow and the 95-percentile flow from the flow duration curve (FDC) are recommended [18]. In this study, the 70-percentile flow is used to identify meteorological and hydrological droughts from precipitation and streamflow series, respectively.

3.2. The Framework for Separating Naturalized and Human-Induced Drought. Distinguishing droughts induced by different factors is essential for objective understanding of the underlying causes of varied regional drought, which also makes sense for water planning and management. In this section, a framework developed by van Loon and van Lanen [19] is applied to separate naturalized and human-induced droughts. Part of this framework is similar to the common method used in hydrology of assessing the impacts of climate change and human activities on hydrological system, while the remaining part focuses on quantitative analysis on hydrological drought.

Specifically, this framework can be divided into three sections. In the first step, the time series of observed hydrometeorological variables are tested so as to find possible change points. The whole period can then be divided into two parts by the change point, that is, the baseline period ("undisturbed") and changed period ("disturbed"). For change point detection, a number of methods are available, such as the Pettitt test [20], Kendall test [21], and the precipitation-runoff double cumulative curves method. The second section focuses on hydrological model simulation and reconstructing runoff series of the changed period. For this purpose, the hydrological model should be firstly calibrated using meteorological forcing of the baseline period. Then, keeping optimized parameters unchanged, the simulation driven by meteorological forcing of the changed period is the reconstructed (simulated) series for which no human disturbances are involved. For hydrological model simulation, various hydrological models can be chosen as long as they are capable of reproducing the natural situation, especially during low flow and drought. The Variable Infiltration Capacity (VIC) model [22] is adopted in this study, and its specific description is given in the following section. The third step is the core of this framework. Hydrological droughts induced by different causes during the changed period can be derived by identifying observed and simulated runoff series with the threshold level method, respectively. The former represents a combination of naturalized and human-induced droughts, while the latter refers to droughts that develop in natural conditions. Therefore, their difference is the human-induced droughts. The threshold values are calculated based on the undisturbed period and applied to the entire time series. Meanwhile, to reduce the impact of modeling errors on drought separation, different threshold values are calculated from observed and simulated runoff series, respectively.

3.3. A Brief Description of the VIC Model. The semidistributed, three-layer Variable Infiltration Capacity (VIC) model [22] is chosen for hydrological modeling. It has been used in many drought related researches, such as reconstructing and analyzing drought events [23–25] and drought prediction [26]. The VIC model considers the dynamic variation in both water and energy balance according to the subgrid heterogeneity represented by soil moisture storage, evaporation, and runoff generation. Partitioning of rainfall into infiltration and surface runoff is controlled by a Variable Infiltration Capacity curve [27]. Vertical water movement occurs within discrete soil layers through diffusion and baseflow is modeled from a lower soil moisture zone as a nonlinear recession [28]. A separate routing model is employed to transport grid cell surface runoff and baseflow to the outlet then into the river system, including a linear transfer function model used to calculate the within-cell

Table 1: Physical meanings and ranges of the sensitive parameters in the VIC model.

Parameter	Physical meaning	Unit	Range
i	Infiltration curve parameter	N/A	0-1
d_1	Thickness of top thin soil moisture layer	m	0.05–0.1
d_2	Thickness of middle soil moisture layer	m	0–2
d_3	Thickness of lower soil moisture layer	m	0–2
D_s	Fraction of D_{smax} where nonlinear baseflow begins	Fraction	0-1
D_{smax}	Maximum velocity of baseflow	mm/day	0–30
W_s	Fraction of maximum soil moisture where nonlinear baseflow occurs	Fraction	0-1

routing and the linearized Saint-Venant equation serving for channel routing [29].

The description of land surface characteristics for each grid cell is mainly implemented through numerous parameters of two categories: vegetation and soil parameters. Vegetation parameters comprise vegetation leaf area index, roughness length, displacement height, architectural resistance, and minimum stomatal resistance with relevant information that can be obtained from the University of Maryland's (UMD) land cover classification [30] and estimated according to the Land Data Assimilation Systems developed by the National Aeronautics and Space Administration (NASA). As for soil parameters, some can be determined from empirical values and need not be adjusted, such as porosity, saturated soil potential, saturated hydraulic conductivity, and the exponent B for unsaturated flow (available from the 5-minute Food and Agriculture Organization data set [12]), while other parameters are subject to calibration based on the agreement between simulated and observed hydrographs. Commonly, calibration is conducted by optimizing the seven sensitive parameters (i, d_1, d_2, d_3, D_s, D_{smax}, and W_s) with two criteria: Nash-Sutcliffe Coefficient of Efficiency (NSCE) and BIAS. The specific meanings and ranges of these sensitive parameters are listed in Table 1.

4. Results and Discussion

4.1. Evolution of Meteorological and Hydrological Droughts. Meteorological drought extracted from monthly precipitation series shows that there is no significant variation trend during the past 46 years (Figure 3(a)). The drought interval is generally stable with most of drought events occurring in the dry season. In contrast, hydrological drought (Figure 3(b)) derived from monthly runoff series shows different pattern with obvious decadal fluctuations observed. Among the five decades, the 1980s (1980–1989) and 2000s (2000–2009) are the two most severe dry decades which suffer consecutive droughts with large deficit volume, whereas for the 1990s (1990–1999) almost no hydrological droughts occur. A comparison of drought characteristics between meteorological and hydrological droughts further demonstrates their difference. Figures 3(c) and 3(d) are the scatterplots of drought duration and deficit volume. Obviously, meteorological droughts occur every decade, but for hydrological droughts they are mostly concentrated in the 1980s and 2000s. Comparing to meteorological drought, the duration of hydrological drought is lengthened (up to 17 months), and deficit volume is attenuated (not more than 6 mm). Meanwhile, the relationship between drought duration and deficit volume is modified and tends to be linear for the hydrological drought.

The above-mentioned differences between the two drought categories, on the one hand, reflect a propagation scheme from meteorological drought to hydrological drought. Due to the effects of climate and catchment control, meteorological droughts are combined into a longer hydrological drought. Meanwhile, the drought signal is weakened in catchment stores during this process [31]. On the other hand, the striking contrast among decades in terms of hydrological drought seems quite abnormal and is far beyond the scope of naturalized drought propagation process. To further explore the reasons for the unusual behavior of hydrological drought during the 1990s, the flow duration curves of precipitation and runoff for each decade are compared, shown in Figure 4. For precipitation, minor decadal difference of the flow duration curves is found, especially in the low flow section, and using the 70-percentile threshold of whole periods would ensure 25%–35% of droughts (accordingly 65%–75% of nondrought) recognized for different decades. However, for runoff, rather large decadal difference is observed. Using the 70-percentile threshold of whole periods would recognize approximately 50%–60% of droughts for the 1980s and 2000s but no more than 10% for the 1990s. This shows the inconsistent behavior between meteorological and hydrological droughts. For drought propagation, catchment control plays an important role in determining process features like duration and deficit. The discrepant performances between these two drought categories suggest that the effect of catchment control is not constant but changes over time. Besides the natural hydrology system, hydrological drought at this catchment scale is potentially disturbed by human activities.

4.2. Analysis on the Changing Environments. To further explore the causes of the abnormal pattern in hydrological drought, a comprehensive analysis on drought related variables (including precipitation, runoff, runoff coefficient, baseflow, and BFI) is conducted. Among them, precipitation provides the antecedent condition for the occurrence of hydrological drought and governs drought deficit volume. Runoff coefficient represents the proportion of runoff in precipitation and can be used to reflect temporally varied

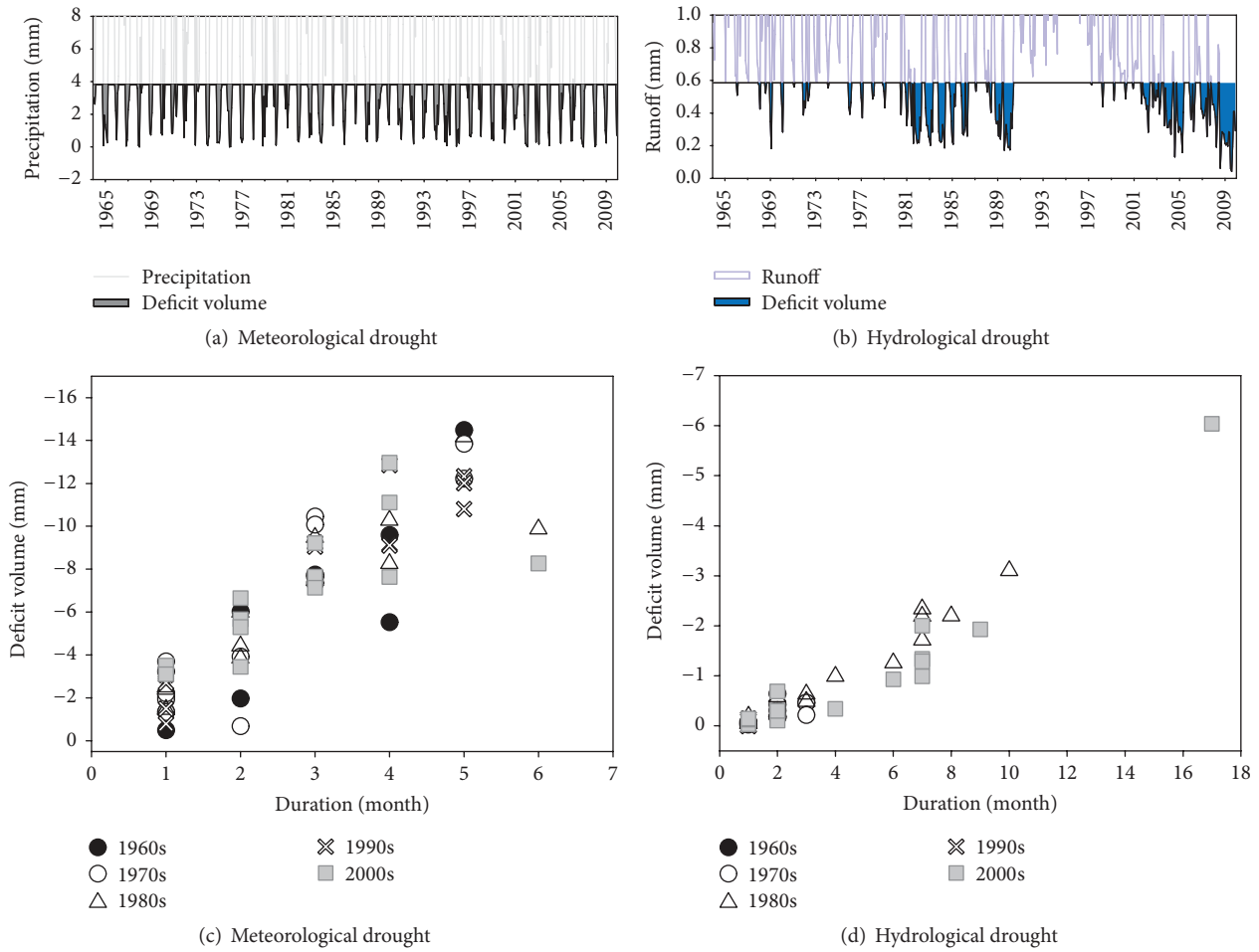

FIGURE 3: Temporal evolutions of identified (a) meteorological drought (derived from precipitation) and (b) hydrological drought (derived from runoff), and the scatterplots of drought duration and deficit volume for (c) meteorological and (d) hydrological droughts.

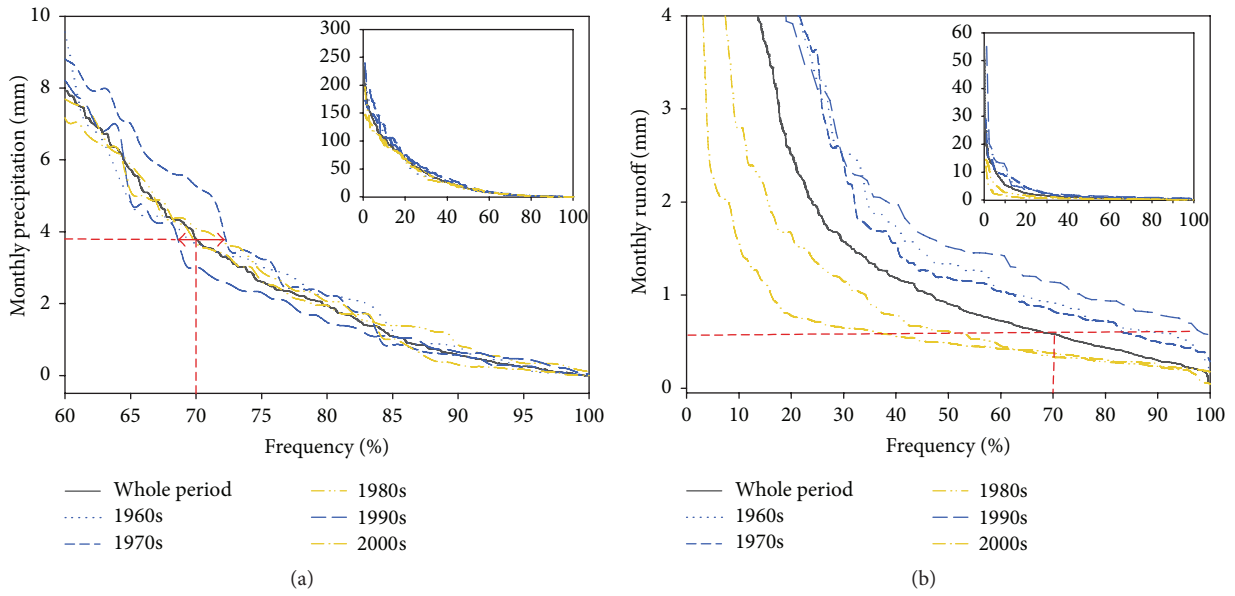

FIGURE 4: Monthly flow duration curves of precipitation (a) and runoff (b) for each decade. Dull yellow and blue lines represent curves for dry and wet decades, respectively.

Table 2: Mean annual precipitation, runoff, runoff coefficient, baseflow, and BFI of every decadal-year over the Laohahe catchment during the past half-century.

	Precipitation (mm)	Streamflow (mm)	Runoff coefficient	Baseflow (mm)	BFI
1964–1969	414.60	38.34	0.09	10.98	0.29
1970–1979	455.01	35.87	0.08	10.06	0.29
1980–1989	396.31	15.95	0.04	4.89	0.35
1990–1999	473.38	42.98	0.09	12.92	0.32
2000–2009	379.06	9.73	0.03	3.70	0.44

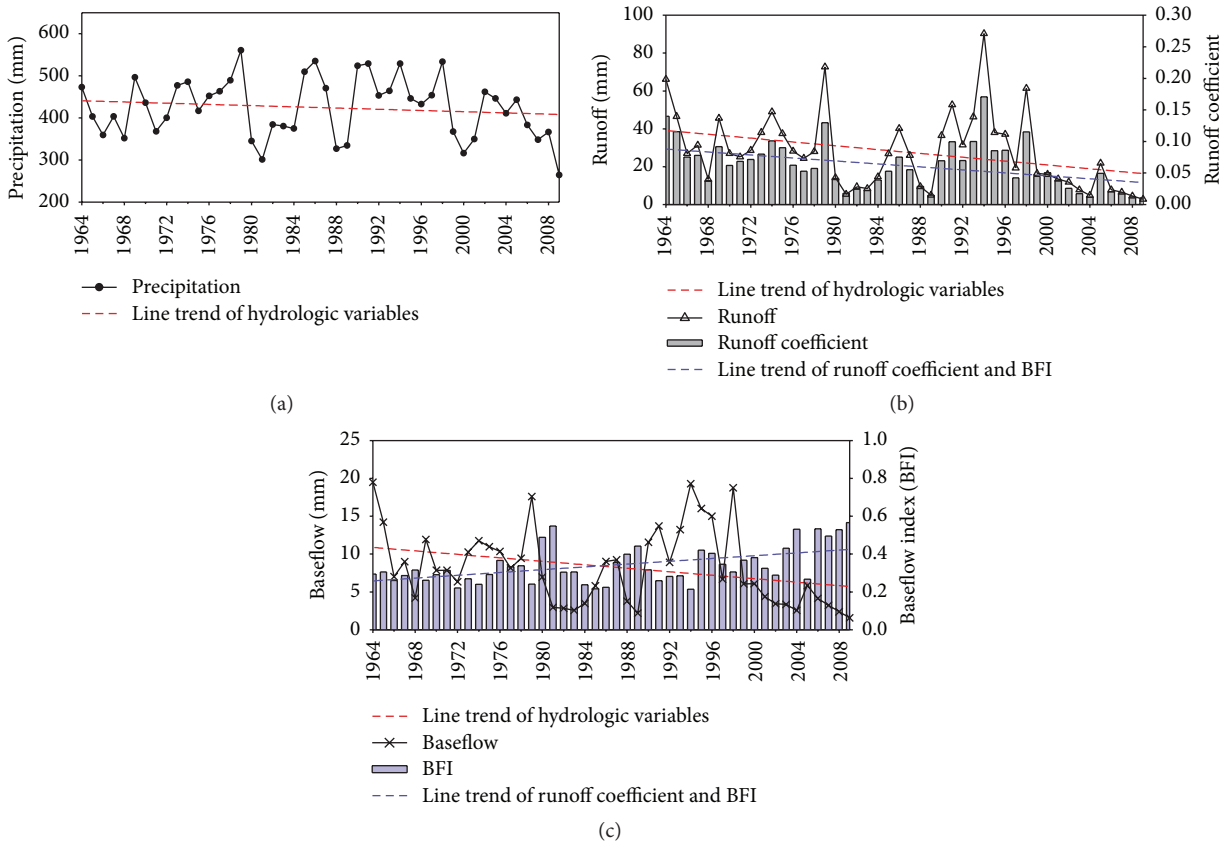

Figure 5: Variations of annual precipitation, runoff, runoff coefficient, baseflow, and baseflow index (BFI) over the Laohahe catchment since 1964. The red dashed line represents linear trend for hydrological variables (precipitation, runoff, and baseflow) and the blue dashed line for runoff coefficient and BFI.

rainfall-runoff relationships. The BFI itself is not a catchment characteristic but it integrates the effect of catchment storage and release properties and is found to have strong positive correlation with hydrological drought duration.

As shown in Figure 5 and Table 2, precipitation (Figure 5(a)) presents a slightly decreasing trend during the past 50 years, accompanied with regularly decadal fluctuation (the 1980s and 2000s are the two driest decades, whereas the 1990s is the wettest decade). Runoff (Figure 5(b)) also shows a descending trend, but in a more rapid rate. This inconsistent pattern between precipitation and runoff is further illustrated by the varied runoff coefficient. Normally, runoff coefficient at this catchment scale varies around 0.09, but in the two driest decades 1980s and 2000s a rather low value (no more than 0.05) is observed, implying the significantly reduced proportion of runoff in precipitation. Meanwhile, runoff components (Figure 5(c)) have also changed and the proportion of baseflow generally increases with an upward trend detected in BFI. This indicates that catchment control like storage and release properties has changed over time, which indirectly influences the development of hydrological drought.

Based on the above analysis, we further investigate the runoff changes (i.e., varied response to precipitation and runoff components) with the double cumulative curves method. Figure 6(a) is the double cumulative curve of precipitation and runoff. From this graph we can find two prominent inflection points where the gradient for the cumulative curve of runoff significantly changes compared with that of precipitation, that is, 1979 and 1998. This deviation is

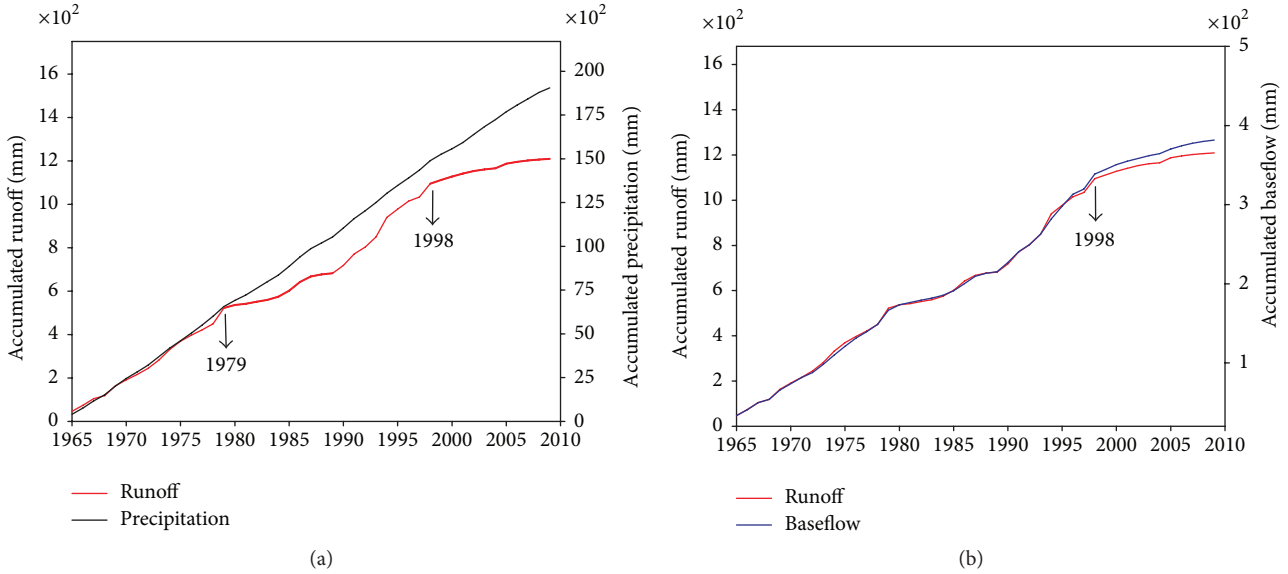

Figure 6: Double cumulative curves of (a) annual precipitation and runoff and (b) annual runoff and baseflow.

quite related to human activities, which lead to sharp decline in runoff [32]. In response to the 1978 land reform policy, most regions in northern China (grain production base) switched their focus to the development of agriculture, and irrigation has become a routine agronomic practice [33]. The Laohahe catchment is one of these cases, as shown in Figure 7; indices like agricultural production (Figure 7(a)) and gross domestic product (GDP, Figure 7(d)) have increased in a staggering speed since 1979. The price paid for the fast-growing agriculture is that more water is consumed and evaporated to meet irrigation demands and livelihood purpose (indicated by a continuous growth in population). The second inflection point which emerged in 1998 implies that reduction in runoff has been aggravated since then. Figure 6(b) shows that, after 1998, runoff decreases more rapidly than baseflow, meaning that consumption from surface water has further increased. During this period, the gross industrial product (GIP) has experienced fast growth (Figure 7(c)), which tremendously contributes to water depletion for the sake of second and third industry development and industrial structure adjustment [11]. In addition, increased reservoir storage capacities during the 2000s might be another reason for surface water reduction. Before 2000s, the Laohahe catchment is mainly regulated by two large reservoirs, namely, the Erdaohezi and Dahushi, with a total regulation capacity of 2.0×10^8 m^3 (a sum of the two reservoirs' storage capacity). In 2003, this regulation capacity has been increased to 5.69×10^8 m^3 with the construction of the San Zuodian reservoir, which potentially brings some pressure to the surface runoff.

As a matter of fact, human activities carried out at this catchment are not limited to the above-mentioned aspects. Other forms such as abstraction from groundwater, land cover and land use change, and livestock breeding all influence runoff patterns in a direct or indirect way. Accordingly, the naturalized process of hydrological drought is disturbed and develops in a more complicated mode. From the perspective of water resources management, our traditional drought mitigation solutions should be adjusted so as to adapt to droughts driven by different causes. This once again shows the significance of making the distinction between naturalized drought and human-induced drought.

4.3. Separating Naturalized and Human-Induced Hydrological Drought. According to the above analysis on the changes of catchment characteristics, the temporal span is divided into two parts, that is, the baseline (undisturbed) period from 1964 to 1979 during which catchment conditions are relatively natural and minor human activities are negligible and the changed (disturbed) period from 1980 to 2010. Following the separating framework described in Section 3.2, we first calibrate the hydrological VIC model using hydrometeorological forcing during the baseline period. Specifically, the VIC model is run at a daily temporal and $0.0625^\circ \times 0.0625^\circ$ spatial resolution. Calibration contains a relative long time, 1964–1974, which aims to ensure an appropriate sample size with both wet and dry years involved and further improves the representativeness of parameters. Accordingly, the remaining five years (1975–1979) belong to the validation period. Figure 8(a) is the monthly simulation results during the baseline period. Overall, a satisfying model performance is found for both calibration and validation periods. Values of NSCE and BIAS are 0.85 and 4.2% for the calibration period and 0.80 and 1.8% for the validation period, respectively, suggesting that VIC is capable of capturing natural variability of the observed hydrograph (e.g., water amounts, peak magnitude, and recession).

With the calibrated model, we reconstructed the streamflow series using hydrometeorological forcing during the changed period (1980–2009). As shown in Figure 8(b), the difference between observed and simulated (reconstructed) series mainly reflects the anthropogenic effects on runoff, combined with minor simulation errors.

Table 3: Drought characteristics (using the 70-percentile monthly threshold) for the observed and simulated runoff during 1980–2009.

Changed period	Number of droughts	Duration (month)		Deficit (mm)	
		Mean	Max	Mean	Max
Observed	27	7.5	29	−3.12	−15.47
Simulated	32	4	6	−1.12	−1.86

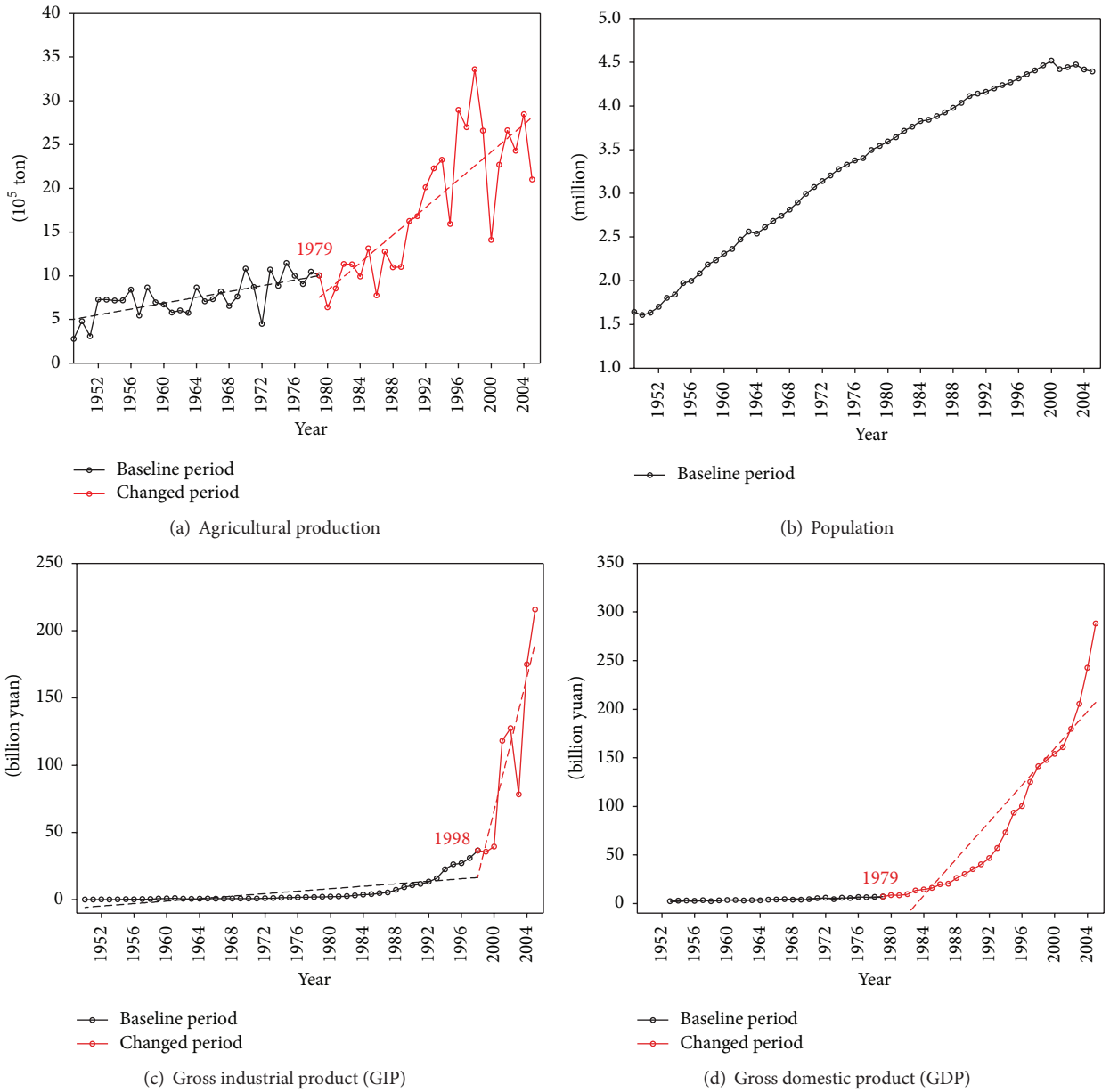

Figure 7: Time series of (a) agricultural products, (b) population, (c) gross industrial product (GIP), and (d) gross domestic product (GDP) in Chifeng, the main city within the Laohahe catchment, from 1949 to 2005.

Figure 9 presents the evolution of hydrological droughts separately identified from observed and simulated streamflow series. Obviously, the upper panel (Figure 9(a)) representing droughts caused by combined effects of natural condition and human disturbances shows a more severe dry pattern than the naturalized condition displayed in the middle panel (Figure 9(b)). Table 3 lists their specific differences in statistics of drought characteristics. Although in the naturalized circumstance five more drought events are observed, drought duration and deficit volume are amplified two to four times and three to eight times, respectively, when human disturbances are involved. This means that the severity of human-induced drought far exceeds that of droughts in naturalized situations. Figure 9(c) is the temporal difference

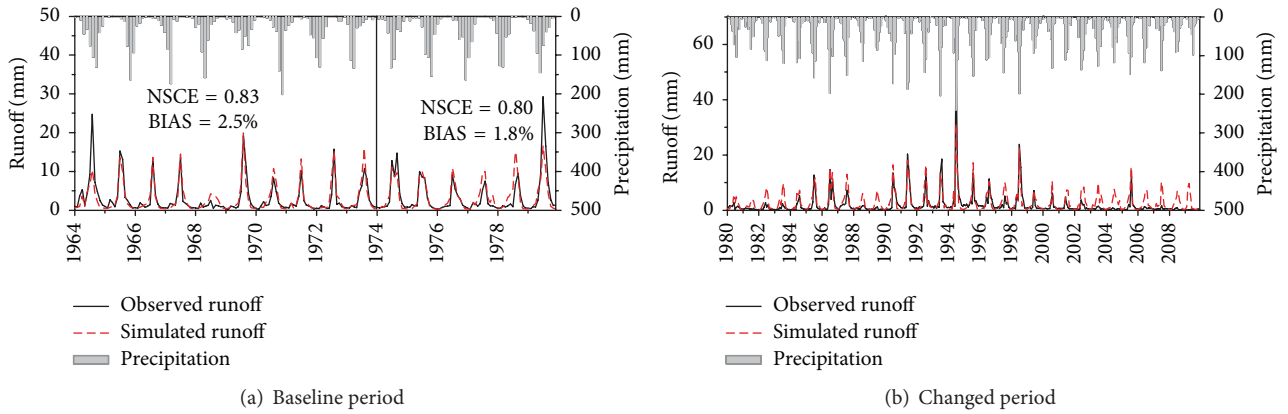

FIGURE 8: VIC simulated monthly runoff at the Xinglongpo hydrologic station for (a) the baseline period 1964–1979 and (b) changed period 1980–2009.

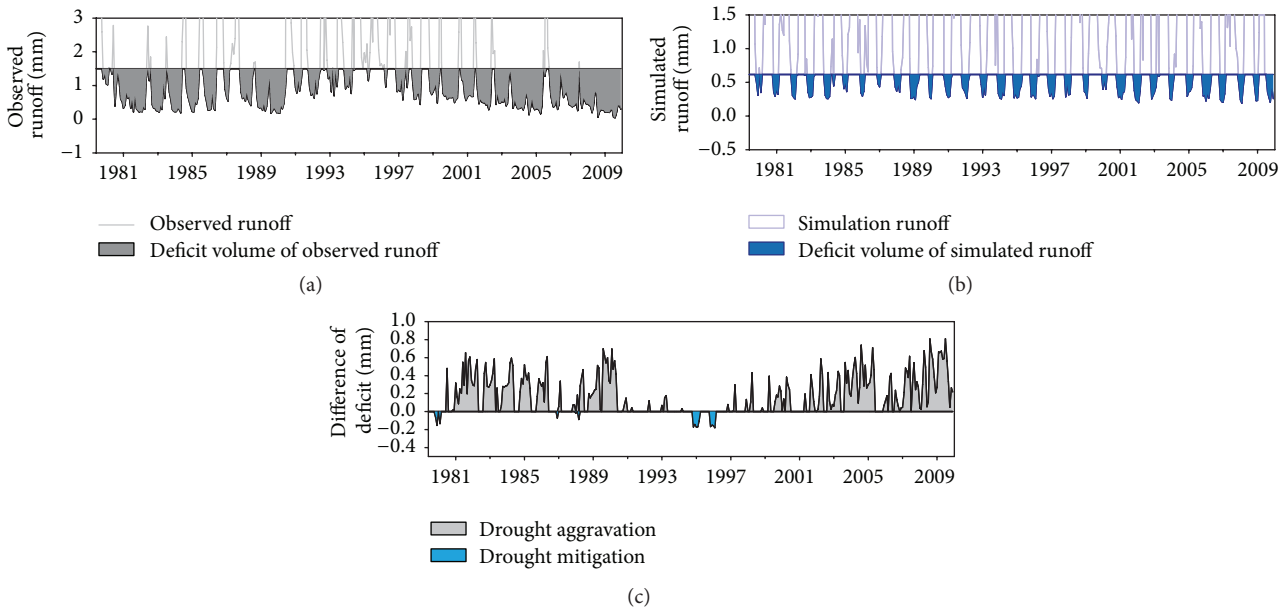

FIGURE 9: Identified hydrological droughts (with 70-percentile threshold derived from the baseline period) during 1980–2009 from (a) observed runoff and (b) simulated runoff series, and (c) is the difference between observed and simulated runoff series representing the net effect of human activities on drought.

between observed and simulated droughts, which reflects the net impact of human activities. The positive values (light grey area) represent a negative role of aggravating drought, whereas the negative values (light blue area) imply a positive effect of drought mitigation. We can find that, during the whole changed period, human activities are more inclined to play a negative role. In particular in the two dry decades 1980s and 2000s, human activities have induced several consecutive drought events with rather long durations, such as droughts from November 1980 to April 1982 (18 months) and from August 2007 to December 2009 (29 months). In contrast, the influence is rather moderate during the wet decade 1990s; even in 1994 and 1995, a positive effect is observed. The abnormal human activity behaviors in these two years may be related to the interannual regulation roles of reservoirs. Figure 10 shows the monthly variations of precipitation and runoff during the past 46 years (only low flow seasons are displayed, from the recession month (September) in this year to May of next year). We can see that precipitation in 1994 and 1995 is generally the lowest; however, corresponding runoff is extremely high. We speculate that the drainage from reservoirs could be one contributing factor. Due to lack of reservoir records, this unusual phenomenon needs to be further analyzed in the future.

In addition, since the whole separation framework of hydrological droughts largely depends on hydrological model simulations, accurate model performance in capturing the characteristics of hydrograph is essential for the separation results between naturalized and human-induced droughts. As many other hydrological simulations, minor biases (errors

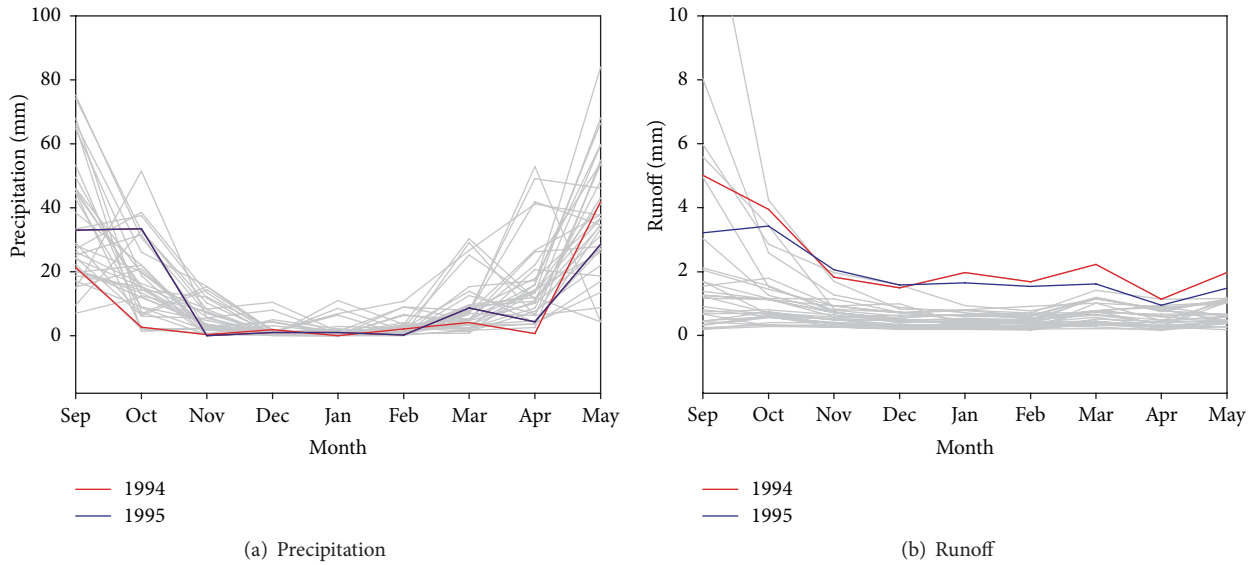

(a) Precipitation (b) Runoff

Figure 10: Monthly variations of (a) precipitation and (b) runoff during the past 46 years. The red and blue lines represent variables in 1994 and 1995, respectively, and the grey lines represent variables in other 44 years.

not more than 2.5%, equivalent to approximately 0.9 mm in streamflow) in produced water amounts are observed during the baseline period, with overestimations in peak streamflow contributing to most of the errors (Figure 8). Since droughts recognized by the fixed threshold are more likely to happen in low flow seasons, this systematic positive deviation in flood peak would not influence our separated results in any significant way as long as the errors for the low flow section are effectively controlled. In a more direct way, we compared the differences between observations and hydrological model simulations identified streamflow deficit volume during the baseline period to analyze the propagated bias in droughts. Results show that, among the 73 months which experience hydrological droughts during the baseline period, the difference between the two datasets on average is 0.01 mm/month, with maximum absolute value no more than 0.05 mm/month. This magnitude in general is rather small compared with the streamflow deficit volume of human-induced droughts, where an order of 0.2–0.8 mm/month is found for most of the drought events (Figure 9(c)). In other words, minor errors derived from model simulations though exist; they will not influence the dominant contribution of human activities substantially, especially for the two driest decades 1980s and 2000s. According to the above findings, we could conclude that, with the participation of human activities, hydrological drought in the Laohahe catchment has been further aggravated and become more severe.

5. Summary and Conclusions

In this paper, a case study over the Laohahe catchment is conducted, which serves as a representative example of the evolution of hydrological drought in the context of changing environments. The common understanding of the hydrological drought development is mainly governed by climate and catchment control. However, for catchments like our studied one which is intensively disturbed by human activities, the causes for hydrological drought become rather complicated and the effects from human activities should be considered.

The comparison between meteorological droughts and hydrological droughts occurring in the Laohahe catchment during 1964–2009 shows an interesting pattern; that is, meteorological droughts occur regularly in every decade, but for hydrological droughts, significant decadal differences are observed: the 1980s and 2000s suffer extremely severe hydrological droughts whereas, for the 1990s, almost no droughts occur. This striking contrast is far beyond the scope of naturalized drought process dominated by climate and catchment control, indicating the potential impact of human disturbances on hydrological drought.

The long-term series of runoff related variables are further analyzed and changes in runoff are confirmed according to several indices, that is, inconsistent trend between precipitation and runoff, varied runoff coefficient, and BFI among decades, which commonly reflect the varied responses of runoff to precipitation and runoff components. Then, the double cumulative curves method is employed to detect the changed points, which further divides the whole period into two parts, that is, the undisturbed period (1964–1979) and disturbed period (1980–2009). Meanwhile, four socioeconomic indices are also analyzed which imply increased water consumption in the changed period.

Based on the divided periods, a separating framework is introduced to distinguish between naturalized drought and human-induced drought during the changed period. From the comparison between their drought characteristics, it can be found that the drought duration and deficit volume of naturalized drought are amplified two to four times and three to eight times, respectively, when human activities are involved.

This reflects the considerable impact of human activities on hydrological drought. Generally, human activities are more inclined to play a negative role which aggravates droughts. In particular in the two dry decades 1980s and 2000s, human activities have induced several consecutive drought events with rather long durations (up to 29 months). With a comprehensive analysis on the individual roles of natural condition and human activities on hydrological drought, this study is promising to provide some theoretical support for future drought mitigation and water resources management.

Conflict of Interests

The authors declare that there is no conflict of interests regarding the publication of this paper.

Acknowledgments

This work was supported by the Special Basic Research Fund for Methodology in Hydrology (Grant no. 2011IM011000) from the Ministry of Sciences and Technology, China, the 111 Project (Grant no. B08048) from the Ministry of Education and State Administration of Foreign Experts Affairs, China, the China Scholarship Council (CSC), the National Key Technology R&D Program by Ministry of Sciences and Technology, China (2013BAC10B02), the Fundamental Research Funds for the Central Universities (2015B14514), the National Natural Science Foundation of China (nos. 51579066, 41501017, and 41201031), the project sponsored by SRF for ROCS, SEM (515025512), and Natural Science Foundation of Jiangsu Province (BK20150815).

References

[1] D. A. Wilhite, "Drought as a natural hazard: concepts and definitions," in *Drought: A Global Assessment*, D. A. Wilhite, Ed., vol. 1, pp. 1–18, Routledge, New York, NY, USA, 2000.

[2] L. M. Tallaksen and H. A. J. van Lanen, *Hydrological Drought—Processes and Estimation Methods for Streamflow and Groundwater*, vol. 48 of *Developments in Water Sciences*, Elsevier, Amsterdam, The Netherlands, 2004.

[3] A. K. Mishra and V. P. Singh, "A review of drought concepts," *Journal of Hydrology*, vol. 391, no. 1-2, pp. 202–216, 2010.

[4] A. Dai, "Increasing drought under global warming in observations and models," *Nature Climate Change*, vol. 3, pp. 52–58, 2010.

[5] K. Stahl, *Hydrological drought—a study across Europe [Ph.D. thesis]*, Albert-Ludwigs-Universitat Freiburg, Freiburger Schriften zur Hydrologie, Freiburg, Germany, no. 15, 2001, http://www.freidok.uni-freiburg.de/volltexte/202.

[6] S. I. Seneviratne, N. Nicholls, D. Easterling et al., "Changes in climate extremes and their impacts on the natural physical environment," in *A Special Report of Working Groups I and II of the Intergovernmental Panel on Climate Change (IPCC)*, chapter 3, pp. 109–230, Cambridge University Press, Cambridge, UK, 2012.

[7] D. A. Wilhite and M. H. Glantz, "Understanding the drought phenomenon: the role of definitions," *Water International*, vol. 10, no. 3, pp. 111–120, 1985.

[8] D. G. Kingston, A. K. Fleig, L. M. Tallaksen, and D. M. Hannah, "North Atlantic sea surface temperature, atmospheric circulation and summer drought in Great Britain," in *Proceedings of the 6th World FRIEND Conference "Global Change: Facing Risks and Threats to Water Resources"*, E. Servat, S. Demuth, A. Dezetter et al., Eds., vol. 340, pp. 598–604, IAHS-AISH Publication, Fez, Morocco, October 2010.

[9] H. A. J. van Lanen, L. Kašpárek, O. Novický et al., *Hydrological Drought—Processes and Estimation Methods for Streamflow and Groundwater*, vol. 48 of *Developments in Water Science*, B.V. Elsevier Science, 2004.

[10] E. Peters, H. A. J. van Lanen, P. J. J. F. Torfs, and G. Bier, "Drought in groundwater—drought distribution and performance indicators," *Journal of Hydrology*, vol. 306, no. 1–4, pp. 302–317, 2005.

[11] L. Ren, F. Yuan, B. Yong et al., "Where does blue water go in the semi-arid area of northern China under changing environments?" in *Evolving Water Resources Systems: Understanding, Predicting and Managing Water-Society Interactions. Proceedings of ICWRS 2014, Bologna, Italy*, vol. 364, IAHS Publications, 2014.

[12] R. G. Allen, L. S. Pereira, D. Raes, and M. Smith, "Crop evapotranspiration: guidelines for computing crop requirements," Irrigation and Drainage Paper 56, FAO, Rome, Italy, 1998.

[13] V. D. Lyne and M. Hollick, "Stochastic time-variable rainfall runoff modelling," in *Proceedings of the Hydrology and Water Resources Symposium*, vol. 32, pp. 89–92, Institution of Engineers, Perth, Australia, September 1979.

[14] J. L. Salinas, G. Laaha, M. Rogger et al., "Comparative assessment of predictions in ungauged basins-part 2: flood and low flow studies," *Hydrology and Earth System Sciences*, vol. 17, no. 7, pp. 2637–2652, 2013.

[15] M. D. Zaidman, H. G. Rees, and A. R. Young, "Spatio-temporal development of streamflow droughts in northwest Europe," *Hydrology and Earth System Sciences*, vol. 6, no. 4, pp. 733–751, 2002.

[16] M. Fendeková and M. Fendek, "Groundwater drought in the nitra river basin—identification and classification," *Journal of Hydrology and Hydromechanics*, vol. 60, no. 3, pp. 185–193, 2012.

[17] V. Yevjevich, "An objective approach to definitions and investigations of continental hydrologic droughts," Hydrology Papers 23, Colorado State University, Fort Collins, Colo, USA, 1967.

[18] A. K. Fleig, L. M. Tallaksen, H. Hisdal, and S. Demuth, "A global evaluation of streamflow drought characteristics," *Hydrology and Earth System Sciences*, vol. 10, no. 4, pp. 535–552, 2006.

[19] A. F. van Loon and H. A. J. van Lanen, "Making the distinction between water scarcity and drought using an observation-modeling framework," *Water Resources Research*, vol. 49, no. 3, pp. 1483–1502, 2013.

[20] A. N. Pettitt, "A non-parametric approach to the change-point problem," *Journal of the Royal Statistical Society Series C: Applied Statistics*, vol. 28, no. 2, pp. 126–135, 1979.

[21] M. G. Kendall, *Rank Correlation Methods*, Charles Griffin, London, UK, 1975.

[22] X. Liang, D. P. Lettenmaier, E. F. Wood, and S. J. Burges, "A simple hydrologically based model of land surface water and energy fluxes for GCMs," *Journal of Geophysical Research D*, vol. 99, no. 7, pp. 14415–14428, 1994.

[23] J. Sheffield, G. Goteti, F. Wen, and E. F. Wood, "A simulated soil moisture based drought analysis for the United States," *Journal of Geophysical Research D: Atmospheres*, vol. 109, no. 24, pp. 1–19, 2004.

[24] K. M. Andreadis and D. P. Lettenmaier, "Trends in 20th century drought over the continental United States," *Geophysical Research Letters*, vol. 33, no. 10, 2006.

[25] A. Wang, T. J. Bohn, S. P. Mahanama, R. D. Koster, and D. P. Lettenmaier, "Multimodel ensemble reconstruction of drought over the continental United States," *Journal of Climate*, vol. 22, no. 10, pp. 2694–2712, 2009.

[26] L. F. Luo and E. F. Wood, "Monitoring and predicting the 2007 U.S. drought," *Geophysical Research Letters*, vol. 34, no. 22, 2007.

[27] R. J. Zhao, Y. L. Zhang, L. R. Fang et al., "The Xinanjiang model, hydrological forecasting," in *Proceedings of the 477th Oxford Symposium*, vol. 129, pp. 351–356, IAHS Publisher, 1980.

[28] L. Dumenil and E. Todini, "A rainfall-runoff scheme for use in the Hamburg climate model," in *Advances in Theoretical Hydrology*, P. O'Kane, Ed., vol. 1 of *European Geophysical Society, Series on Hydrological Sciences*, pp. 129–157, Elsevier, Amsterdam, The Netherlands, 1992.

[29] D. Lohmann, E. Raschke, B. Nijssen, and D. P. Lettenmaier, "Regional scale hydrology: I. Formulation of the VIC-2L model coupled to a routing model," *Hydrological Sciences Journal*, vol. 43, no. 1, pp. 131–141, 1998.

[30] M. C. Hansen, R. S. Defries, J. R. G. Townshend, and R. Sohlberg, "Global land cover classification at 1 km spatial resolution using a classification tree approach," *International Journal of Remote Sensing*, vol. 21, no. 6-7, pp. 1331–1364, 2000.

[31] A. F. van Loon, M. H. J. van Huijgevoort, and H. A. J. van Lanen, "Evaluation of drought propagation in an ensemble mean of large-scale hydrological models," *Hydrology and Earth System Sciences*, vol. 16, no. 11, pp. 4057–4078, 2012.

[32] L. Ren, M. Wang, C. Li, and W. Zhang, "Impacts of human activity on river runoff in the northern area of China," *Journal of Hydrology*, vol. 261, no. 1–4, pp. 204–217, 2002.

[33] Z. Zhang, X. Chen, C.-Y. Xu, L. Yuan, B. Yong, and S. Yan, "Evaluating the non-stationary relationship between precipitation and streamflow in nine major basins of China during the past 50 years," *Journal of Hydrology*, vol. 409, no. 1-2, pp. 81–93, 2011.

Hindawi Publishing Corporation
Advances in Meteorology
Volume 2016, Article ID 1634787, 8 pages
http://dx.doi.org/10.1155/2016/1634787

Research Article

Robust Response of Streamflow Drought to Different Timescales of Meteorological Drought in Xiangjiang River Basin of China

Lin Zhao,[1] Jianjun Wu,[2] and Jian Fang[1]

[1]*School of Resource and Environmental Sciences, Wuhan University, Wuhan 430079, China*
[2]*Academy of Disaster Reduction and Emergency Management, Beijing Normal University, Beijing 100875, China*

Correspondence should be addressed to Jian Fang; fj20061028@126.com

Received 2 June 2015; Accepted 1 October 2015

Academic Editor: Maurits W. Ertsen

Meteorological drought can evolve into all aspects of hydrologic system such as soil layer, groundwater, and river discharge, leading to agricultural drought, groundwater drought, and streamflow drought, respectively. How does it propagate? Is there any strong relationship between meteorological drought and others? These issues need further understanding regarding different climate regions. In this paper, monthly SRI and SPEI at different timescales during 1976 and 2005 were utilized to understand how streamflow drought responded to meteorological drought in Xiangjiang river basin, a semihumid basin of Central China. Impressive findings included that strong correlations between SRI and SPEI were found. SPEI of 2-month timescale behaved best when correlating with SRI ($R = 0.79$). Longer timescales of SPEI seemed not to be useful for streamflow drought identification. At seasonal scale, higher correlation coefficients were obtained during dry season, whereas lower coefficients were found in wet season. The maximum R reached up to 0.89 in November at 2-month timescale. Besides, robust response relation between streamflow drought and meteorological drought was also found. The average response rate (R_r) was considerably high (75.4%), with the maximum obtained at 2-month timescale ($R_r = 82.9\%$). Meanwhile, important seasonal difference of response rate has also been pointed out.

1. Introduction

Drought is a multifaceted phenomenon that occurs across a range of temporal and spatial scales [1], characterized by periods of more than normal water deficit. It is one of the most damaging natural disasters all over the world [2], causing significant damage to different sectors of natural environment, such as vegetation growth [3, 4], crop yield [5, 6], water supply [7], desertification [8], and forest fire [9]. Due to global warming, the dry land areas have increased significantly in the past fifty years [10] and widespread severe droughts in the next 30–90 years over many land areas were also simulated by most models [11].

Four basic categories of drought have been identified by Wilhite and Glantz in 1985 [12], which are meteorological drought, agricultural drought, hydrological drought, and socioeconomic drought. Prolonged severe meteorological drought will gradually propagate into different sectors of water resources, such as soil moisture, groundwater, and river discharge, leading to soil drought, groundwater drought, and streamflow drought. The propagation of drought through hydrologic system is complex, which may be affected by underlying conditions such as land cover, vegetation, and topography [13–15]. Understanding of this propagation procedure and how it behaves in different area would not only be helpful for drought monitoring and early warning, but also provide further support in theory and practical implications for making regional drought plans.

A few number of previous studies have reported on the relationship between hydrological drought and meteorological drought. Part of studies have paid attention to the evolution of drought characteristics when it propagated through different hydrologic systems. Hisdal and Tallaksen conducted a study on the comparison between regional characteristics of meteorological drought and hydrological drought in Denmark and found that hydrological droughts were less homogeneous over Denmark, less frequent, and lasted for longer time periods than meteorological drought [16]. Peters et al.

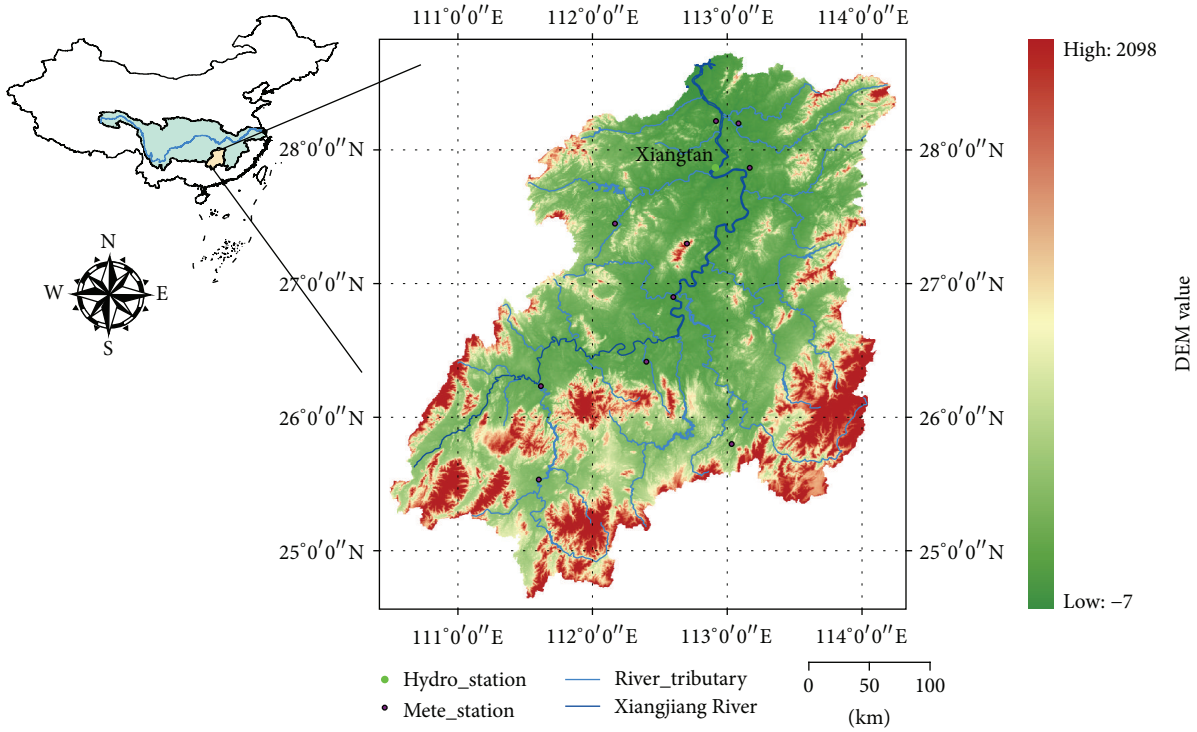

Figure 1: Study area and the location of all gauging stations.

have also provided an evidence that the propagation of meteorological drought to groundwater drought decreased the number of drought events and caused a shift in the drought severity distribution [17]. Major related researches have been devoted to how the response of hydrological drought to meteorological drought varied in different timescales and the time-lag of hydrological drought to meteorological drought. Vicente-Serrano and López-Moreno found that surface flows responded to short time scales of meteorological drought (1–4 months) in a mountainous Mediterranean Basin [18]. Tabrizi et al. found that annual time scale of meteorological drought in the upstream of the Doroodzan watershed in Iran was useful in investigating occurrence of streamflow drought in the downstream [19]. Good correlation between annual PDSI, SPI, and Percentage of Rainfall Anomaly was found in ten major basins across China [20]. Four-month timescale of Standardized Precipitation Index (SPI) was proved to be the most suitable indicator when relating with standardized runoff index (SRI) in a typical semiarid inland basin of China [21]. A time-lag of 127 days regarding comparison between streamflow drought and meteorological drought was also found in this area [21]. Similar time lag of 7 months was found in a study conducted in the Awash River basin of Ethiopia [22]. At a small drought-prone basin in Oklahoma of USA, there was a time-lag of 2 months between SRI and SPI in model projection [23].

Considering limited related previous studies on the relationship between hydrological drought and meteorological drought in Asia, the scope of this research lies in the response of streamflow drought to meteorological drought in a humid basin in Southern China. As indicated in a recent study [24], PET, in the face of climate change, an important component in the hydrologic cycle, should not be ignored in drought monitoring. Different to SPI, PET has been integrated into the Standardized Precipitation Evapotranspiration Index (SPEI) calculation [25], making it more efficient than SPI in drought monitoring at humid and semihumid areas, in which both precipitation and temperature are vital for drought identification.

The main purpose is to test the usefulness of different timescales of SPEI to indicate streamflow drought and how the relation between streamflow drought and meteorological drought behaves in different seasons at humid regions, especially under trend of global warming. The objective is to select the most suitable timescale of SPEI to identify drought in river discharge. Results will be helpful in regional water resources planning and drought management.

2. Materials and Methods

2.1. Study Area and Data. Xiangjiang River basin is one of the largest subbasins of Yangtze River Basin. It is located in the southcentral China and most of the basin is within Hunan Province (Figure 1). As a main tributary of the Yangtze River, the Xiangjiang River originates from the mountainous area in the southwest and flows into the Dongting Lake in the northeast. It has a total length of 844 km and forms a basin of 94,660 km^2. The streamflow in this basin is mainly charged by precipitation. Robust linear relationship between monthly mean runoff and monthly precipitation during 1976 and 2005 was found in Figure 2. The elevation in the

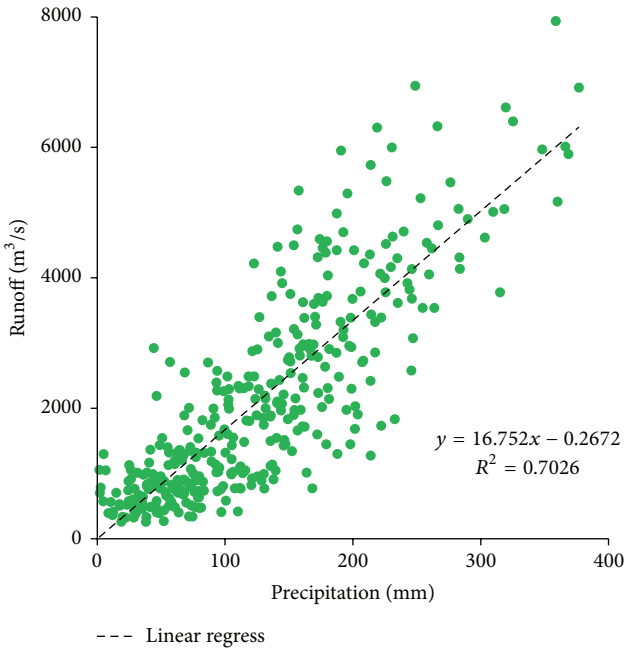

Figure 2: Scatter diagram of monthly mean runoff and monthly precipitation during 1976 and 2005.

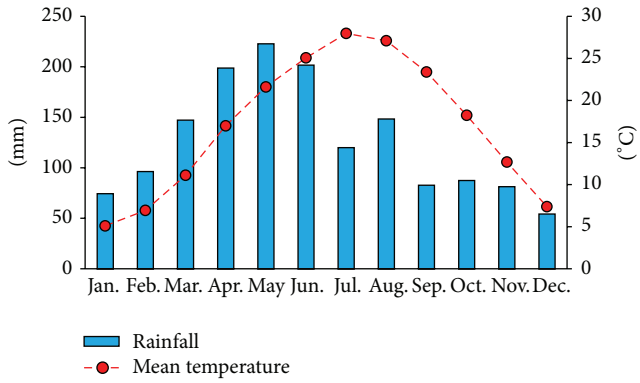

Figure 3: Intra-annual variation of monthly average temperature and monthly rainfall during 1976 and 2005.

basin varies from 2098 m to 0 m, with high mountains in the south and southwest part and flat plains in the north. The basin is characterized as a humid subtropical monsoon climate by averaging monthly temperature and monthly rainfall during 1976 and 2005 (Figure 3). The annual average temperature is about 17.1°C and annual average evaporation is around 1200 mm. The annual rainfall ranges from 1170 mm to 2160 mm and it is unevenly distributed, making it prone to frequent flood and drought.

There are six meteorological stations in this basin (see black dots in Figure 1). They provide the meteorological information used in this study. The monthly precipitation and mean temperature data covering the period between 1960 and 2014 were provided by the China Meteorological Administration. The daily discharge data were obtained in Xiangtan station (green dot in Figure 1) which is the key hydrological station in the downstream of Xiangjiang River, covering the period between 1976 and 2005. The hydrological data were provided by the Changjiang Water Resources Commission (CWRC) of China. Quality test of meteorological data and discharge data has been conducted before calculation of SPEI and SRI.

Table 1: Pearson correlation between the average data series and the series of each meteorological station.

Station	Precipitation	Temperature
Shuangfeng	0.8731	0.9986
Nanyue	0.8852	0.9977
Yongzhou	0.8962	0.9996
Hengyang	0.8895	0.9991
Daoxian	0.8783	0.9989
Chenzhou	0.8583	0.9988

To avoid inhomogeneity in the meteorological data, we tested its homogeneity by correlating data series of each meteorological station with the regional average. Table 1 shows the coefficients of Pearson correlation among the monthly precipitation and mean temperature series in each station and the regional average series. Correlation coefficients are very high and significant ($P < 0.01$) in all meteorological stations ($R \geq 0.87$).

2.2. Methods

2.2.1. Evaluation of Meteorological Drought. Meteorological drought events were evaluated based on the newly developed Standardized Precipitation Evapotranspiration Index (SPEI) [25]. The robustness of multiscale characteristics of time for SPEI is similar to the SPI [26]. And it also combines temperature into the model, which is used for calculating potential evapotranspiration (PET). We followed the Thornthwaite approach to calculate PET [27], which proved to be reliable in SPEI calculation [28].

Computation of the SPEI requires long-term monthly meteorological data, which were arranged to appropriate time scales based on different goals, for example, 3 months, 6 months, 9 months, and 12 months. The different timescales (i-month) mean the different time lengths for accumulating precipitation data and averaging temperature data by backtracking. In this study, i-month timescale of SPEI was written in SPEIi by short. More detailed calculation procedures could be found in related references [25]. Input monthly precipitation and mean temperature for calculating SPEI were obtained by averaging the data from six meteorological stations, covering the period between 1960 and 2014. In this study, 1- to 12-month timescales of SPEI during 1976 and 2005 were extracted to coincide with the time span of SRI.

The classification of meteorological drought based on SPEI value was given in Table 2 [25]. Four major drought intensities were classified by the different values of SPEI.

2.2.2. Evaluation of Streamflow Drought. The SRI [29] was utilized to identify streamflow drought in this study. It was

Table 2: Classification of drought intensity.

SPEI/SRI value	Drought intensity
(−1.00, −0.00]	Mild drought
(−1.50, −1.00]	Moderate drought
(−2.00, −1.50]	Severe drought
(−∞, −2.00]	Extreme drought

calculated in a manner similar to normal standardization procedure, which was given as

$$\mathrm{SRI}_{ij} = \frac{\left(R_{ij} - \overline{R_j}\right)}{\sigma_j}, \quad (1)$$

where i and j were the year and month of the year, respectively ($i = 1976, 1977, \ldots, 2005$; $j = 1, 2, 3, \ldots, 12$); $\overline{R_j}$ and σ_j were the mean and the standard deviation of R_{ij}, respectively. R_{ij} was the natural logarithm of the monthly mean discharge for the given ith year and the jth month. The timescale of SRI was one month.

The classification of streamflow drought based on SRI value was given in Table 2. Four major drought intensities were classified by the different values of SRI.

2.2.3. The Response Rate of Streamflow Drought to Meteorological Drought. In this study, we used the response rate (R_r) to indicate the percentage of streamflow drought when meteorological drought occurred. It stands for how streamflow drought responds to different timescales of meteorological drought. The higher R_r means this response is more sensitive and vice versa. The specific algorithm for R_r was given below:

$$R_r = \frac{n}{m} \times 100\%, \quad (2)$$

where m was the occurrence times of meteorological drought (SPEI < 0) during 1976 and 2005 and n was the occurrence times of streamflow drought (SRI < 0) under the condition that SPEI was less than 0.

3. Results

3.1. Temporal Variability of SRI and SPEI. Monthly SRI and different timescales of SPEI in this basin were depicted in Figure 4, covering the period between 1976 and 2005. Four main streamflow drought periods were recognized from SRI series, which were AUG/1977-SEP/1981 (streamflow drought period 1 (SDP1)), JUL/1983-APR/1993 (SDP2), AUG/1998-JUN/1999 (SDP3), and JUN/2003-JUN/2004 (SDP4). SDP1 and SDP2 were also characterized by intermittent short wet periods. The other two periods were much shorter, covered by continuous streamflow drought. The most severe streamflow drought occurred in SDP3, which was characterized by extremely low SRI value of consecutive three months (SRI of FMA/1999 < −2).

From views of SPEI at different timescales (Figure 4), evolution of meteorological drought at different timescales can be identified. Higher drought frequency was found at

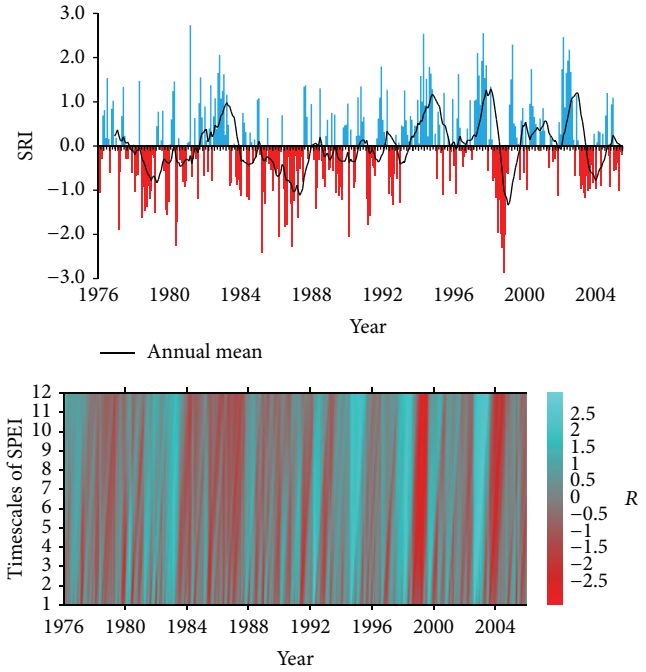

Figure 4: Time series of SRI and different timescales of SPEI during 1976 and 2005.

shorter timescales of SPEI. Drought occurrence time of longer timescales lagged that of shorter timescales, which was indicated by that the red vertical stripes (drought events) inclined towards right. In addition, dominant drought spells along with their magnitude and duration can also be clearly seen from Figure 4. The most severe meteorological drought occurred in 1998-1999. Furthermore, a good correspondence between streamflow drought and meteorological drought can be found from the comparative analysis of SRI and SPEI at different timescales. Two severe or extreme meteorological drought periods mentioned above (1998-1999, 2003-2004) characterized by SPEI at all timescales correspond with SDP3 and SDP4 very well. This result indicated that consecutive severe meteorological drought could lead to severe or consecutive streamflow drought in this basin.

3.2. Relationship between SRI and Different Timescales of SPEI. The Pearson correlation coefficients between SRI and SPEI at different timescales were shown in Figure 5. Correlation coefficients were high and significant at all timescales ($R > 0.55$, $P < 0.01$). There were significant differences with regard to timescales. The maximum correlation coefficient was obtained at 2-month timescale ($R = 0.79$). The correlation decreased gradually along with the increasing timescales. It also indicated that the runoff of Xiangjiang River was mainly charged by rainfall of the current and previous months.

A further analysis of the relationship between SRI and SPEI of different timescales at different months has been conducted. Significant seasonal difference regarding different timescales was found in Figure 6. Higher correlation coefficients were found from October to March at all timescales (mean $R > 0.75$, $P < 0.01$). The lowest correlation coefficient

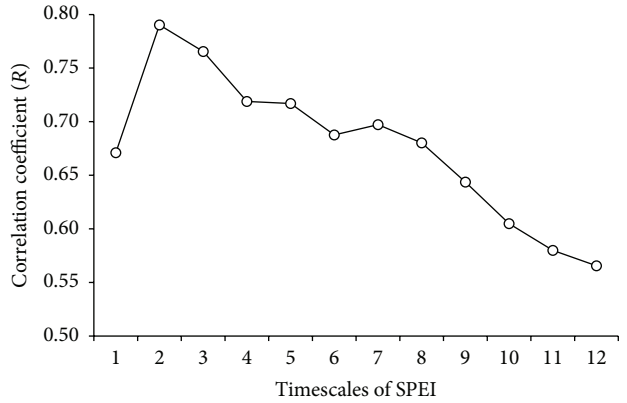

Figure 5: Correlation between SRI and the SPEI at different time scales.

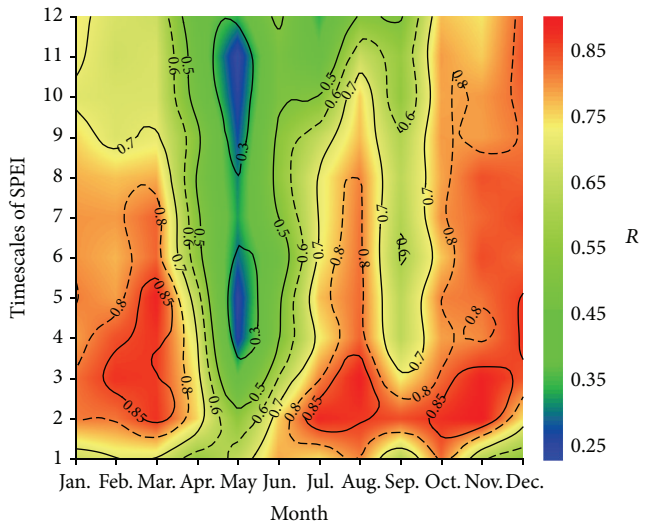

Figure 6: Monthly correlation coefficients between SRI and SPEI at different time scales.

was found in May, with most R at different timescales less than 0.5. Regarding timescales, the correlation at 1-month scale was low. It appeared much higher at 2-month scale and decreased gradually when timescale increased. The highest correlation was found at three parts in Figure 6 (the red region with R greater than 0.85). The top three high correlation coefficients were obtained in November at 2-month scale ($R = 0.89$), August at 3-month scale ($R = 0.88$), and March at 5-month scale ($R = 0.88$). Figure 7 showed the SRI series and SPEI series at 2-month timescale in November. It can be clearly found that the fluctuation of SRI accorded with that of SPEI2 very well. Near all the peak and valley of SRI series corresponded to that of SPEI2.

3.3. Response of Streamflow Drought to Meteorological Drought. The response rate (R_r) of streamflow drought to meteorological drought at different timescales was shown in Figure 8. Strong response relationship was found between them. The R_r was considerably high at all timescales, with the average 75.4%. At short to medium timescales (1 to 8

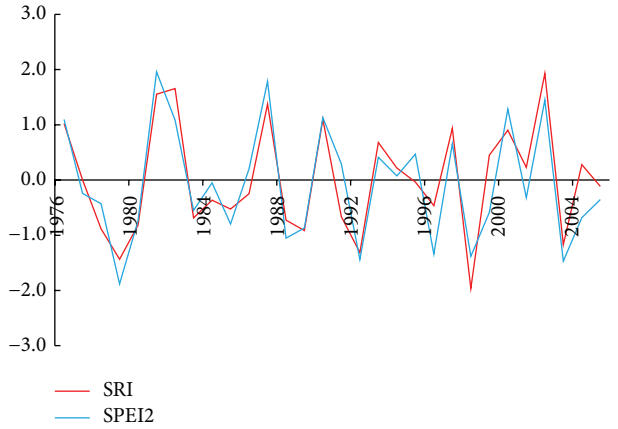

Figure 7: SRI and SPEI2 in November during 1976 and 2005.

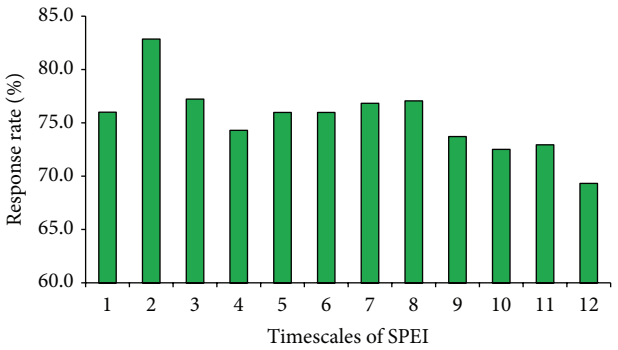

Figure 8: Response rate of streamflow drought to meteorological drought at different timescales.

months), the R_r remained at about 75% except that the peak value appeared at 2-month timescale ($R_r = 82.9\%$). After 8-month scale, R_r declined gradually along with the increase of timescale and reached the minimum at 12-month scale ($R_r = 69.3\%$). Results indicated that streamflow drought in Xiangjiang River basin responded to meteorological drought at 2-month timescale very well. When meteorological drought occurred (SPEI2 < 0), the probability of streamflow drought would reach up to 82.9%.

Figure 9 reflected the seasonal difference of response between streamflow drought and meteorological drought. Robust response relation was also found at monthly scale. A majority of response rate was larger than 70%. Moreover, remarkable monthly difference of R_r was shown clearly. The sensitivity of streamflow drought to meteorological drought differed in seasons and timescales. Shorter (1–4 months) timescales of SPEI could indicate streamflow drought (SRI < 0) better during January and July, whereas medium timescales (5–9 months) of SPEI perform better for indicating streamflow drought from August to December. Higher response rate was found during autumn and winter months (dry seasons). The possible reason is that streamflow responds to rainfall sensitively in dry seasons, while, in wet seasons, this relationship could be affected by other factors such as much more frequent heavy rainfall, stronger evapotranspiration

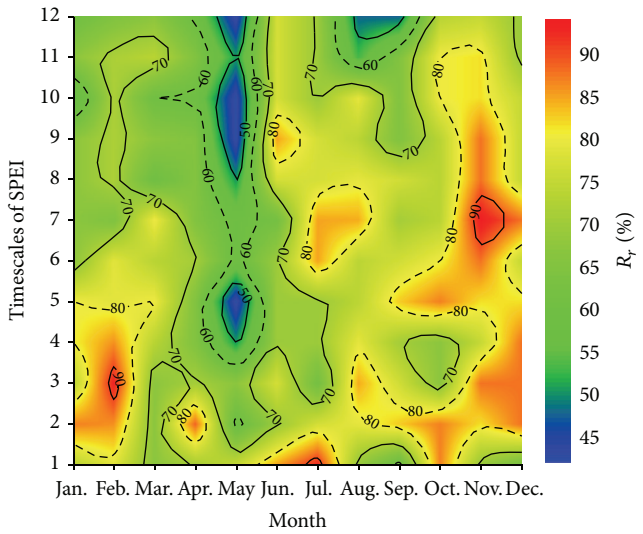

FIGURE 9: Monthly response rate of streamflow drought to meteorological drought at different timescales.

associated with high temperature, and higher water demand such as agricultural irrigation and higher domestic water demands of urban and rural inhabitants. The top three high response rates were obtained in November at 7-month scale (R_r = 93.8%), February at 3-month scale (R_r = 92.9%), and July at 1-month scale (R_r = 92.3%). The lowest R_r appeared in May, with the minimum equal to 41.7%.

4. Discussion and Conclusion

In order to understand how streamflow drought responded to meteorological drought in the Xiangjiang River basin, monthly SRI and SPEI of different timescales during 1976 and 2005 were calculated to identify streamflow drought and meteorological drought, respectively. Correlation and response relationship have been investigated. Robust relation between streamflow drought and meteorological drought was found in this basin. The main conclusions were summarized as below:

(1) Relationship between streamflow drought and meteorological drought can be investigated well by the comparative analysis of SRI and SPEI at different timescales. Continuous severe meteorological drought would propagate to severe or consecutive streamflow drought in this basin, whereas intermittent or moderate meteorological drought may lead to separate streamflow drought.

(2) Robust correlation between SRI and SPEI was found. SPEI of 2-month timescale behaved best in correlating with SRI (R = 0.79, P < 0.01). The longer the timescale of SPEI was, the weaker the correlation was. At seasonal scale, significant difference of correlation was found. Higher correlation coefficients were obtained during dry season (October to March), with the maximum R reaching up to 0.89, whereas the minimum was found in wet season (April to June). These findings agreed with the results carried out in the Aragon River basin of the central Spanish Pyrenees [18].

(3) Remarkable results were also found regarding to the response rate of streamflow drought to meteorological drought. The average response rate was considerably high (75.4%). Maximum R_r was obtained at 2-month timescale (R_r = 82.9%). It stated again that SPEI2 could be used as a good indicator in streamflow drought identification. Besides, R_r differed greatly in different seasons. Shorter timescales of meteorological drought could indicate streamflow drought better during winter and spring, whereas streamflow drought in late summer to autumn responded to meteorological drought at medium timescales.

In this study, important relationship between streamflow drought and meteorological drought has been pointed out. This relation would provide scientific support in drought mitigation and regional water resources management. It is also necessary to test the most suitable timescale of meteorological drought index before drought monitoring of different hydrologic variables. Generally, shorter timescales of meteorological drought indices proved to be better when relating to streamflow. Vicente-Serrano and López-Moreno have indicated that 1–4 months of SPI could relate to the surface flows quite well in a mountainous Mediterranean Basin [18]. A case study conducted in two reservoirs in central Spain has shown that very high correlations (>0.9) were found between hydrological and climatic droughts for timescales between 3 and 5 months, by relating SPI, SPEI to the z-standardized inflows [30]. In a plain basin surrounded by high mountains in Greece, higher correlations have also been obtained with the 3-month SPI and 6-month SPI when relating to a standardized runoff index [31]. In another case study conducted in a semiarid basin of China, similar results had indicated that SPI of 4-month timescale correlated with SRI better [21].

In addition, seasonality must also be investigated carefully. Different timescales of meteorological drought indices may behave totally different in various seasons. Streamflow response to climatic droughts may be very different as a function of the river regimes [32]. So, the selection of the most suitable timescale regarding different months before utilizing SPEI to indicates that streamflow drought is of great importance. In this study, SPEI2 was proved to be the most suitable index when relating to SRI generally, whereas SPEI1 and SPEI7 behaved best in July and November, respectively. In central Spain, very high correlations were found between hydrological and climatic droughts from January to March for timescales between 3 and 5 months. In contrast, correlations during summer months were very low at the shortest timescales [30]. However, in some high-latitude Asian basins that drain to the Arctic Ocean, correlations between SPEI and SSI were much higher in July than in January [32].

The noticeable timescale issue and seasonality may depend on the basin characteristics, elevation, terrain, climate zone, vegetation cover, and water resources regulation. How do these factors affect the sensitivity of streamflow

drought to meteorological drought? Maybe it can be explained by comparison among similar basins in the future research. Besides, interannual variability of the propagation procedure under global warming could be obtained if there is long-term hydrologic and climatic data. Furthermore, how meteorological drought propagate through the hydrologic system quantitatively and the time lag between meteorological drought and other types of drought are also interesting issues that should be addressed in a future study.

Conflict of Interests

The authors declare that there is no conflict of interests regarding the publication of this paper.

Acknowledgments

This work is supported by National Natural Science Foundation of China (Grant no. 41301586) and China Postdoctoral Science Foundation (Grants nos. 2013M540599 and 2014T70731).

References

[1] D. A. Wilhite, "Drought as a natural hazard: concepts and definitions," in *Drought: A Global Assessment*, D. A. Wilhite and O. Vanyarkho, Eds., Routledge, New York, NY, USA, 2000.

[2] FEMA, *National Mitigation Strategy: Partnerships for Building Safer Communities*, Federal Emergency Management Agency, Washington, DC, USA, 1995.

[3] S. M. Vicente-Serrano, C. Gouveia, J. J. Camarero et al., "Response of vegetation to drought time-scales across global land biomes," *Proceedings of the National Academy of Sciences of the United States of America*, vol. 110, no. 1, pp. 52–57, 2013.

[4] Z. T. Wu, J. J. Wu, B. He et al., "Drought offset ecological restoration program-induced increase in vegetation activity in the Beijing-Tianjin Sand Source Region, China," *Environmental Science and Technology*, vol. 48, no. 20, pp. 12108–12117, 2014.

[5] R. B. Austin, C. Cantero-Martínez, J. L. Arrúe, E. Playán, and P. Cano-Marcellán, "Yield-rainfall relationships in cereal cropping systems in the Ebro river valley of Spain," *European Journal of Agronomy*, vol. 8, no. 3-4, pp. 239–248, 1998.

[6] Q. F. Wang, J. J. Wu, T. J. Lei et al., "Temporal-spatial characteristics of severe drought events and their impact on agriculture on a global scale," *Quaternary International*, vol. 349, pp. 10–21, 2014.

[7] A. T. De Gaetano, "A temporal comparison of drought impacts and responses in the New York City metropolitan area," *Climatic Change*, vol. 42, no. 3, pp. 539–560, 1999.

[8] S. E. Nicholson, C. J. Tucker, and M. B. Ba, "Desertification, drought, and surface vegetation: an example from the west African Sahel," *Bulletin of the American Meteorological Society*, vol. 79, no. 5, pp. 815–829, 1998.

[9] J. G. Pausas, "Changes in fire and climate in the eastern Iberian Peninsula (Mediterranean basin)," *Climatic Change*, vol. 63, no. 3, pp. 337–350, 2004.

[10] A. Dai, "Drought under global warming: a review," *Wiley Interdisciplinary Reviews: Climate Change*, vol. 2, no. 1, pp. 45–65, 2011.

[11] A. G. Dai, "Increasing drought under global warming in observations and models," *Nature Climate Change*, vol. 3, no. 1, pp. 52–58, 2013.

[12] D. A. Wilhite and M. H. Glantz, "Understanding the drought phenomenon: the role of definitions," *Water International*, vol. 10, no. 3, pp. 111–120, 1985.

[13] K. C. Mo, "Model-based drought indices over the United States," *Journal of Hydrometeorology*, vol. 9, no. 6, pp. 1212–1230, 2008.

[14] V. Mishra and K. A. Cherkauer, "Retrospective droughts in the crop growing season: implications to corn and soybean yield in the Midwestern United States," *Agricultural and Forest Meteorology*, vol. 150, no. 7-8, pp. 1030–1045, 2010.

[15] V. Mishra, K. A. Cherkauer, and S. Shukla, "Assessment of drought due to historic climate variability and projected future climate change in the midwestern United States," *Journal of Hydrometeorology*, vol. 11, no. 1, pp. 46–68, 2010.

[16] H. Hisdal and L. M. Tallaksen, "Estimation of regional meteorological and hydrological drought characteristics: a case study for Denmark," *Journal of Hydrology*, vol. 281, no. 3, pp. 230–247, 2003.

[17] E. Peters, H. A. J. Van Lanen, P. J. J. F. Torfs, and G. Bier, "Drought in groundwater: drought distribution and performance indicators," *Journal of Hydrology*, vol. 306, no. 1–4, pp. 302–317, 2005.

[18] S. M. Vicente-Serrano and J. I. López-Moreno, "Hydrological response to different time scales of climatological drought: an evaluation of the Standardized Precipitation Index in a mountainous Mediterranean basin," *Hydrology and Earth System Sciences*, vol. 9, no. 5, pp. 523–533, 2005.

[19] A. A. Tabrizi, D. Khalili, A. A. Kamgar-Haghighi, and S. Zand-Parsa, "Utilization of time-based meteorological droughts to investigate occurrence of streamflow droughts," *Water Resources Management*, vol. 24, no. 15, pp. 4287–4306, 2010.

[20] J. Q. Zhai, B. D. Su, V. Krysanova, T. Vetter, C. Gao, and T. Jiang, "Spatial variation and trends in PDSI and SPI indices and their relation to streamflow in 10 large regions of china," *Journal of Climate*, vol. 23, no. 3, pp. 649–663, 2010.

[21] L. Zhao, A. F. Lyu, J. J. Wu et al., "Impact of meteorological drought on streamflow drought in Jinghe River Basin of China," *Chinese Geographical Science*, vol. 24, no. 6, pp. 694–705, 2014.

[22] D. C. Edossa, M. S. Babel, and A. D. Gupta, "Drought analysis in the Awash river basin, Ethiopia," *Water Resources Management*, vol. 24, no. 7, pp. 1441–1460, 2010.

[23] L. Liu, Y. Hong, and C. N. Bednarczyk, "Hydro-climatological drought analyses and projection using meteorological and hydrological drought indices: a case study in Blue River Basin, Oklahoma," in *Proceedings of the 36th NOAA Annual Climate Diagnostics and Prediction Workshop*, Fort Worth, Tex, USA, October 2011.

[24] M. A. A. Zarch, B. Sivakumar, and A. Sharma, "Droughts in a warming climate: a global assessment of Standardized precipitation index (SPI) and Reconnaissance drought index (RDI)," *Journal of Hydrology*, vol. 526, pp. 183–195, 2015.

[25] S. M. Vicente-Serrano, S. Beguería, and J. I. López-Moreno, "A multiscalar drought index sensitive to global warming: the standardized precipitation evapotranspiration index," *Journal of Climate*, vol. 23, no. 7, pp. 1696–1718, 2010.

[26] T. B. McKee, N. J. Doesken, and J. Kleist, "The relationship of drought frequency and duration to time scales," in *Proceedings of the 8th Conference on Applied Climatology*, pp. 179–184, Anaheim, Calif, USA, January 1993.

[27] C. W. Thornthwaite, "An approach toward a rational classification of climate," *Geographical Review*, vol. 38, no. 1, pp. 55–94, 1948.

[28] M. X. Yu, Q. Li, M. J. Hayes, M. D. Svoboda, and R. R. Heim, "Are droughts becoming more frequent or severe in China based on the standardized precipitation evapotranspiration index: 1951–2010?" *International Journal of Climatology*, vol. 34, no. 3, pp. 545–558, 2014.

[29] I. Nalbantis and G. Tsakiris, "Assessment of hydrological drought revisited," *Water Resources Management*, vol. 23, no. 5, pp. 881–897, 2009.

[30] J. Lorenzo-Lacruz, S. M. Vicente-Serrano, J. I. López-Moreno, S. Beguería, J. M. García-Ruiz, and J. M. Cuadrat, "The impact of droughts and water management on various hydrological systems in the headwaters of the Tagus River (central Spain)," *Journal of Hydrology*, vol. 386, no. 1–4, pp. 13–26, 2010.

[31] L. Vasiliades, A. Loukas, and N. Liberis, "A water balance derived drought index for Pinios River Basin, Greece," *Water Resources Management*, vol. 25, no. 4, pp. 1087–1101, 2011.

[32] S. M. Vicente-Serrano, S. Beguería, J. Lorenzo-Lacruz et al., "Performance of drought indices for ecological, agricultural, and hydrological applications," *Earth Interactions*, vol. 16, no. 10, pp. 1–27, 2012.

Hindawi Publishing Corporation
Advances in Meteorology
Volume 2016, Article ID 7986568, 10 pages
http://dx.doi.org/10.1155/2016/7986568

Research Article

Drought Assessment by a Short-/Long-Term Composited Drought Index in the Upper Huaihe River Basin, China

Meixiu Yu,[1,2,3] Xiaolong Liu,[3] Li Wei,[4] Qiongfang Li,[1,2] Jianyun Zhang,[3] and Guoqing Wang[3]

[1]*College of Hydrology and Water Resources, Hohai University, Nanjing 210098, China*
[2]*Center for International River Research, School of Business, Hohai University, Nanjing 210098, China*
[3]*Hydrology and Water Resources Department, Nanjing Hydraulic Research Institute, Nanjing 210024, China*
[4]*Hydrology Bureau of Jiangxi Province, Nanchang 332000, China*

Correspondence should be addressed to Meixiu Yu; meixiuyu1985@gmail.com and Qiongfang Li; li_qiongfang@hotmail.com

Received 29 May 2015; Accepted 4 October 2015

Academic Editor: Mohsin Hafeez

Accurate and reliable drought monitoring is of primary importance for drought mitigation and reduction of social-ecological vulnerability. The aim of the paper was to propose a multiscale composited drought index (CDI) which could be widely used for drought monitoring and early warning in China. In the study, the upper Huaihe River basin above the Xixian gauge station, which has been hit by severe droughts frequently in recent decades, was selected as the case study site. The newly built short-term/long-term CDI comprehensively considered three natural forms of drought (meteorological, hydrological, and agricultural) by selection of different variables that are related to each drought type. The short-term/long-term CDI was developed using the Principle Component Analysis of related drought components. The thresholds of the short-term/long-term CDI were determined according to frequency statistics of different drought indices. Finally, the feasibility of the two CDI was investigated against the self-calibrating Palmer drought severity index, the standardized precipitation evapotranspiration index, and the historical drought records. The results revealed that the short-term/long-term CDI could capture the onset, severity, and persistence of drought events very well with the former being better at identifying the dynamic evolution of drought condition and the latter better at judging the changing trend of drought over a long time period.

1. Introduction

Drought is one of the most damaging natural hazards and often results in devastating effects to social and ecological systems (Hao and Aghakouchak, [1]). The annual economic damage of severe droughts across China is estimated to be 2.5–3.5 percent of the gross domestic product. The frequency of severe and extreme droughts in China increased significantly from 26.8 percent during 1950–1990 to 47.6 percent during 1991–2011 [2], and the drought percentage area increased by 3.92 percent/10a from 1990s (Yu et al., [3]). Thus, accurate and reliable drought monitoring and prediction are of critical importance for risk assessment and decision making. Different drought indices have been developed and applied for drought monitoring and assessment. The Palmer drought severity index (PDSI; Palmer [4]) and self-calibrating PDSI (scPDSI; Wells et al. [5]) are widely used for drought characterization. The standardized precipitation index (SPI; McKee et al. [6]) and the standardized precipitation evapotranspiration index (SPEI; Vicente-Serrano et al., [7]) are commonly used for meteorological drought monitoring. The standardization concept was also applied to other drought indices such as the standardized soil moisture index (SMI) and the standardized streamflow index (SSI, Vicente-Serrano et al., [8]). However, the performance of different drought index differs in detecting the drought onset, persistence, and termination. Wilhite [9] concluded that using a single index to reveal the diversity and complexity of drought conditions and impact is one of the major limitations to drought monitoring. Due to the fact that no single index

can represent all aspects of meteorological, agricultural, and hydrological droughts, a multi-index approach should be proposed for drought monitoring, assessment, and prediction (Hao and Aghakouchak, [1]). Located in a transition zone between the climates of North and South China, the Huaihe River basin was determined to be the region being easily hit by floods and droughts frequently. Xie et al. [10] investigated the feasibility of six drought indices (Rainfall Anomaly Index (RAI), Z index, SPI index, Relative Moisture Index, Composited Meteorological Index (CMI), and modified CMI) in the Huaihe River basin during 1961–2010 and concluded that the CMI and the modified CMI were better at identifying drought events. Zhang et al. [11] assessed the drought condition of the upper Huaihe River basin by the PDSI and the RAI, and the result revealed that the RAI was much more sensitive than the PDSI in drought monitoring. Zhang et al. [12] analyzed the evolution of hydrological drought features under the regulation of two cascade reservoirs in the Huaihe River of China and indicated that although the downstream reservoir leads to an overall increase in the drought severity, it mitigates the severe and extreme droughts; the reservoir storage functions to smooth streamflow variation in that it reduces the drought frequency and extends the duration. Admittedly, the drought assessment and monitoring in the Huaihe River basin have been a focus of many meteorologists and hydrologists (Zhang et al., [13]; Cai et al., [14]; Wang et al., [15]; Duan et al., [16]; Yan et al., [17]). However, previous research on drought in the study area is mostly based on one single drought index or only considered one type of drought. The aim of this paper is to introduce and evaluate a short-term/long-term composited drought index (S_CDI/L_CDI) which comprehensively considered three natural forms of drought (meteorological, hydrological, and agricultural) by selection of different variables that are related to each drought type in the upper Huaihe River basin. The output of the study could provide valuable references for the drought monitoring and early warning system development in the Huaihe River basin and other regions/basins in China.

2. Short-/Long-Term CDI Development

2.1. Selection of CDI Components. Based on the differences in time scales and drought types of drought index, the scPDSI, the 1- and 3-month SPEI, ZIND, and the SMI were selected to develop the short-term CDI by using the Principle Component Analysis (PCA), while the Palmer Hydrology Drought Index (PHDI), the 6-, 12-, 18-, and 24-month SPEI, the SSI, and the SMI were chosen to formulate the long-term CDI. The dynamic evolution of drought condition can be obtained by the short-term CDI while the changing trend of drought over a long time period could be known by the long-term CDI.

2.2. Principle Component Analysis. The PCA method is a technique applied to multivariate analysis for dimensionality reduction [18]. The original intercorrelated variables could be reduced to a small number of new linearly uncorrelated ones that explain most of the total variance.

Considering k variables in a given time period i, $X_{i,1}, X_{i,2}, \ldots, X_{i,k}$, k principle components (PCs) are produced for the same time period, $Y_{i,1}, Y_{i,2}, \ldots, Y_{i,k}$, using linear combinations of the first ones, according to

$$\begin{aligned} Y_{i,1} &= e_{11}X_{i,1} + e_{12}X_{i,2} + \cdots + e_{1k}X_{i,k} \\ Y_{i,2} &= e_{21}X_{i,1} + e_{22}X_{i,2} + \cdots + e_{2k}X_{i,k} \\ &\vdots \\ Y_{i,k} &= e_{k1}X_{i,1} + e_{k2}X_{i,2} + \cdots + e_{kk}X_{i,k}. \end{aligned} \tag{1}$$

In the applications the variables $X_{i,k}$ refer to scPDSI, SPEI1, SPEI3, ZIND, SMI, and series for short-term CDI, and refer to PHDI, SPEI6, SPEI12, SPEI18, SPEI24, SSI, and SMI series for long-term CDI. k is equal to the number of drought indices (5 for short-term CDI and 7 for long-term CDI) and i represents the length of drought indices series.

In (1) $Y_{i,1}$ explains most of the variance, $Y_{i,2}$ explains the reminiscent amount of variance, and so on. PCs extraction could be based on variance/covariance or correlation matrix of data with $\{e_{11}, e_{21}, \ldots, e_{1k}\}$ being the first eigenvector and $\{e_{11}, e_{21}, \ldots, e_{1k}\}$ being the eigenvector of k order and each eigenvector includes the coefficients of the k principal component. Finally, the amount of variance explained by the first PC is called the first eigenvalue λ_1, and the second is λ_2, so that $\lambda_1 \geq \lambda_2 \geq \cdots \geq \lambda_k$. Since each eigenvalue represents the fraction of the total variance in the original data and is explained by each component, proportion of each component can be calculated as $\lambda_j / \sum \lambda_j$. Thus, the short-term/long-term CDI can be expressed as follows:

$$\begin{aligned} \mathrm{CDI}_i = {} & \frac{\lambda_1}{\lambda_1 + \lambda_2 + \cdots + \lambda_k} Y_{i,1} + \cdots \\ & + \frac{\lambda_j}{\lambda_1 + \lambda_2 + \cdots + \lambda_k} Y_{i,j} + \cdots \\ & + \frac{\lambda_n}{\lambda_1 + \lambda_2 + \cdots + \lambda_k} Y_{i,k}, \end{aligned} \tag{2}$$

where λ_j is eigenvalue of the jth principal component, $Y_{i,j}$ is the jth principal component of the ith month, CDI_i is the short-term/long-term CDI in the ith month.

2.3. Short-/Long-Term CDI Formulation. According to (1) and (2), the short-term CDI can be formulated as follows:

$$\begin{aligned} \mathrm{S\_CDI}_i &= \sum_{1}^{k} \frac{\lambda_j}{\lambda_1 + \lambda_2 + \cdots + \lambda_k} X_{\mathrm{S}} E_{\mathrm{S}}, \\ X_{\mathrm{S}} &= \left(x_{\mathrm{scPDSI},i}, x_{\mathrm{ZIND},i}, x_{\mathrm{SPEI1},i}, x_{\mathrm{SPEI3},i}, x_{\mathrm{SMI},i}\right); \\ E_{\mathrm{S}} &= \left(e_{\mathrm{scPDSI},i,j}, e_{\mathrm{ZIND},i,j}, e_{\mathrm{SPEI1},i,j}, e_{\mathrm{SPEI3},i,j}, e_{\mathrm{SMI},i,j}\right)^T. \end{aligned} \tag{3}$$

And the long-term CDI can be formulated as follows:

$$\begin{aligned} \text{L\_CDI}_i &= \sum_{1}^{k} \frac{\lambda_j}{\lambda_1 + \lambda_2 + \cdots + \lambda_k} X_{\text{L}} E_{\text{L}}, \\ X_{\text{L}} &= \left(x_{\text{SMI},i}, x_{\text{PHDI},i}, x_{\text{SSI},i}, x_{\text{SPEI6},i}, x_{\text{SPEI12},i}, x_{\text{SPEI18},i}, x_{\text{SPEI24},i}\right); \\ E_{\text{L}} &= \left(e_{\text{SMI},i,j}, e_{\text{PHDI},i,j}, e_{\text{SSI},i,j}, e_{\text{SPEI6},i,j}, e_{\text{SPEI12},i,j}, e_{\text{SPEI18},i,j}, e_{\text{SPEI24},i,j}\right)^T, \end{aligned} \tag{4}$$

where λ_j are eigenvalues of the jth principal component, $e_{i,j}$ are eigenvectors of the jth principal component of the ith month, X_i is the drought index series in the ith month, S_CDI_i and L_CDI_i are the short-term CDI and the long-term CDI in the ith month.

It should be noted that the monthly scPDSI, ZIND, PHDI, and SPEI (in time scales of 1-month, 3-month, 6-month, 12-month, 18-month, and 24-month, resp.) could be obtained based on the daily air temperature and precipitation from meteorological stations in/around the study basin, while the monthly SMI and the SSI need to be calculated by soil water volume and generated runoff based on the hydrological modelling. The gridded Xinanjiang model (XAJ; Zhao, [19]), a model of runoff formation on saturation of storage, used widely in humid and semi-humid regions in China, was adopted to simulate the gridded soil water and generated runoff in the upper Huaihe River basin.

2.4. XAJ Model. The XAJ model is a rainfall-runoff, distributed, basin model for use in humid and semi-humid regions. The evapotranspiration component is represented by a model of three soil layers. Runoff production occurs on repletion of storage to capacity values which are assumed to be distributed throughout the basin. Prior to 1980, runoff was separated into surface and groundwater components using Horton's concept of infiltration. Subsequently, the concept of hillslope hydrology was introduced with an additional component, interflow, being identified. Runoff concentration to the outflow of each subbasin is represented by a unit hydrograph or by a lag and route technique. The damping or routing effects of the channel system connecting the subbasins are represented by Muskingum routing. There are fifteen parameters in all, of which the model is particularly sensitive to six. Optimization of the parameters is achieved with different objective functions according to the nature of each parameter. The model has been widely used in China since 1980, mainly for flood forecasting, though more recently it is also being used for other purposes.

2.5. Determination of the Drought Intensity Threshold Levels of the CDI Categories. The drought intensity threshold levels of the short-term CDI were conducted as in the following steps: firstly, calculate the drought event frequency $F_{i,j}$ (i for the drought intensity level, j for different drought index) of all the short-term drought components with different drought intensity level in the upper Huaihe River basin above the Xixian station; secondly, average $F_{i,j}$ for the same drought intensity level, and then a series of new drought frequencies f_i (i for the drought intensity level) of different drought intensity levels for the short-term CDI was obtained; thirdly, determine the drought intensity threshold levels of the short-term CDI according to f_i. The drought intensity threshold levels of the long-term CDI can also be acquired by following the above steps.

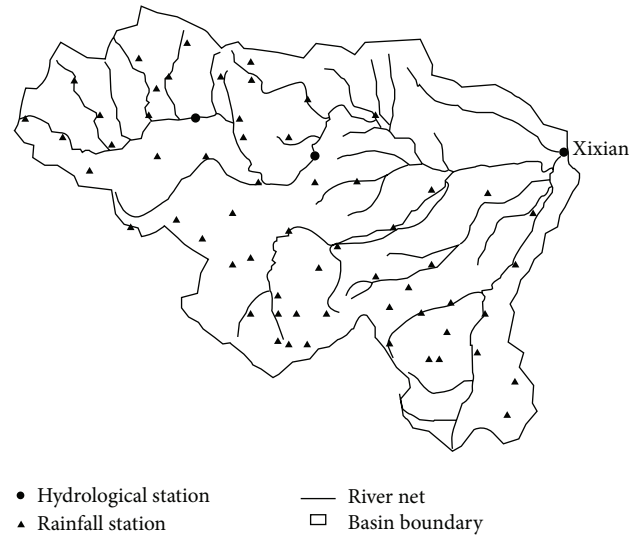

Figure 1: Sketch map of the upper Huaihe River basin.

3. Application of the Short-/Long-Term CDI

3.1. Case Study Site. The Huaihe River basin is one of seven major river basins in China and lies in the warm temperature semi-humid monsoon region, which is a transition zone between the climates of North and South China. Special geographical location determined that the Huaihe River basin was a region easily hit by floods and droughts over many centuries, particularly in recent decades, and severe droughts occurred much more frequently which caused huge economic and social loss. To propose a short-/long-term CDI which could be widely used for drought monitoring and early warning in China, this paper selected the upper Huaihe River basin above Xixian gauge station as the case study site with a catchment area of 10 190 km^2 (see Figure 1).

3.2. Data Preparation and Processing. Considering the spatial unevenness of underlying conditions and meteorological variables, the study areas were divided into grids with a size of 1 km × 1 km. Based on the daily observed meteorological variables (precipitation and air temperature) from closer six meteorological stations during 1988–2005, the inverse distance-squared weighted method was used to acquire the meteorological data for every grid. Before the interpolation,

Table 1: Calibrated parameters for the daily Xinanjiang model in upper Huaihe River above the Xixian station.

Parameters	Meaning	Values
KC	Ratio of potential evapotranspiration to pan evaporation	0.89
UM	Areal mean tension water capacity in the upper layer (mm)	28
LM	Areal mean tension water capacity in the lower layer (mm)	85
c	Coefficient of deep evapotranspiration	0.167
WM	Areal mean tension water capacity (mm)	150
b	Exponent of the tension water capacity curve	0.45
IM	Ratio of the impervious to the total area of the basin	0.001
SM	Areal mean of the free water capacity of the surface soil layer (mm)	15
EX	Exponent of the free water capacity curve	1.5
KG	Outflow coefficient of the free water storage to groundwater relationship	0.55
CS	Recession constant of surface water storage	0.62
CI	Recession constant of interflow water storage	0.85
CG	Recession constant of groundwater storage	0.998
L	Lag time (d)	2
KE	Parameter of the Muskingum method	24
XE	Parameter of the Muskingum method	0.3

digital elevation model was used to correct the meteorological variables according to meteorological variable-elevation relationships. Monthly gridded scPDSI, ZIND, PHDI, and SPEI (1-month, 3-month, 6-month, 12-month, 18-month, and 24-month, resp.) was calculated on the basis of the gridded meteorological variables, and then the monthly areal drought indices were obtained by averaging their gridded values.

3.3. Application of the XAJ Model. Based on the topography, hydrological, and meteorological data in 1988–2005, the daily gridded XAJ model was adopted to simulate gridded soil water and generated runoff in the upper Huaihe River basin above Xixian station. The calibration and validation periods were 1988–2002 and 2003–2005, respectively (Tables 1 and 2). The result revealed that the daily XAJ model was simulated with satisfactory accuracy, which indicated that the calculated gridded soil water and generated runoff could be used for the further CDI construction. The monthly gridded SMI and SSI were computed based on the gridded soil water and generated runoff, and then the areal monthly SMI and SSI were carried out by averaging the gridded values. It should be noted that the soil field capacity was obtained from the International Geosphere-Biosphere Programme (IGBP) which provides the gridded Profile Available Water Capacity with the spatial resolution of 10 km × 10 km. Figure 2 showed the temporal variations of the areal averaged soil moisture index in the upper Huaihe River basin.

Table 2: Calibration and validation results of the daily XAJ model in the upper Huaihe River basin.

Periods	P (mm)	R_o (mm)	R_c (mm)	RE %
Calibration				
1988	787.6	193.8	202.2	4.3
1989	1153	475.1	457.6	−2.6
1990	877.6	295.9	284.3	−3.9
1991	1197.7	609.8	584.6	−3
1992	744.2	149.8	164.5	11.1
1993	840.5	224.5	222.8	−0.8
1994	849.6	179.0	192.8	7.7
1995	881.2	214.8	232.8	9.6
1996	1141.5	521.0	508.7	−1.2
1997	782.3	226.0	221.4	−2
1998	1166.6	616.4	511.5	−17
1999	573.8	80.3	86.8	8.1
2000	1328	578.4	624.6	9.2
2001	456.6	104.6	96.5	−7.7
2002	1108.1	348.2	411.1	19.4
Validation				
2003	1145.9	611.5	512.7	−16.2
2004	933.7	279.0	327.9	17.5
2005	1253.2	601.3	608.2	1.15

Note: P is for precipitation, R_o for observed runoff, R_c for calculated runoff, and RE for relative error.

3.4. Application of the Short-/Long-Term CDI. Based on the time series of areal monthly scPDSI, ZIND, 1-month SPEI, 3-month SPEI, and SMI, according to (3), the short-term CDI in the upper Huaihe River basin above the Xixian station was carried out with the SPSS package. The eigenvalues and eigenvectors in (3) can be referred to in Table 3. And the drought intensity threshold levels of the short-term CDI were determined according to Section 2.5 (Table 4).

Based on the time series of areal monthly PHDI, 6-month SPEI, 12-month SPEI, 18-month SPEI, 24-month SPEI, SSI, and SMI, according to (4), the long-term CDI in the upper Huaihe River basin above the Xixian station was carried out

Table 3: Eigenvalues and eigenvectors of the PCA for short-term/long-term CDI in the upper Huaihe River basin.

CDI	Eigenvalues			Eigenvectors e_1, e_2, e_3							
	λ_1	λ_2	λ_3								
S_CDI	2.82	0.8	0.69	e_1	e_{1sc_PDSI} 0.23	e_{1ZIND} 0.30	e_{1SPEI1} 0.23	e_{1SPEI3} 0.28	e_{1SMI} 0.28		
				e_2	e_{2sc_PDSI} 0.75	e_{2ZIND} −0.21	e_{2SPEI1} 0.48	e_{2SPEI3} −0.62	e_{2SMI} −0.16		
				e_3	e_{3sc_PDSI} −0.65	e_{3ZIND} −0.42	e_{3SPEI1} 0.85	e_{3SPEI3} −0.08	e_{3SMI} 0.36		
L_CDI	3.77	1.24	0.6	e_1	e_{1SMI} 0.61	e_{1PHDI} 0.71	e_{1SSI} 0.75	e_{1SPEI6} 0.81	$e_{1SPEI12}$ 0.76	$e_{1SPEI18}$ 0.72	$e_{1SPEI24}$ 0.76
				e_2	e_{2SMI} 0.59	e_{2PHDI} −0.28	e_{2SSI} 0.32	e_{2SPEI6} −0.18	$e_{2SPEI12}$ −0.48	$e_{2SPEI18}$ −0.41	$e_{2SPEI24}$ 0.53
				e_3	e_{3SMI} 0.43	e_{3PHDI} 0.27	e_{3SSI} −0.51	e_{3SPEI6} −0.27	$e_{3SPEI12}$ 0.09	$e_{3SPEI18}$ 0.08	$e_{3SPEI24}$ 0.03

Notes: λ_1, λ_2, λ_3 are eigenvalues; e_1, e_2, e_3 are eigenvectors.

Table 4: Drought categories of the short-term/long-term CDI.

Drought category	Short-term CDI	Long-term CDI
Normal	(−0.37, +∞)	(−0.33, +∞)
Mild drought	(−0.69, −0.37)	(−0.78, −0.33)
Moderate drought	(−0.97, −0.69)	(−1.16, −0.78)
Severe drought	(−1.36, −0.97)	(−1.39, −1.16)
Extreme drought	(−∞, −1.36)	(−∞, −1.39)

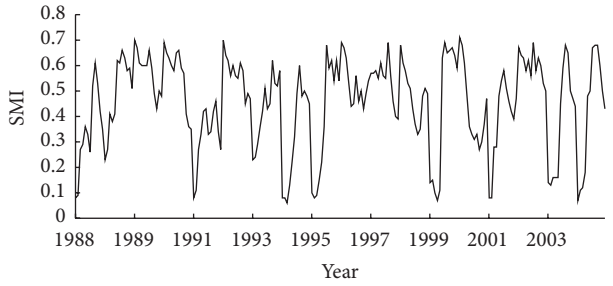

Figure 2: Temporal variations of the SMI in the upper Huaihe River basin.

with the SPSS package. The eigenvalues and eigenvectors in (4) can be referred to in Table 3. And the drought intensity threshold levels of the long-term CDI were determined according to Section 2.5 (Table 4).

4. Results and Discussion

4.1. Temporal Variations of the Short-Term/Long-Term CDI and Other Drought Indices. The chronological comparison between the S_CDI and the scPDSI and the S_CDI and the 1-month SPEI time series in the upper Huaihe River basin above Xixian station during 1988–2005 was displayed in Figure 3. It has been found that the three drought indices identified most dry conditions of the upper Huaihe River basin: the drier the conditions, the lower the drought index

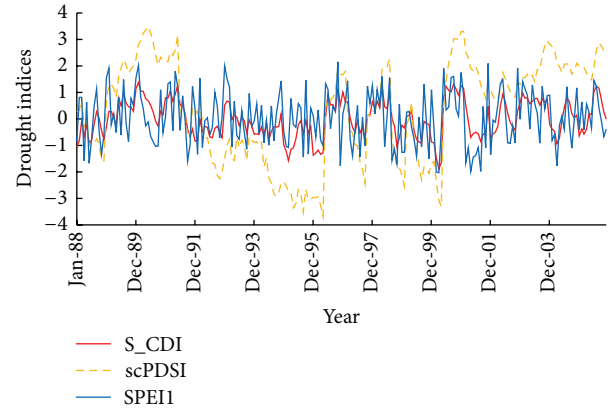

Figure 3: Temporal variations of the short-term CDI and its components.

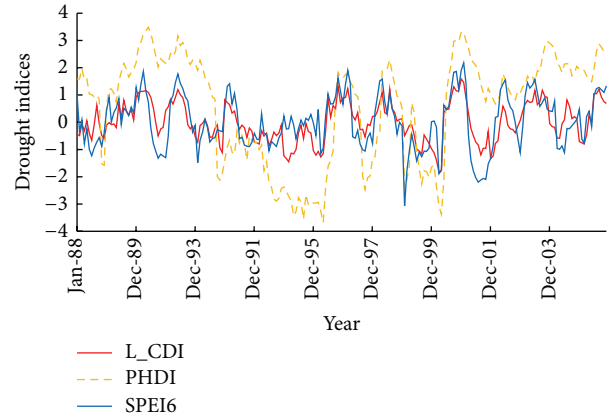

Figure 4: Temporal variations of the long-term CDI and its components.

values and the basin was in relatively dry condition in 1990s and early 2000s. Similar variation trends were also found in the L_CDI and the PHDI and the L_CDI and the 6-month SPEI time series (Figure 4).

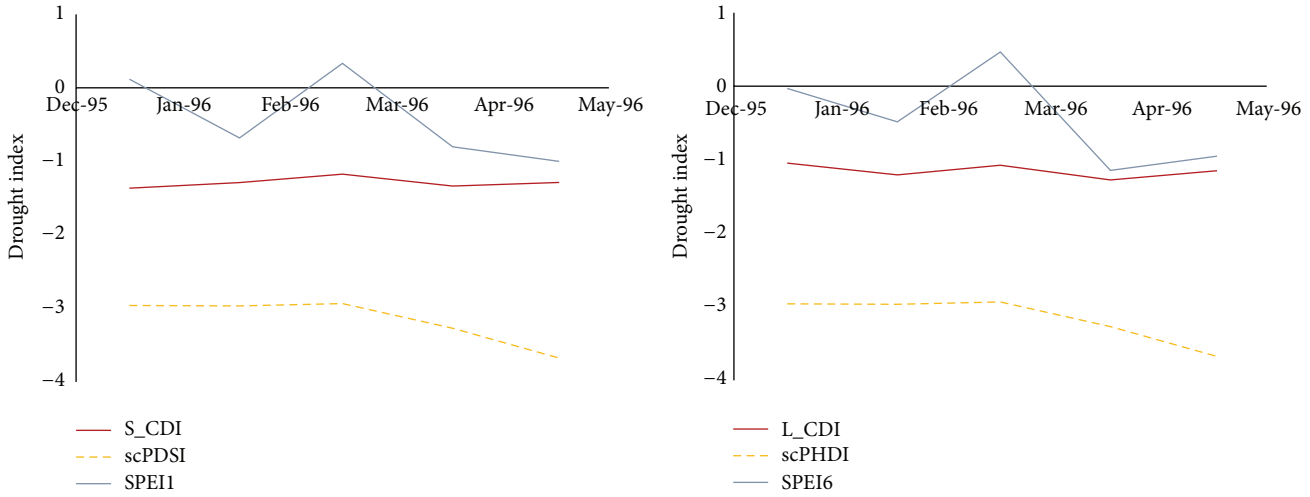

(a) S_CDI (b) L_CDI

Figure 5: The 1996 drought.

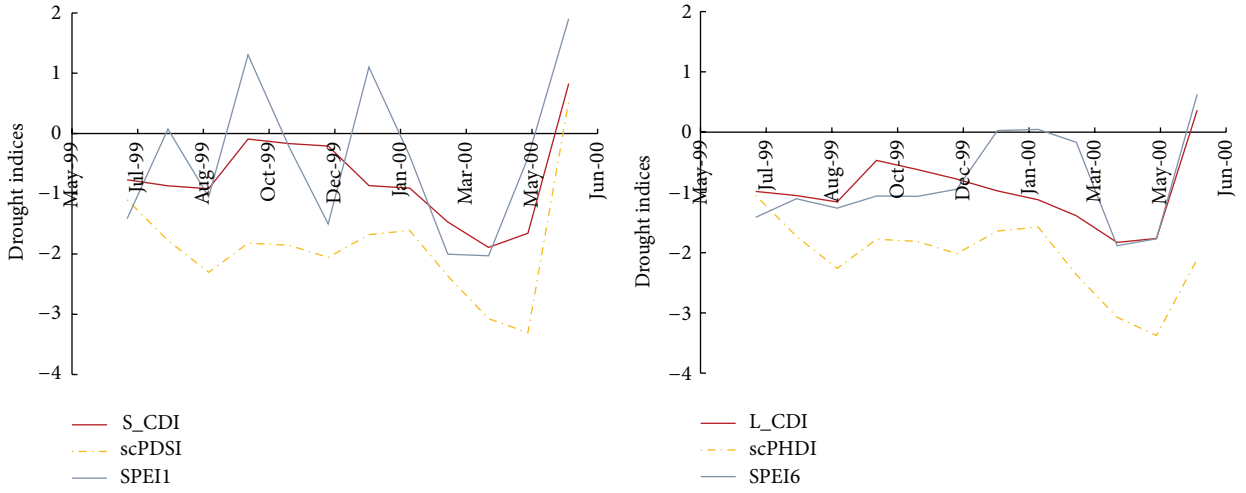

(a) S_CDI (b) L_CDI

Figure 6: The 2000 drought.

Correlations between the CDI and scPDSI/SPEI time series were also investigated by the Spearman correlation coefficient, which is the application of the Pearson correlation coefficient performed upon data ranks instead of the data themselves (e.g., Wilks., [20]), with the range of the Spearman coefficient being constrained within ±1. Rank correlation is a robust measure that is insensitive to the underlying data distribution and is recognized as a competent tool for determining the best aggregate correlation (Wilks, [20]).

Rank correlation between the S_CDI and scPDSI/1-month SPEI was found to behave similarly to that between the L_CDI and PHDI/6-month SPEI, that is, Spearman correlation coefficients being of 0.83, 0.72, respectively, between the S_CDI and the scPDSI, and the S_CDI and the 1-month SPEI time series, and Spearman correlation coefficients being of 0.75, 0.82, respectively, between the L_CDI and the PHDI, and the L_CDI and the 6-month SPEI time series.

The variation trends of all the drought indices are consistent with each other; however, the drought severity, onset, and termination identified by different drought indices varied differently.

4.2. Drought Assessment of Critical Drought Events. Two critical drought events—the long-term 2000 drought and the short-term 1996 drought—were used to assess the fidelity of the S_CDI, the L_CDI, and their drought components.

4.2.1. Historical Records of Critical Droughts. The 2000 drought, which actually began from September of 1999 and developed to the severe spring and early summer drought

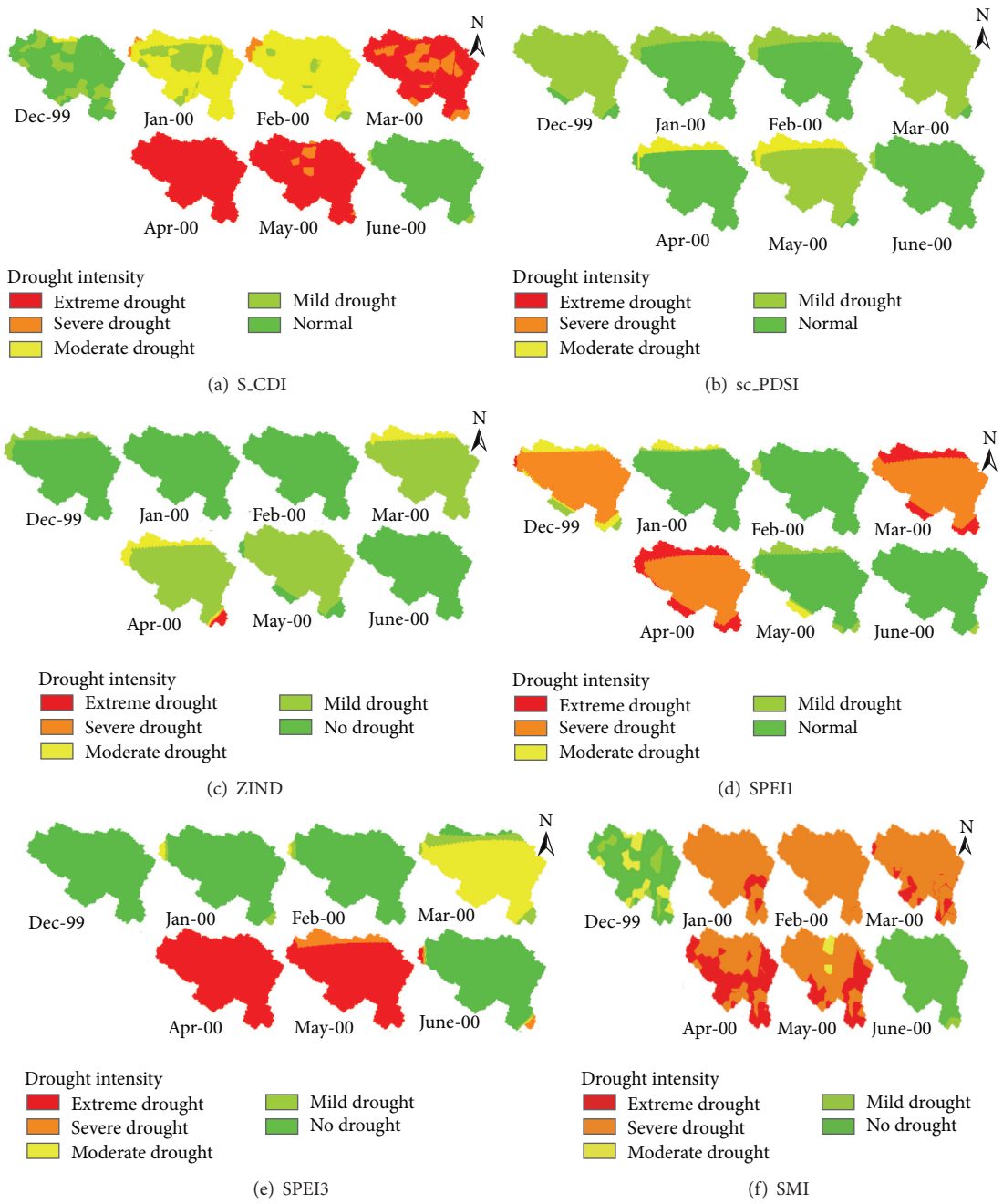

Figure 7: Dynamic spatial distributions of the S_CDI and its components in the upper Huaihe River basin.

in 2000, was one of the most famous extreme droughts in the Huaihe River basin in history (Zhang, [21]). During this drought, the total precipitation during January–May of 2000 was less than 45 percent of normal, no flow in the main river during April and May. According to incomplete statistics, the precipitation in Shangdong province—one of the major provinces in the Huaihe River basin—decreased 84 percent of normal during March and April, and 50% large and middle-sized reservoirs in the Province were operated under dead storage level and all the small reservoirs were depleted. The extreme drought in 1996 was also chosen to assess the feasibility of the newly developed CDI. Fortunately this drought event only persisted for a short period.

4.2.2. Drought in 1996. From Figure 5(a), it can be found that severe and extreme droughts in early 1996 were identified by the S_CDI, while only moderate and severe droughts were identified by the scPDSI and no drought by the 1-month SPEI. From Figure 5(b), only moderate and severe droughts were recognized by the L_CDI and the PHDI, and mild drought by the 6-month SPEI. Compared with the historical records, it can be concluded that the S_CDI best described the actual

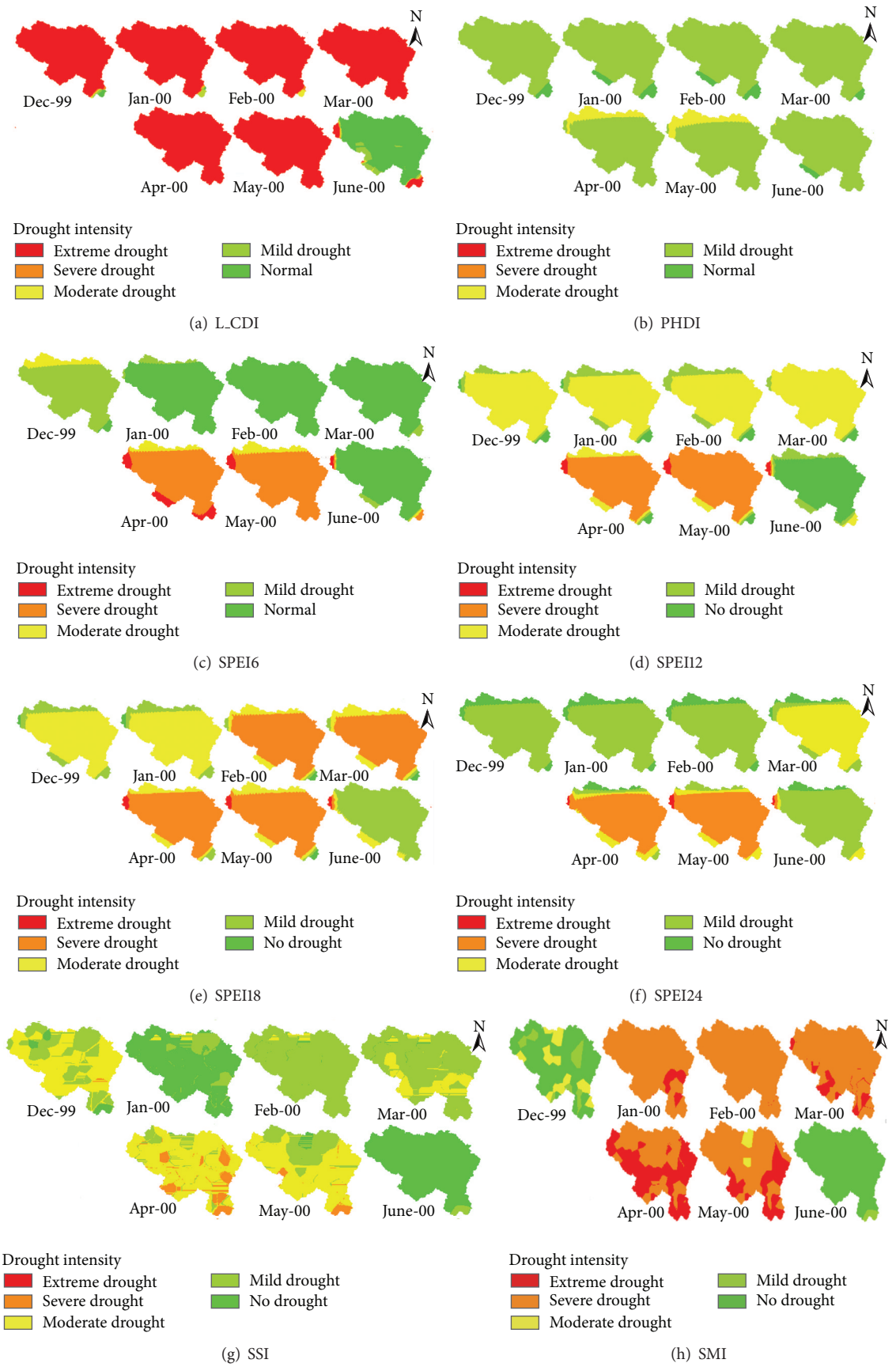

Figure 8: Dynamic spatial distributions of the L_CDI and its components in the upper Huaihe River basin.

dry condition of the short-term drought event in 1996. It indicated that the S_CDI could well capture the relative timely dynamic variation of the short-term drought evolution.

4.2.3. Drought in 2000. Both the S_CDI and the 1-month SPEI identified extreme droughts in March and April of 2000. However, the extreme drought continued developing till May of 2000 and it was only detected by the S_CDI, while no drought was found by the 1-month SPEI (Figure 6(a)). In the meanwhile, severe drought was detected by the scPDSI. From Figure 6(b), the L_CDI identified extreme droughts in March–May of 2000 while the 6-month SPEI identified this extreme drought only in April and May. Moreover, moderate drought was also detected from November of 1999 to January of 2000 by the L_CDI, while almost no drought occurred identified by the 6-month SPEI. Severe drought was detected by the PHDI only in April and May. The above comparison demonstrated that the S_CDI and L_CDI best characterized the extreme drought in 2000. Since this drought persisted a relatively long time period, the L_CDI was better identifying the whole drought evolution since the L_CDI detected the severe drought in September of 1999 while the S_CDI did not judge accurately.

4.3. Dynamic Spatial Distributions of Typical Drought Events. Dynamic spatial distributions of the S_CDI and its components in the upper Huaihe River basin were presented in Figure 7. A small part of the basin was firstly found in extreme drought in January 2000 by SMI with the rest in severe drought, while the 1-month SPEI identified the boundary area in extreme drought condition in March 2000 with the rest in severe drought condition. No extreme drought was found by the 3-month SPEI until April and May 2000. The S_CDI discovered moderate drought in January and February 2000, and most part was discovered in extreme drought in March 2000, almost all basin in extreme drought in April and May 2000, and no drought in June 2000. The scPDSI and the ZIND only identified mild drought over the whole period. In general, the S_CDI performed better than any other drought components; however, it was not the best choice while in comparison with the historical records of the 2000 drought. Figure 8 showed dynamic spatial distributions of the L_CDI and its components in the upper Huaihe River basin. Almost the whole upper Huaihe River basin was in extreme drought condition in December 1999 by the L_CDI, and such drought condition continued to May 2000, and the dry condition relieved in June 2000. The SPEI with different time scales only discovered severe drought during the period, and moderate drought was discovered by SSI and only mild drought by PHDI. Comparing Figures 7 and 8, it can be concluded that the L_CDI best described the drought process, including the drought onset, severity, and termination month.

5. Conclusions

The short-term/long-term CDI were developed and applied in the upper Huaihe River basin. The performance of the short-term/long-term CDI was compared with their drought index components and historical records, respectively. The result revealed that the newly built short-term CDI could better capture the drought severity, onset, and termination than the scPDSI and the 1-month SPEI for relatively short-term droughts, while the long-term CDI behaved better than the PHDI and the 6-month SPEI on drought persistence and magnitude for relatively long-term droughts; the S_CDI is better at drought assessment of short-term drought events while the L_CDI is better at drought assessment of long-term drought events; to obtain a more comprehensive and accurate result during drought assessment, the S_CDI is suggested to be adopted for drought assessment during drought initial period while the L_CDI is used after the drought persisting for a relatively long time period. The output of the paper could provide valuable references for drought estimation and monitoring of other river basins/regions in China.

Conflict of Interests

The authors declare that there is no conflict of interests regarding the publication of this paper.

Acknowledgments

Financial support is gratefully acknowledged from the National Science Foundation Commission under Grant no. 41171220, China, and the project (2014B04314) supported by the Fundamental Research Funds for the Central Universities.

References

[1] Z. C. Hao and A. Aghakouchak, "A nonparametric multivariate multi-index drought monitoring framework," *Journal of Hydrometeorology*, vol. 15, no. 1, pp. 89–101, 2014.

[2] M. X. Yu, *Development and application of the composited drought index [Ph.D. thesis]*, Hohai University, Nanjing, China, 2013.

[3] M. X. Yu, Q. F. Li, M. J. Hayes, M. D. Svoboda, and R. R. Heim, "Are droughts becoming more frequent or severe in China based on the Standardized Precipitation Evapotranspiration Index: 1951–2010?" *International Journal of Climatology*, vol. 34, no. 3, pp. 545–558, 2014.

[4] W. Palmer, "Meteorological droughts," Weather Bureau Research Paper, U.S. Department of Commerce, 1965.

[5] N. Wells, S. Goddard, and M. J. Hayes, "A self-calibrating palmer drought severity index," *Journal of Climate*, vol. 17, no. 12, pp. 2335–2351, 2004.

[6] T. McKee, N. Doesken, and J. Kleist, "The relationship of drought frequency and duration to time scales," in *Proceedings of the 8th Conference on Applied Climatology*, pp. 179–184, American Meteorological Society, Anaheim, Calif, USA, January 1993.

[7] S. M. Vicente-Serrano, S. Beguería, and J. I. López-Moreno, "A multiscalar drought index sensitive to global warming: the Standardized Precipitation Evapotranspiration Index," *Journal of Climate*, vol. 23, no. 7, pp. 1696–1718, 2010.

[8] S. M. Vicente-Serrano, J. I. López-Moreno, S. Beguería, J. Lorenzo-Lacruz, C. Azorin-Molina, and E. Morán-Tejeda, "Accurate computation of a streamflow drought index," *Journal of Hydrologic Engineering*, vol. 17, no. 2, pp. 318–332, 2012.

[9] D. A. Wilhite, *Drought and Water Crises: Science, Technology, and Management Issues*, Taylor & Francis, 2005.

[10] W. Xie, S. Wang, W. Tang, R. Wu, and J. Dai, "Comparative analysis on the applicability of drought indexes in the Huaihe River Basin," *Journal of Applied Meteorological Science*, vol. 25, no. 2, pp. 176–184, 2014.

[11] W. Zhang, Y. Liu, Q. Li, L. Ren, and T. Cai, "Drought evaluation for upper reaches of the Huaihe River," *Journal of China Hydrology*, vol. 29, no. 5, pp. 69–72, 2009.

[12] R. Zhang, X. Chen, Z. Zhang, and P. Shi, "Evolution of hydrological drought under the regulation of two reservoirs in the headwater basin of the Huaihe River, China," *Stochastic Environmental Research and Risk Assessment*, vol. 29, no. 2, pp. 487–499, 2015.

[13] W. Zhang, S. Pan, L. Cao et al., "Changes in extreme climate events in eastern China during 1960–2013: a case study of the Huaihe River Basin," *Quaternary International*, vol. 380-381, pp. 22–34, 2015.

[14] X. Cai, H. Mao, and W. Wang, "Study of the adaptability of multiscale drought indices in Yangtse-Huaihe River basins," *Journal of Glaciology and Geocryology*, vol. 35, no. 4, pp. 978–989, 2013.

[15] Q. Wang, P. Shi, T. Lei et al., "The alleviating trend of drought in the Huang-Huai-Hai Plain of China based on the daily SPEI," *International Journal of Climatology*, 2015.

[16] K. Duan, W. Xiao, Y. Mei, and D. Liu, "Multi-scale analysis of meteorological drought risks based on a Bayesian interpolation approach in Huai River basin, China," *Stochastic Environmental Research and Risk Assessment*, vol. 28, no. 8, pp. 1985–1998, 2014.

[17] D.-H. Yan, D.-M. Han, G. Wang, Y. Yuan, Y. Hu, and H.-Y. Fang, "The evolution analysis of flood and drought in Huai River Basin of China based on monthly precipitation characteristics," *Natural Hazards*, vol. 73, no. 2, pp. 849–858, 2014.

[18] I. T. Jolliffe, *Principal Component Analysis*, Springer, 2nd edition, 2002.

[19] Z. Ren-Jun, "The Xinanjiang model applied in China," *Journal of Hydrology*, vol. 135, no. 1–4, pp. 371–381, 1992.

[20] D. S. Wilks, *Statistical Methods in the Atmospheric Sciences: An Introduction*, vol. 59 of *International Geophysics Series*, Academic Press, San Diego, Calif, USA, 1995.

[21] S. F. Zhang, *Historic Droughts of China 1949–2000*, Hohai University Press, Nanjing, China, 2008.

Hindawi Publishing Corporation
Advances in Meteorology
Volume 2016, Article ID 1536135, 10 pages
http://dx.doi.org/10.1155/2016/1536135

Research Article

Spatial-Temporal Variation of Aridity Index of China during 1960–2013

Huiping Huang,[1,2,3] Yuping Han,[1,3] Mingming Cao,[2] Jinxi Song,[2] and Heng Xiao[1]

[1]*School of Resources and Environment, North China University of Water Resources and Electric Power, Zhengzhou 450045, China*
[2]*College of Urban Environmental Science, Northwest University, Xi'an 710127, China*
[3]*Collaborative Innovation Center of Henan Province, Zhengzhou 450045, China*

Correspondence should be addressed to Yuping Han; han0118@163.com

Received 16 March 2015; Revised 7 August 2015; Accepted 17 August 2015

Academic Editor: Mark D. Svoboda

Aridity index, as the ration of potential evapotranspiration and precipitation, is an important indicator of regional climate. GIS technology, Morlet wavelet, Mann-Kendall test, and principal component analysis are utilized to investigate the spatial-temporal variation of aridity index and its impacting factors in China on basis of climate data from 599 stations during 1960–2013. Results show the following. (1) Boundaries between humid and semihumid region, and semihumid and semiarid region coincide with 400 mm and 800 mm precipitation contour lines. (2) Average annual aridity index is between 3.4 and 7.5 and shows decrease trend with a tendency of –0.236 per decade at 99% confidence level. (3) The driest and wettest month appear in December and July, respectively, in one year. (4) Periods of longitudinal and latitudinal shift of aridity index 1, 1.5, and 4 contours coordinate are 10 and 25 years, 6 and 26 years, and 5 and 25 years, respectively. (5) Four principal components which affect aridity index are thermodynamic factors, water and radiation factors, geographical and air dynamic factors, and evaluation factor, respectively.

1. Introduction

Aridity index is the ratio of annual potential evapotranspiration (ET_0) and annual precipitation (UNESCO [1], FAO [2], and UNEP [3]) and it usually reflects the degree of climatic drought. Regions where aridity index is less than 1.0 are classified as wet areas (Ponce et al. [4]); the regions where aridity index is more than 1 are classified as dry areas since the evaporative demand cannot be met by precipitation. China is classified as humid area, semihumid area, semiarid area, and arid area mainly based on aridity index assisted by precipitation. Humid area is the region where aridity index is less than 1, semihumid area is the region where aridity index is between 1.5 and 1, semiarid area is the region where aridity index is between 1.5 and 4, and arid area is the region where aridity index is more than 4 (Zheng et al. [5], Zheng et al. [6]). ET_0 refers to the largest amount of evaporation that will occur if the sufficient water surface is available and it is a function of temperature, vapor pressure, wind speed, humidity, and solar radiation (Penman [7]). So the spatial-temporal variation of aridity index change is the reflection on change of all climatic factors.

Effect of climate changes on hydrological regimes, especially hydrological extremes, for example, droughts and floods, has become a priority area both for process research and for water management practices (Zhang et al. [8]). Many researchers have reported impacts of changes in climatic variables, such as precipitation, air temperature, sunshine hour, and wind speed, on the world. In China, 400 mm and 800 mm rainfall contours had a shifting trend toward west and south during 1960–2010 (Yuan et al. [9]). Aridity index in northwest China indicated that the region became wetter from 1960 to 2010 (Liu et al. [10]). Investigation shows that aridity index in Turkey during 1930 to 2000 increased at many stations (Türkeş [11]). There is decrease in aridity index in Iran and decrease was more obvious in the semiarid region than in the humid region (Tabari and Aghajanloo [12]). During 1960–2005, eastern Greece has shifted from the "humid" class towards the "subhumid" and "semiarid" classes and at the end of the twenty-first century drier conditions are

expected to appear in Greece (Nastos et al. [13]). Based on collected meteorological data, we present a detailed analysis of spatial-temporal variations and its impacting factors in aridity index in China.

2. Data and Methodology

2.1. Data. Daily and yearly precipitation, maximum, minimum, and mean air temperature, wind speed (at 10 m aboveground surface), humidity, vapor pressure, and sunshine hour covering from 1960 to 2013 were collected from 599 meteorological stations from the China Meteorological Administration (CMA) and National Meteorological Information Center of China (NMIC). The data was released as the data set (SURF_CLI_CHN_MUL_DAY) after quality control in the Web site http://data.cma.gov.cn/. Missing data were estimated by the average value of the other years observed at the same station (missing data are mainly concentrated in 1967, 1968, and 1969) (Huang et al. [14]). There exist 10 first-level river basins in China and they are, namely, Songhua River Basin (SRB), Liao River Basin (LRB), Hai River Basin (HaRB), Yellow River Basin (YeRB), Huai River Basin (HuRB), Yangtze River Basin (YaRB), Southeast Rivers Basin (SERB), Pearl River Basin (PRB), Southwest Rivers Basin (SWRB), and Northwest Rivers Basin (NWRB). The DEM data of China is from Computer Network Information Center, Chinese Academy of Sciences. The location of the meteorological stations and 10 river basins is shown in Figure 1.

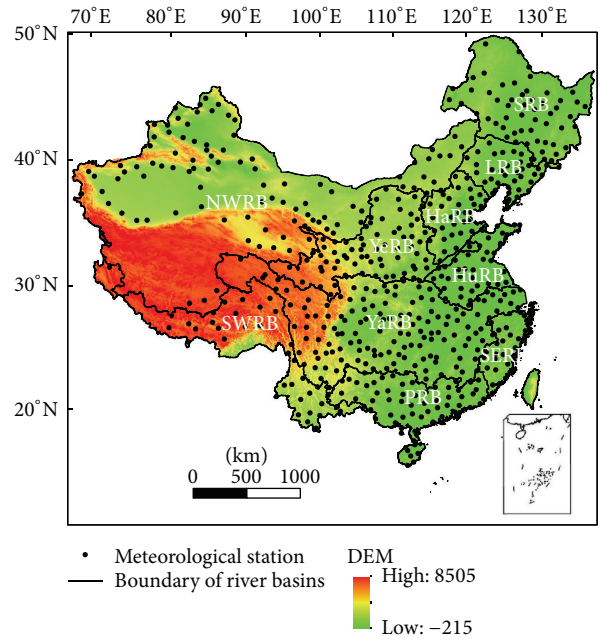

Figure 1: Spatial distribution of meteorological stations in China.

2.2. Methodology

2.2.1. Potential Evaporation (ET_0). According to definition of aridity index of UNEP (1992), calculation of aridity index needs reference evapotranspiration (ET_0) and precipitation data. ET_0 is estimated using the Penman-Monteith (PM) equation (Allen et al. [15]) which is the standard equation for ET_0. The formula is given as

$$ET_0 = \frac{0.408\Delta\left(R_n - G\right) + \gamma\left(900/\left(T + 273\right)\right)U_2\left(e_s - e_a\right)}{\Delta + \gamma\left(1 + 0.34U_2\right)}, \quad (1)$$

where ET_0 is daily potential evapotranspiration ($mm \cdot d^{-1}$); yearly and monthly ET_0 data are used in this paper; R_n is the net radiation at the top surface ($MJ \cdot m^{-2} \cdot d^{-1}$); G is the soil heat flux density ($MJ \cdot m^{-2} \cdot d^{-1}$); T is mean daily air temperature at 2 m height (°C); U_2 is daily average wind speed at 2 m height ($m \cdot s^{-1}$); e_s is saturation vapor pressure (kPa); e_a is actual vapor pressure (kPa); Δ is slope of e vapor pressure curve ($kPa \cdot °C^{-1}$); γ is the psychrometric constant ($kPa \cdot °C^{-1}$).

2.2.2. Calculation of Aridity Index. Aridity index (ϕ) is the ratio of potential evapotranspiration and precipitation which can be expressed as

$$\phi = \frac{ET_0}{P}, \quad (2)$$

where ET_0 is the potential evapotranspiration (mm) and P is the precipitation (mm) in statistical period.

2.2.3. Interpolation of ET_0 and Precipitation. This paper uses collaborative Craig interpolation method (COK) to transfer yearly meteorological data of each station into 10 km × 10 km grid map. COK changes the best estimating method of regional variables from one single attribute to 2 or more than 2 attributes. One of the attributes is main and others are auxiliary. COK combines self-correlation of main attribute and interaction of main and auxiliary attributes into unbiased optimal estimation. It is applicable for multiple regional variables which related to each other; it can estimate the required variables with one or more secondary variables and has been widely used (Hevesi et al. [16], Hevesi et al. [17]). Based on Cokriging tool embedded in geostatistical analysis module in ArcGIS software, precipitation and ET_0 are interpolated in this paper.

2.2.4. Mean Center of Aridity Index Contour Line. The aridity index contour lines of 1, 1.5, and 4 in every year during 1960 to 2013 are extracted from the aridity index grid map. In order to get the average location of each contour line, this paper adopts weighted average of aridity index contour line to characterize its spatial position. The spatial changes in aridity index line can be characterized on the extracted center coordinates of each contour line in every year (Wang et al. [18]). The weighted average location of aridity index contour can be obtained using Mean Center tools in ArcGIS which located in the Spatial Statistical Tools.

2.2.5. Spatial and Temporal Trend Analysis. The simple linear regression method was used to estimate the trend magnitudes (slope) in aridity index and other climatic variables including

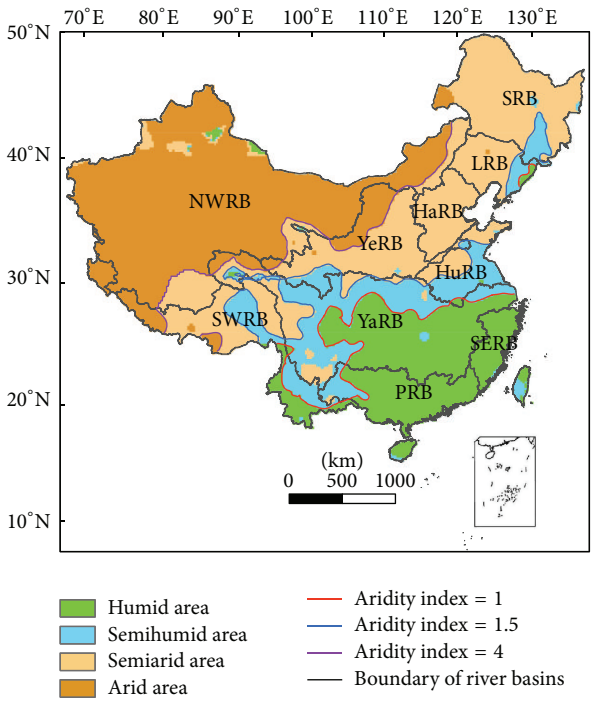

Figure 2: Distribution of average annual aridity index in China.

air temperature (°C), relative humidity (%), 2 m wind speed ($m\,s^{-1}$), and sunshine hours (h) used in P–M method (Xing et al. [19]). Meanwhile we apply the Mann-Kendall (MK) method (Mann [20], Kendall [21]) which is distribution-free, is robust against outliers, and has a higher power than many other commonly used tests (Dinpashoh et al. [22]) to recognize the temporal trend of aridity index. This paper decomposed the shift of weighted average position of aridity index contour line into longitudinal and latitudinal shift, and analysis of the periodic shift used Morlet wavelet.

3. Results

3.1. Spatial Change of Multiyear Average Aridity Index

3.1.1. Annual Distribution of Aridity Index. China is divided into 4 types of regions based on average aridity index (Zhang et al. [8]). Figure 2 shows the spatial distribution of different regions. Arid region is located in mainly NWRB, a little part of northwest in YeRB and northwest of SWRB. The semiarid region includes most part of SRB, LRB, YeRB, and SWRB, whole part of HaRB and half of HuRB in the north part. Semihumid region consists of east SRB, LRB, south of HuRB, north of YaRB, east of SWRB, and west of PRB. Humid region includes most of YaRB, PRB, and all of SERB. Boundary between arid area and semiarid area basically coincided with the 400 mm contour of precipitation; boundary between semihumid area and humid area basically coincided with the 800 mm contour of precipitation (Fu et al. [23]). There exist enclaves in every kind of region such as two parts of humid regions located in the arid area in NWRB. The reason humid claves locate arid area in NWRB is that in Tianshan mountain area precipitation is more than other regions for its terrain. The reason other enclaves exist is because of the different aridity index associated with the terrain there.

3.1.2. Seasonal Distribution of Aridity Index. Aridity index shows different distribution pattern in spring, summer, autumn, and winter (Table 1 and Figure 3). Summer is the wettest season and winter is the driest in one year. In winter, only SERB belongs to the humid area; HaRB, HuRB, YeRB, NWRB, and SWRB belong to arid area. In summer, YaRB, SERB, SRB, SWRB, and PRB all belong to humid area. Autumn is relatively wetter than spring and no season is humid in HaRB, HuRB, YeRB, LRB, and NWRB.

It can be seen from Figure 3 that scope of arid region is the minimum in summer and maximum in winter. Arid only exists in most part of NWRB and a little part of SWRB in summer and exists in most part of all China including all of YeRB, HaRB, most part of NWRB, SWRB, and LRB, and west part of PRB, YaRB, and SRB. Area of arid in autumn is basically the same with that of the whole year. Semiarid area is different in autumn and winter from other times. Semihumid region is the smallest and the region is like a stripe among semiarid region and humid region in spring and winter. Humid region is different in autumn compared with the other seasons; it only locates in the middle part of YaRB and a little southeast part of SWRB.

Among aridity index calculation in seasonal scale, there exists condition that there is no precipitation in some stations. When precipitation is 0 in one station in one statistical time, we adopt the maximum aridity index in the same station in the same season in 1960–2013. Precipitation is 0 which indicates the extreme drought in one region. In spring, precipitation is 0 in 9 stations in 1968, 7 stations in 1963 and 1994. In Lenghu station, which locates in NWRB, precipitation is 0 during 17 years. There are 29 stations which exist in one or more years when precipitation is 0. Among the 29 stations 26 stations are located in NWRB. In summer, in Bachu station which locates in NWRB, there are 12 years when precipitation is 0. In autumn, stations where there is no precipitation peak are 18 in 1991. There are 35 stations which exist in one or more years when there is no precipitation; the no-precipitation years are more than 10 in 9 stations which all belong to NWRB. In winter, which is the driest season in China, it is only in 1995 that all stations have precipitation. There are 116 stations which exist in one or more years when there is no precipitation and the no-precipitation years are more than 10 years in 20 stations.

3.2. Temporal Change of Aridity Index

3.2.1. Change of Annual Aridity Index in China. Figure 4(a) shows the spatial distribution of aridity index change trends for 599 meteorological stations from 1960 to 2013 in China. There are 309 stations present increasing trend and they are mainly located in the middle part of China, including west of SRB, most of HaRB and YeRB, west of YaRB and PRB, and east of SWRB. In NWRB, aridity index in 10 stations increases and aridity index of other 133 stations decreases. Particularly, 39 stations show significant decrease (95% confidence level),

Table 1: Seasonal aridity index in different river basins.

	YaRB	SERB	HaRB	SRB	HuRB	YeRB	LRB	NWRB	SWRB	PRB
Annual	0.922	0.723	2.107	1.316	2.135	1.689	1.738	7.021	1.238	0.776
Spring	0.96	0.518	5.221	2.111	3.49	3.756	3.843	10.948	2.188	0.736
Summer	0.788	0.756	1.229	0.901	1.607	1.012	1.182	5.894	0.693	0.568
Autumn	0.988	1.068	2.411	1.408	1.61	2.029	1.944	7.009	1.184	0.989
Winter	1.363	0.719	7.752	2.26	6.574	4.39	2.349	4.826	4.65	1.654

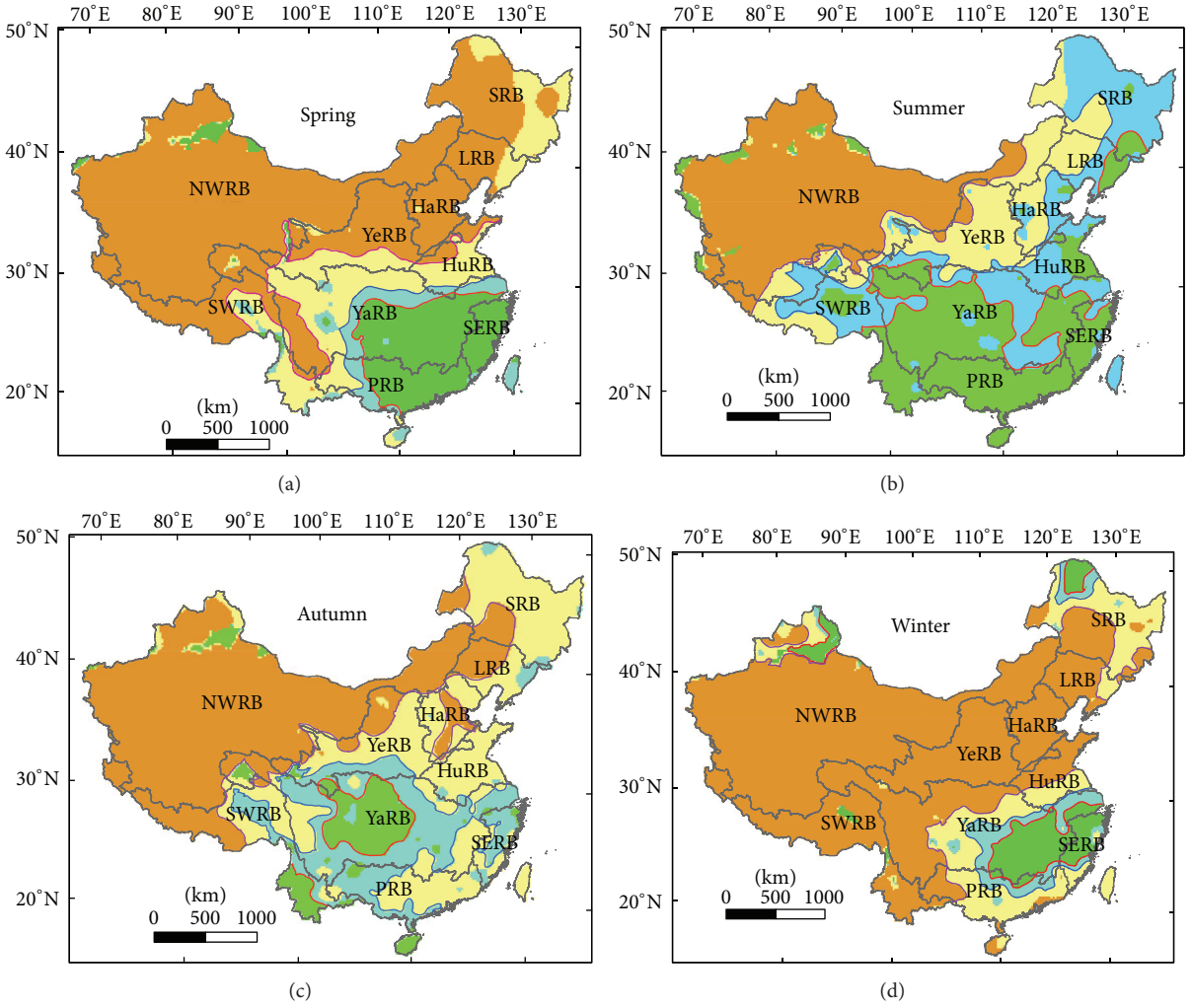

Figure 3: Distribution of seasonal aridity index in China. (The legend is the same as Figure 2.)

accounting for 69.6% of all the significant decrease in China. In SERB, 20 stations show decrease which account for 71.4% of the region.

Figure 4(b) indicates change of annual aridity index averaged by weight of Thiessen polygon of 599 stations in 1960–2013. Average of aridity index is between 3.4 and 7.5; the driest year appears in 1980 and the wettest year appears in 2003. Annual aridity index shows decrease trend with a tendency of −0.236 per decade at 99% confidence level which indicates that China became wetter during 1960–2013.

3.2.2. Change of Monthly Aridity Index. Aridity index has the obvious monthly characteristics and Figure 5 shows the variation of it in 10 river basins in whole China. In NWRB, HaRB, HuRB, LRB, NWRB, SRB, and whole China, July is the wettest month, in PRB, SERB, and YaRB, June is the wettest month, and in YeRB September is the wettest month. The driest month dispersed in January, March, April, October, and December. In all the monthly statistical data, maximum data 11.62 appears in NWRB in April and minimum data 0.44 appears in SERB in June. The wettest region is SERB and there

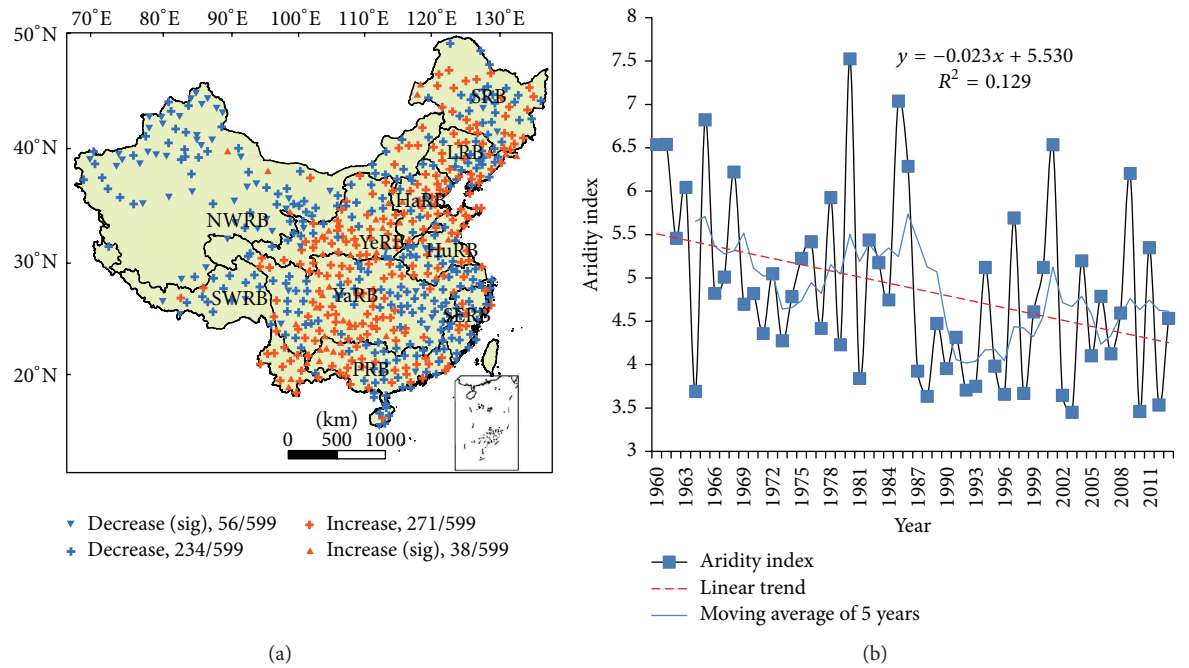

Figure 4: Change of annual aridity index.

are eight months in which aridity index is less than 1 but in YeRB and NWRB data in all months are more than 1. In China as a whole, aridity index is between 0.95 and 2.3, and maximum value appears in December.

3.2.3. Space Change Trend of Interannual Aridity Index Contour Line. In China, average coordinate for aridity index contour lines of 1, 1.5, and 4 is (115.1, 35.24), (113.35, 37.91), and (95.87, 32.74), and the points locate in northeast of HuRB, middle of HaRB, and north of SWRB, respectively. Figure 6 shows coordinate for aridity index contour lines of 1, 1.5, and 4 during 1960–2013. In 1960–2013, point of aridity index contour line moves towards to south and west. Slope of contour 1 is −0.057 and −0.081, slope of contour 1.5 is −0.107, −0.062, and slope of contour 4 is −0.017, −0.032 in longitudinal and latitudinal direction, respectively. Shift of aridity index 1.5 in longitudinal direction is significant; other shifts of the mean center coordinate vibrate so the trend is not significant. All the shifts indicate that the climate is changing towards wet in China in 1960–2013.

3.2.4. Periodic Analysis of Interannual Aridity Index Contour Line. Figure 7 is modular square map of Morlet wavelet transform coefficients for mean center coordinates of different aridity index contour lines. Red lines indicate positive phase and comparative big data period; blue lines indicate negative phase and comparative small data period. Figures clearly reflect fluctuation of mean center coordinates of different aridity index contour lines. There exist different periodic changes in mean center for longitude and latitude coordinate. 10 and 25 years' periods exist in shift of aridity index 1 contour coordinate in both longitudinal and latitudinal direction, of which 10 years is the main cycle. 6 and 26 years' cycles exist in shift of aridity index 1.5 contour coordinate in both longitudinal and latitudinal direction and 5 years is the main cycle. 5 and 25 years' cycles exist in shift of aridity index 4 contour coordinate in both longitudinal and latitudinal direction and 5 years is the main cycle.

3.3. Interaction between Changes in Aridity Index and Climate Variables

3.3.1. Change in Climate Variables. Table 2 shows slope of climate variables averaged by meteorological stations in each river basin from 1960 to 2013. Except for T_{max} in HuRB, all temperature variables show increase trend significantly, of which increase in T_{min} is the biggest and increase of T_{min} in NWRB reached 0.486°C per decade. Humidity in all regions shows decrease trend and decrease in 7 basins is significant, but the descendent is less in LRB, NWRB, SWRB, and YeRB. Change trend in vapor pressure is significant in SRB, HuRB, LRB, and NWRB with slope being 0.077, 0.187, 0.074, and 0.049, respectively. However, trend in SERB and PRB is decrease. Significant decrease is detected in wind speed change and slope in SRB is the biggest. Except increase in SWRB, sunshine hour is decreasing significantly in other river basins. Precipitation change is different and there is no consistent trend in 10 river basins. Except in NWRB, change of precipitation is insignificant.

3.3.2. Principal Component Analysis of Aridity Index. There are many methods to quantify the contributions of climate variables change in aridity index, because meteorological variables impacted each other and they are not totally

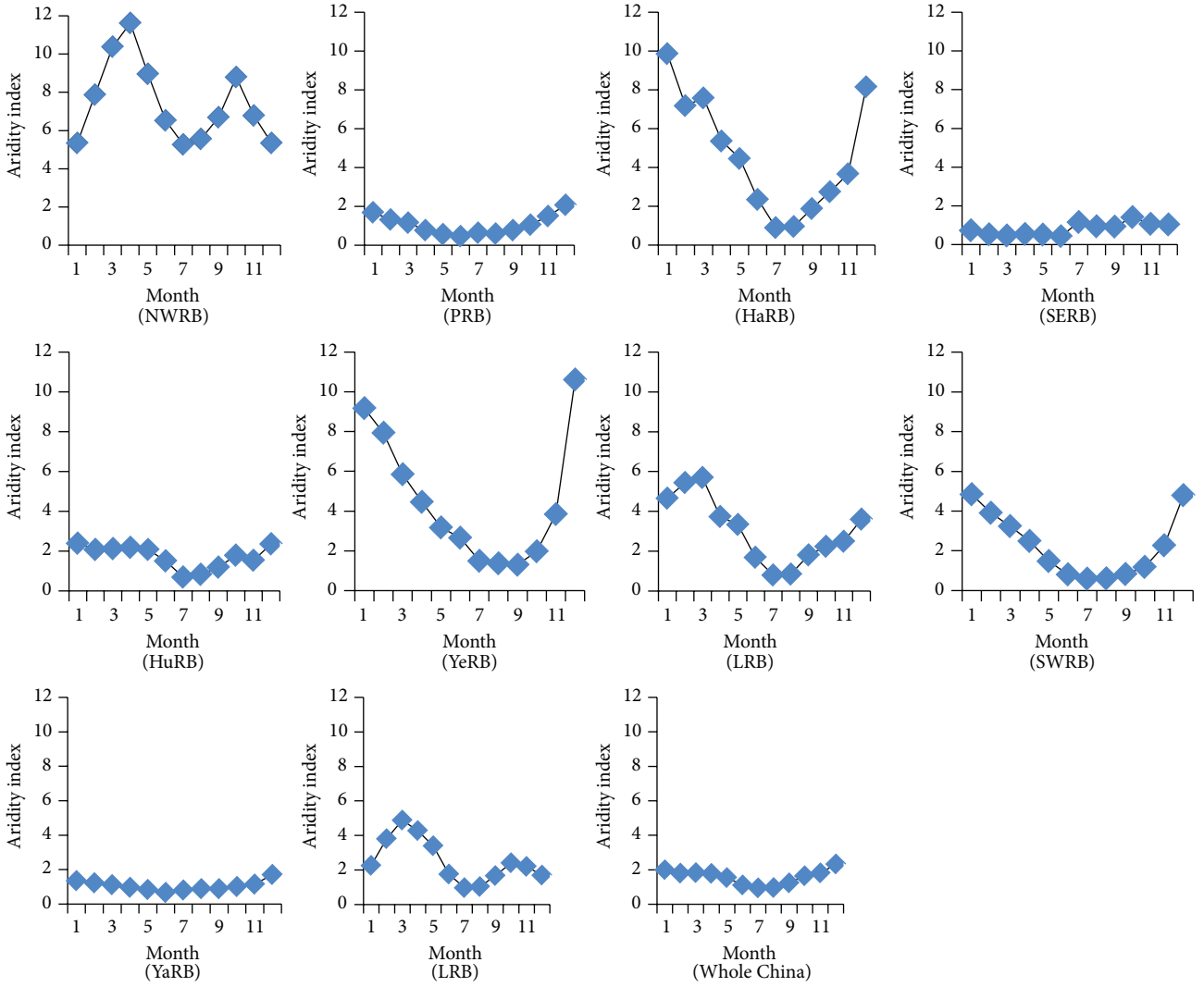

Figure 5: Monthly distribution of aridity index in different river basin.

Table 2: Variations of various climate variables averaged from 1960 to 2013.

	YaRB	SERB	HaRB	SRB	HuRB	YeRB	LRB	NWRB	SWRB	PRB
T_{max} (°C)	0.226**	0.258**	0.273**	0.275**	0.111	0.353**	0.231**	0.345**	0.333**	0.125*
T_{mean} (°C)	0.18**	0.214**	0.285**	0.337**	0.202**	0.277**	0.238**	0.343**	0.282**	0.14**
T_{min} (°C)	0.238**	0.243**	0.41**	0.485**	0.246**	0.331**	0.343**	0.486**	0.358**	0.199**
Humidity (%)	−0.536**	−0.836**	−0.6**	−0.465**	−0.877**	−0.511*	−0.117	−0.133	−0.34	−0.637**
Vapor pressure (kPa)	0.003	−0.029	0.055	0.077*	0.187**	0.027	0.076**	0.074**	0.049*	−0.034
Wind speed ($m \cdot s^{-1}$)	−0.087**	−0.132**	−0.163**	−0.189**	−0.108**	−0.075**	−0.185**	−0.152**	−0.053**	−0.044**
Sunshine hour (h)	−0.112**	−0.164**	−0.233**	−0.095**	−0.185**	−0.084**	−0.185**	−0.043**	0.009	−0.133**
Precipitation (mm)	−2.813	20.316	−13.107	0.679	−8.647	−8.508	−4.768	6.018**	3.049	4.445

**99% confidence level; *95% confidence level; the slope is the value of aridity index per decade.

independent. For example, increase in precipitation may lead to an increase in humidity but decrease in air temperature. In addition, partial derivatives of aridity index to climate variables are not constant but fluctuated in statistical period. This paper adopts principal component analysis to discuss main factors impacting aridity index and operation is completed in SPSS. The adopted influencing factors in this paper include 11 variables which include climate variables listed in Table 2 and longitude, latitude, and evaluation. Evaluation of every metrological station is extracted from DEM data of China.

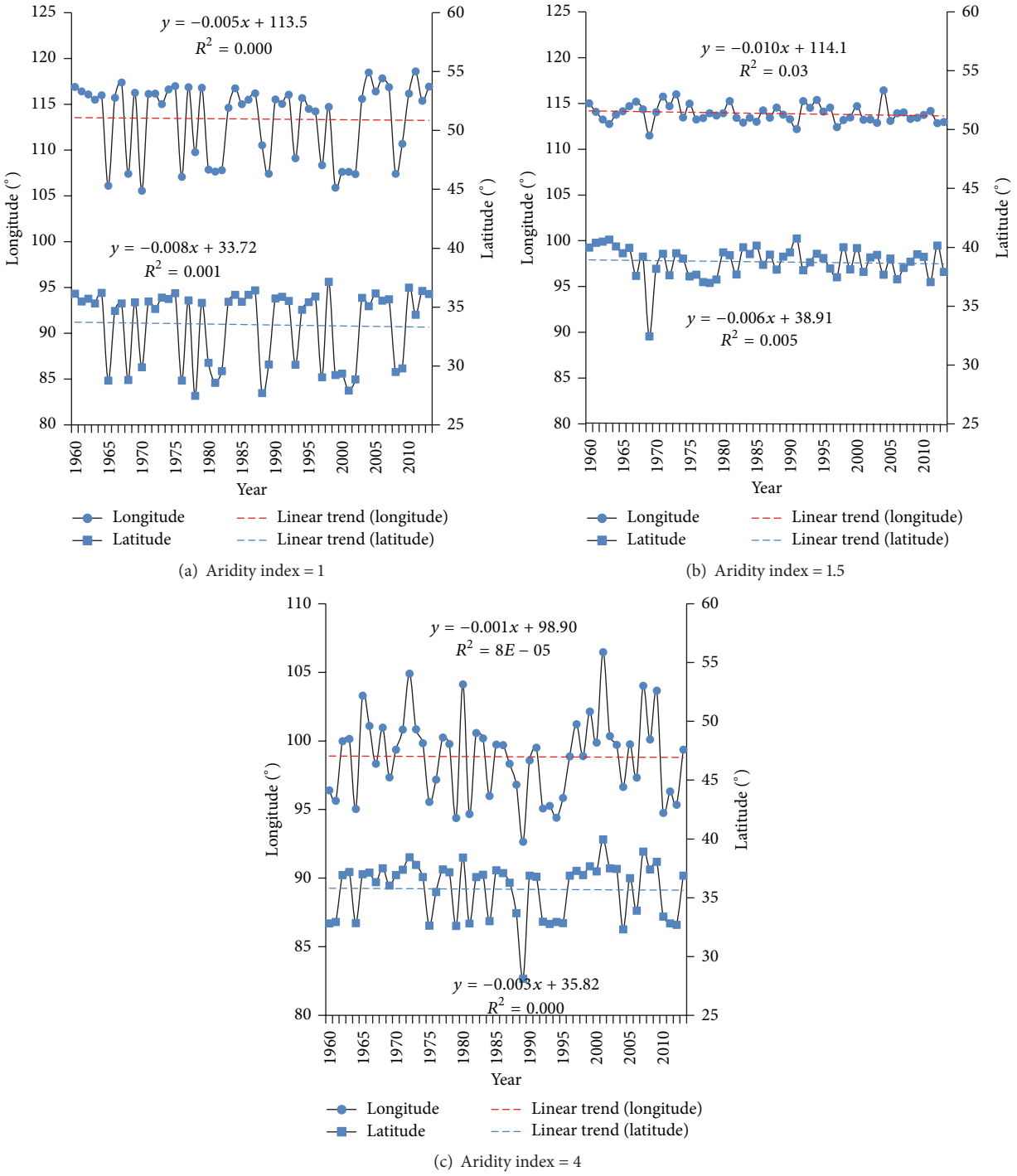

FIGURE 6: Annual spatial shift of mean center of different aridity index contour line.

Table 3 is total variance decomposition for each factor; it can be seen that characteristics of the first 4 principal components account for 90.62% of the total variance. That is, the first 4 principal components have covered most information of the 11 factors. So the first 4 principal components are selected to substitute for the 11 factors and the first principal carries 58.77% information of the total factors.

Although the first 4 principal components have summarized 90.62% information of all the influencing factors, there is little difference in the coefficients of each primitive variable. Variance maximization rotation is adopted on the loading matrix in this paper in order to explain the factor better and Table 4 is the rotated component matrix. It can be seen from Table 4 that the first principal component

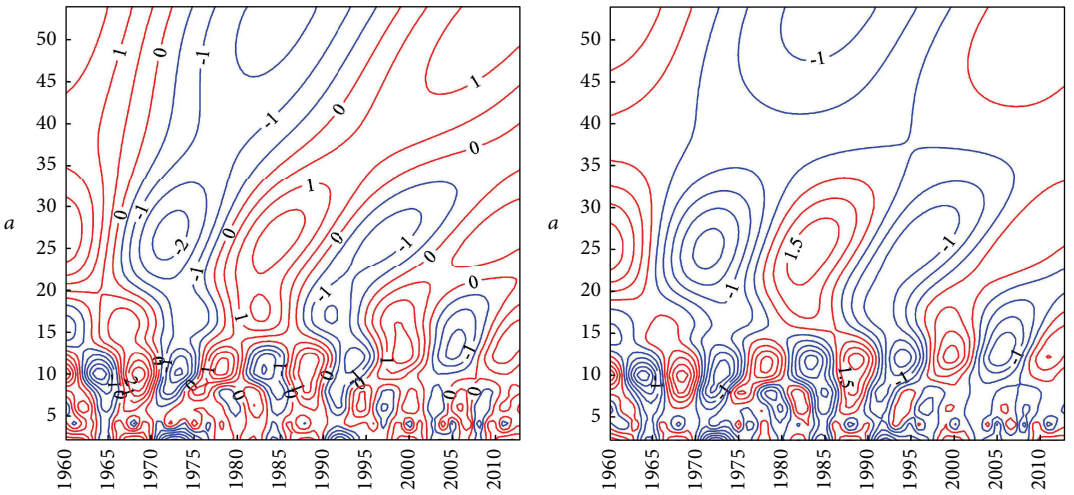

(a) Aridity index = 1 (longitude)

(b) Aridity index = 1 (latitude)

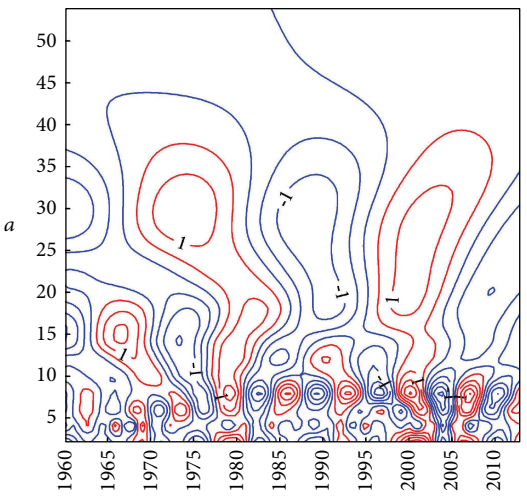

(c) Aridity index = 1.5 (longitude)

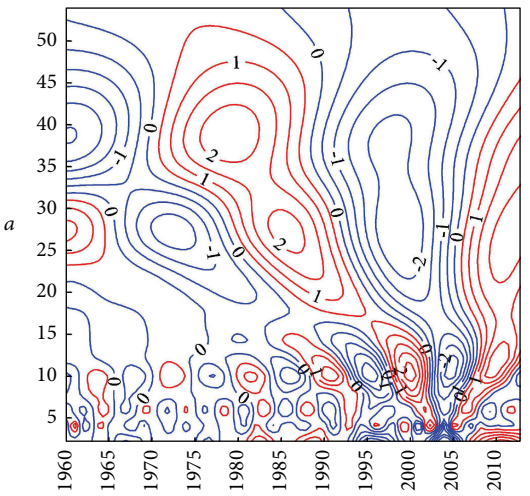

(d) Aridity index = 1.5 (latitude)

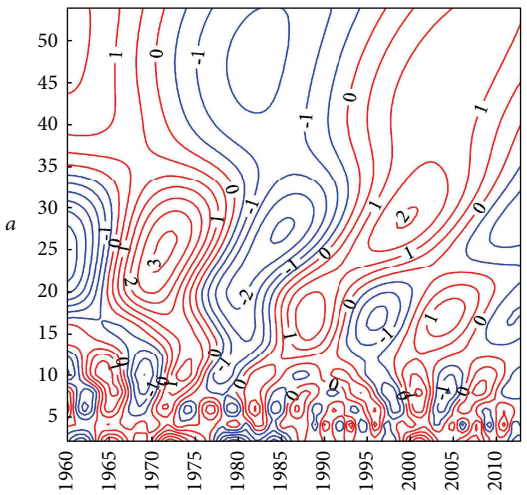

(e) Aridity index = 4 (longitude)

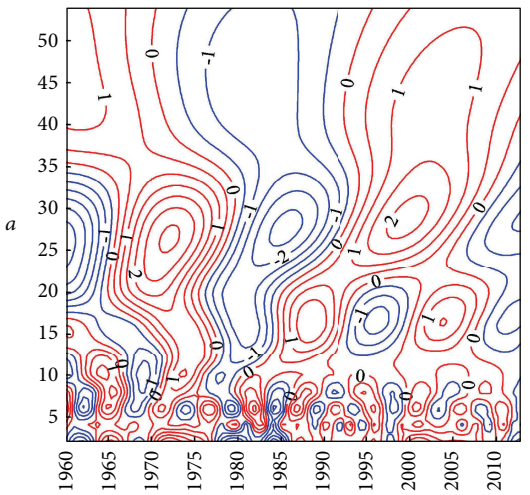

(f) Aridity index = 4 (latitude)

Figure 7: Wavelet variance diagrams of the mean centers.

Table 3: Eigenvalues and squared loadings of the principal components.

	1	2	3	4	5	6	7	8	9	10	11
Eigenvalues	6.46	1.71	0.97	0.83	0.37	0.28	0.25	0.09	0.03	0.02	0.00
Contributions	58.77	15.52	8.79	7.55	3.32	2.56	2.24	0.82	0.27	0.14	0.03
Accumulated contributions	58.77	74.29	83.08	90.62	93.94	96.50	98.74	99.56	99.83	99.97	100.00

Table 4: Rotated component matrix.

	a	b	c	d	e	f	g	h	i	j	k
1	0.00	−0.77	−0.28	0.95	0.94	0.91	−0.20	−0.32	0.42	0.81	0.48
2	0.25	0.27	−0.08	0.16	0.21	0.21	0.02	−0.87	0.82	0.21	0.84
3	0.93	0.09	−0.27	−0.02	0.03	0.05	0.88	−0.19	0.25	0.19	0.16
4	0.16	−0.18	−0.91	0.11	0.16	0.21	−0.13	−0.09	0.34	0.21	0.22

a: Longitude; b: Latitude; c: Evaluation; d: T_{max}; e: T_{mean}; f: T_{min}; g: Wind speed; h: Sunshine hour; i: Humidity; j: Vapor pressure; k: Precipitation.

has bigger loading on T_{max}, T_{mean}, T_{min}, and vapor pressure and the loading value reduces in turn, of which the temperature variables loading values are more than 0.9. Vapor pressure, latitude, and temperature can be considered as thermodynamic factors and they are the most critical factors influencing aridity index. Humidity, sunshine hour, and precipitation have bigger absolute value of load on the second principal component. Humidity and precipitation belong to the moisture factor and have positive relationship with the second principal component. Sunshine hour belongs to the radiation factor. Longitudes and wind speed which belong to the geographical, dynamic factor, respectively, have big absolute value of load on the third principal component. Absolute value of evaluation load is the biggest in the fourth principal component and it belongs to geographical factor.

4. Conclusions

Using the Penman formulation of ET_0, precipitation, and other geographical variables during 1960–2013 in China, authors analyze the spatial and temporal variation of the aridity index and explore its influencing factors (i.e., four principal components). The following conclusions are drawn from this research.

(1) Spatial distribution of aridity index: arid region locates in mainly NWRB, a little part of northwest in YeRB and northwest of SWRB. The semiarid region includes most part of SRB, LRB, YeRB, and SWRB, whole part of HaRB, and half of HuRB in the north part. Semihumid region consists of east SRB, LRB, south of HuRB, north of YaRB, east of SWRB, and west of PRB. Humid region includes most of YaRB, PRB, and all of SERB. Scope of arid region is the minimum in summer and maximum in winter.

(2) Temporal change of aridity index: annual average of aridity index is between 3.4 and 7.5; the driest year appeared in 1980 and the wettest year appeared in 2003 and it shows decrease trend with a tendency of −0.236 per decade at 99% confidence level. In NWRB, HaRB, HuRB, LRB, NWRB, SRB, and whole China, July is the wettest month, in PRB, SERB, and YaRB, June is the wettest month, and in YeRB, September is the wettest month. The driest month dispersed in January, March, April, October, and December.

(3) Spatial and periodic characteristics of interannual aridity index contour line: the average coordinate for aridity index contour lines of 1, 1.5, and 4 is (115.1, 35.24), (113.35, 37.91), and (95.87, 32.74). Mean center point of aridity index contour line moves towards the south and the west during 1960–2013. In both longitudinal and latitudinal direction, there exist 10-year and 25-year cycles in shift for aridity index 1 contour coordinate, 6-year and 26-year cycles in shift for aridity index 1.5 contour coordinate, and 5-year and 25-year cycles in shift for aridity index 1.5 contour coordinate.

(4) Principal components influencing aridity index: there are 4 principal components which influence the change of aridity index. T_{mean}, T_{max}, T_{min}, vapor pressure, and latitude comprise the first component and they all can be considered as thermodynamic factors. Humidity, precipitation, and sunshine hour consist of the second principal component and they belong to the moisture factor and radiation factor. Longitudes and wind speed which belong to the geographical, dynamic factor, respectively, are the third principal component. Evaluation which belongs to geographical factor consists of the fourth principal component.

Conflict of Interests

The authors declare that there is no conflict of interests regarding the publication of this paper.

Acknowledgments

This study was supported by the National Natural Science Foundation of China (Grant no. 51279063), the Program for the New Century Excellent Talents in University (Grant no. NCET-13-0794), the Key Projects in the National Science & Technology Pillar Program during the Twelfth Five-year Plan Period (Grant no. 2012BAC19B00), the Plan for Scientific Innovation Talent of Henan Province in China (Grant no. 144100510014), and the Support Plan of the Education Department of Henan Province for Science and Technology Innovation Teams (Grant no. 15IRTSTHN030).

References

[1] UNESCO, *Map of the World Distribution of Arid Regions: Map at Scale 1:25,000,000 with Explanatory Note*, United Nations Educational, Scientific and Cultural Organization, Paris, France, 1969.

[2] Food and Agriculture Organization, "Arid zone forestry: a guide for field technicians," in *FAO Conservation Guide*, J. P. Lanly, Ed., FAO, Rome, Itlay, 1989.

[3] United Nations Environment Programme (UNEP), *World Atlas of Desertification*, Edward Arnold, London, UK, 1992.

[4] V. M. Ponce, R. P. Pandey, and S. Ercan, "Characterization of drought across climatic spectrum," *Journal of Hydrologic Engineering*, vol. 5, no. 2, pp. 222–224, 2000.

[5] J.-Y. Zheng, Y.-H. Yin, and B.-Y. Li, "A new scheme for climate regionalization in China," *Acta Geographicasinica*, vol. 6, no. 1, pp. 3–11, 2010.

[6] J.-Y. Zheng, J.-J. Bian, Q.-S. Ge, and Y.-H. Yin, "The climate regionalization in China for 1951–1980 and 1981–2010," *Geographical Research*, vol. 32, no. 6, pp. 988–997, 2013.

[7] H. L. Penman, "Natural evaporation from open water, bare soil and grass," *Proceedings of the Royal Society of London, Series A: Mathematical and Physical Sciences*, vol. 193, pp. 120–145, 1948.

[8] Q. Zhang, C.-Y. Xu, and Z.-X. Zhang, "Observed changes of drought/wetness episodes in the Pearl River basin, China, using the standardized precipitation index and aridity index," *Theoretical and Applied Climatology*, vol. 98, no. 1-2, pp. 89–99, 2009.

[9] Z. Yuan, D.-H. Yan, Z.-Y. Yang, J. Yin, and Y. Yuan, "Research on temporal and spatial change of 400 mm and 800 mm rainfall contours of China in 1961–2000," *Advances in Water Science*, vol. 25, no. 4, pp. 494–502, 2014.

[10] X.-M. Liu, D. Zhang, Y.-Z. Luo, and C.-M. Liu, "Spatial and temporal changes in aridity index in northwest China: 1960 to 2010," *Theoretical and Applied Climatology*, vol. 112, no. 1-2, pp. 307–316, 2013.

[11] M. Türkeş, "Spatial and temporal variations in precipitation and aridity index series of Turkey," in *Mediterranean Climate: Variability and Trends*, H.-J. Bölle, Ed., Regional Climate Studies, chapter 5, pp. 181–213, Springer, Berlin, Germany, 2003.

[12] H. Tabari and M.-B. Aghajanloo, "Temporal pattern of aridity index in Iran with considering precipitation and evapotranspiration trends," *International Journal of Climatology*, vol. 33, no. 2, pp. 396–409, 2013.

[13] P. T. Nastos, N. Politi, and J. Kapsomenakis, "Spatial and temporal variability of the aridity index in Greece," *Atmospheric Research*, vol. 119, pp. 140–152, 2013.

[14] H.-P. Huang, Y.-P. Han, M.-M. Cao, J.-X. Song, H. Xiao, and W.-L. Cheng, "Spatiotemporal characteristics of evapotranspiration paradox and impact factors in China in the period of 1960–2013," *Advances in Meteorology*, vol. 2015, Article ID 519207, 10 pages, 2015.

[15] R. G. Allen, L. S. Pereira, D. Raes, and M. Smith, "Crop evapotranspiration guidelines for computing crop water requirements," FAO Irrigation and Drainage Paper 56, Food and Agriculture Organization of the United Nations, Rome, Italy, 1998.

[16] J. A. Hevesi, J. D. Istok, and A. L. Flint, "Precipitation estimation in mountainous terrain using multivariate geostatistics. Part I: structural analysis," *Journal of Applied Meteorology*, vol. 31, no. 7, pp. 661–676, 1992.

[17] J. A. Hevesi, A. L. Flint, and J. D. Istok, "Precipitation estimation in mountainous terrain using multivariate geostatistics. Part II: isohyetal maps," *Journal of Applied Meteorology*, vol. 31, no. 7, pp. 677–688, 1992.

[18] H. Wang, D.-H. Yan, D.-Y. Qin, and J.-H. Wang, "A study of the spatial shift of 400 mm rainfall contours in the Yellow River Basin during recent 50 years," *Advances in Earth Science*, vol. 20, no. 6, pp. 649–655, 2005.

[19] W.-Q. Xing, W.-G. Wang, Q.-X. Shao, S.-Z. Peng, Z.-B. Yu, and J. Taylor, "Changes of reference evapotranspiration in the Haihe River Basin: present observations and future projection from climatic variables through multi-model ensemble," *Global and Planetary Change*, vol. 115, pp. 1–15, 2014.

[20] H. B. Mann, "Non-parametric tests against trend," *Econometrica*, vol. 13, pp. 245–259, 1945.

[21] M. G. Kendall, *Rank Correlation Measures*, Charles Griffin, London, UK, 1975.

[22] Y. Dinpashoh, D. Jhajharia, A. Fakheri-Fard, V. P. Singh, and E. Kahya, "Trends in reference crop evapotranspiration over Iran," *Journal of Hydrology*, vol. 399, no. 3-4, pp. 422–433, 2011.

[23] J.-L. Fu, W.-H. Qian, and X. Lin, "Trends in graded precipitation in China from 1961 to 2000," *Advances in Atmospheric Sciences*, vol. 25, no. 2, pp. 267–278, 2008.

Hindawi Publishing Corporation
Advances in Meteorology
Volume 2016, Article ID 2905198, 14 pages
http://dx.doi.org/10.1155/2016/2905198

Research Article

Possible Future Climate Change Impacts on the Hydrological Drought Events in the Weihe River Basin, China

Fei Yuan,[1] Mingwei Ma,[1] Liliang Ren,[1] Hongren Shen,[1] Yue Li,[2] Shanhu Jiang,[1] Xiaoli Yang,[1] Chongxu Zhao,[1] and Hao Kong[1]

[1] *State Key Laboratory of Hydrology-Water Resources and Hydraulic Engineering, College of Hydrology and Water Resources, Hohai University, 1 Xikang Road, Nanjing 210098, China*
[2] *Patent Examination Cooperation Center of the Patent Office, SIPO, Henan, Zhengzhou 450000, China*

Correspondence should be addressed to Fei Yuan; fyuan@hhu.edu.cn

Received 29 May 2015; Revised 23 September 2015; Accepted 28 September 2015

Academic Editor: Maurits W. Ertsen

Quantitative evaluation of future climate change impacts on hydrological drought characteristics is one of important measures for implementing sustainable water resources management and effective disaster mitigation in drought-prone regions under the changing environment. In this study, a modeling system for projecting the potential future climate change impacts on hydrological droughts in the Weihe River basin (WRB) in North China is presented. This system consists of a large-scale hydrological model driven by climate outputs from three climate models (CMs) for future streamflow projections, a probabilistic model for univariate drought assessment, and a copula-based bivariate model for joint drought frequency analysis under historical and future climates. With the observed historical climate data as the inputs, the Variable Infiltration Capacity hydrological model projects an overall runoff reduction in the WRB under the Intergovernmental Panel on Climate Change A1B scenario. The univariate drought assessment found that although fewer hydrological drought events would occur under A1B scenario, drought duration and severity tend to increase remarkably. Moreover, the bivariate drought assessment reveals that future droughts in the same return period as the baseline droughts would become more serious. With these trends in the future, the hydrological drought situation in the WRB would be further deteriorated.

1. Introduction

Nowadays our societies are in much more urgent need of water resources, particularly in the drought-prone territories in China and in other parts of the world. In such regions, increasingly frequent droughts are becoming a main threat to local socioeconomic and ecoenvironment systems [1]. Even in humid areas of South China, where droughts used to be less frequent, several long-lasting, severe, and widespread drought events were witnessed in the 2000s and 2010s, causing serious water shortage problems and sharp damage (e.g., the severe 2010 drought in Southwest China) [2, 3]. In Northern China, such as the Yellow River basin (YRB), drought situations can be even worse because of the semiarid to arid climatology and limited atmospheric water sources [4]. Therefore, the focus of this study is on the largest tributary of YRB, that is, the drought-prone Weihe River basin (WRB), where large human population, extensive areas of rainfall and/or irrigation-fed agriculture, rapid industrial and economic developments, and vulnerable ecological and environmental systems meet and conflict between water supply and demand. Several studies have shown that the WRB suffered from disastrous drought periods in history (e.g., 1962, 1972, 1987, and 1990s) and the drought trends of this region tend to deteriorate as well [5, 6]. For mitigation purposes, the water volume stored in river systems (e.g., streamflow) is often analyzed to define hydrological droughts. Based on the theory of runs, drought variables (e.g., duration and severity) can also be extracted to investigate their univariate and multivariate probabilistic properties and frequency analysis [7, 8]. However, the hydrological drought characteristics of the YRB have not yet been systematically investigated and

reported. On the other hand, although [9–12] studied the variations of runoff/streamflow and its responses to climate change in the WRB, it is still unclear how potential climate change (especially the global warming) impacts future extreme hydrological drought events in this region.

Therefore this study aims to propose an effective framework to evaluate historical (1961–1990 as baseline period) drought conditions and to project future (2011–2040 as climate change period) hydrological drought properties in the WRB. Specifically, the new framework consists of four components: (1) the Variable Infiltration Capacity (VIC) hydrologic model driven by climate outputs from three climate models (CMs) for future streamflow projections, (2) a drought variable identification model for drought severity and duration based on the theory of runs, (3) a probabilistic model for univariate drought assessment and frequency analysis (duration and severity) under historical and future climates, and (4) a copula-based model for bivariate drought assessment and joint frequency analysis. This framework provides quantitative evaluation of climate change impacts on hydrological drought characteristics in the WRB.

Though [13] applied similar approaches to a river basin in USA, they adopted the Thornthwaite water balance model (a simple conceptual hydrologic model) to simulate future runoff and used the standardized streamflow index to define hydrological droughts. In this study, the authors employed the physically based VIC distributed hydrological model for historical streamflow simulations and future runoff projections. In addition, streamflow at certain levels was directly used as truncation thresholds to define hydrological drought duration and severity. This approach makes it more convenient to compare historical and future drought properties and to interpret climate change impacts on drought characteristics. Moreover, the adopted CMs and univariate and copula-based multivariate models are also quite different from those of [13]. In general, such a study using multimodels (climatic, hydrological, and multivariate probabilistic) has not been documented in the WRB. This work is expected to fill the research gap of future climate change impacts on hydrological droughts and to provide reliable data support for upgrading water resources management and adaptation strategies in response to changing environment in this region.

2. Study Area

The Weihe River is the longest tributary of the Yellow River in North China, with a drainage area of 1.348×10^5 km^2 (Figure 1). The river basin is dominated by continental monsoon climate and characterized as semiarid region. The annual mean temperature ranges between 9.3°C and 14.4°C. The mean annual precipitation is 511.3~659.1 mm, with a distinct increase from northwest to southeast. Precipitation mainly occurs from June to November, which accounts for 70.8~74.2% of annual precipitation. Snow generally occurs in winter in the entire basin. The spatiotemporal distribution of runoff is similar to precipitation, with basin-averaged mean annual runoff depth being less than 100 mm. The basin is prone to droughts. Agricultural losses due to local drought disasters occupy over 50% of the total losses. Recent climate

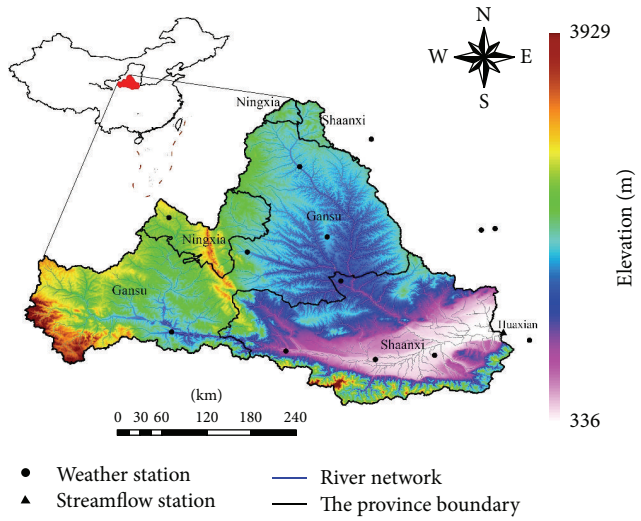

Figure 1: Map of study area.

change has deteriorated the water shortage situation in the WRB and resulted in more severe drought events. Thus it is necessary to assess the possible climate change impacts on regional hydrological drought events. In this study, the area controlled by Huaxian streamflow station (upstream area of 1.065×10^5 km^2, Figure 1) was selected as the study region.

3. Data and Methodology

3.1. Data. Historical meteorological data of thirteen weather stations within or nearby the basin (Figure 1) were obtained from China Meteorological Administration. These data include daily records of maximum and minimum air temperature and precipitation during the period of 1961–2012. The whole basin was divided into 213 grid cells at a 0.25° resolution. All the station-based daily precipitation and air temperature data were interpolated to each 0.25° grid cell by the nearest neighbor method. Topographical effects were not considered in precipitation interpolation, while near-surface air temperature was assumed to decrease by 0.65°C per altitude rise of 100 m.

China's land-use/cover data sets with 5 or 10 yr intervals between 1980 and 2010 [14] were used to analyze the land-use change in the study area. It shows that cropland, the dominant land-use type in the region of the middle and lower reaches, has a downward trend since late 1980s. The cover ratio of woodland in the upstream region drops sharply since late 1980s and approximately trends to be stable after the 1990s. The built-up area increased notably since 1980, implying the rapid urbanization in this region. The coverage of water bodies, which refer to the lakes, reservoirs, ponds, and other water retaining projects for the irrigations, has also shown an upward trend. Furthermore, the Pettitt jump test for the annual runoff depth time series from 1961 to 2012 at Huaxian station indicates that the year 1990 is the abrupt change point in annual runoff with a significant decrease trend since 1990. Meanwhile, the consistency test with the double mass curve of the cumulative annual areal mean precipitation and observed

runoff depth shows that runoff coefficient tends to decrease since 1990 as well. Therefore, considering the change patterns of land-use, precipitation and runoff, the period of 1961–1990 was defined as the baseline period for hydrological drought projections in this study.

Climate data sets from three climate models (CMs) were adopted in this study. They are Australian Commonwealth Scientific and Research Organization (CSIRO) Mk 3.5 Global Climate Model (GCM), German Max Planck Institute for Meteorology (MPI) ECHAM 5 GCM, and Hadley Centre's Providing Regional Climates for Impacts Studies (PRECIS) regional climate model (RCM). The CSIRO and MPI GCMs run at a spatial resolution of $1.875^\circ \times 1.875^\circ$ and $2.0^\circ \times 2.0^\circ$, respectively. The output of these two GCMs was statistically downscaled to a 50 km × 50 km resolution by the bilinear interpolation and quantile-mapping methods. The PRECIS RCM dynamically downscales the HadAM3H GCM data from the $1.25^\circ \times 1.875^\circ$ resolution to 50 km × 50 km. The three CM data sets are composed of the simulated daily maximum and minimum air temperature and precipitation in the baseline period of 1961–1990 and in the years of 2011–2040 under A1B scenario of the Intergovernmental Panel on Climate Change (IPCC) Special Report on Emission Scenarios (SRES) [15]. The IPCC-SRES A1B shows rapid economic growth, especially in developing nations, with a balance across all energy sources for economic development, and it has been adopted as the most commonly used emission scenario for climate change studies in China [16, 17]. Furthermore, linear interpolation was performed to transform the three downscaled CM data sets (50 km × 50 km) to a 0.25° resolution. In this study, the observed historical climate data set in 1961–1990 was directly employed as the baseline climatology. To bias-correct the CM data sets, the delta-change method was used, which superimposes the mean monthly anomalies between the CM-simulated baseline and A1B climate data on the observed historical meteorology to represent future climate. In this way, three future climate data sets were finally constructed for three future scenarios, namely, A1B PRECIS, A1B CSIRO, and A1B MPI.

3.2. Variable Infiltration Capacity Hydrological Model. The Variable Infiltration Capacity (VIC) model [18, 19] is a state-of-the-art physically based distributed hydrological model. It simulates radiative fluxes, turbulent fluxes of momentum, sensible heat, unsaturated liquid water transport, saturated gravitational drainage, surface runoff, bottom drainage evapotranspiration, freezing, and thawing of soil ice at each land grid cell. Additionally, a conceptual streamflow routing model is included to route the computed runoff depth at each grid cell to the watershed outlets. The routing model simulates two processes: (1) runoff concentration on the outflow of each grid cell is represented by the linear reservoir method; (2) the routing effect of channel system connecting grid cells is represented by the Muskingum routing algorithm [20].

In this study, the vegetation and soil parameters of the VIC model were spatially estimated a priori according to vegetation and soil texture classes at each grid cell. For each type of vegetation, the vegetation parameters, such as architectural resistance r_a (s/m), albedo α, minimum stomata resistance r_{smin} (s/m), leaf-area index LAI, roughness length z_0 (m), and zero-plane displacement d_0 (m), were derived on the basis of the vegetation parameter information from Land Data Assimilation Systems (LDAS, http://ldas.gsfc.nasa.gov/gldas/GLDASmapveg.php). The individual soil parameters used in VIC, such as porosity θ_s, saturated soil potential ψ_s, saturated hydraulic conductivity K_s, and bulk density BD, were derived according to the work of [21, 22]. In addition, two insensitive hydrologic parameters of VIC were estimated a priori according to the work of [23]. These parameters are the following: (1) D_{soil}: soil depth of each soil layer (three layers in this study) is set as 0.1 m, 0.5 m, and 1.5 m, respectively; (2) W_s: the fraction of the maximum soil moisture (of the lowest soil layer) where nonlinear baseflow occurs is defined as 0.99. Other sensitive VIC hydrologic parameters (such as Ds_{max}, maximum baseflow that can occur from the lowest soil layer; Ds, fraction of Ds_{max} where nonlinear baseflow begins; and b_{inf}, coefficient defining the shape of the Variable Infiltration Capacity curve) and runoff routing parameters were calibrated by fitting the daily calculated streamflow time series against the observed records. These sensitive parameters are calibrated within the predefined rational physical value ranges by the Shuffled Complex Evolution (SCE-UA) automatic optimization method [24], with the log-transformed Nash-Sutcliffe model efficiency coefficient as the objective function.

In this study, the gridded baseline and three future climate data sets were, respectively, used to drive the VIC model for daily streamflow simulations and projections at Huaxian station. Subsequently, the monthly simulated streamflow time series accumulated from the daily time series were analyzed to assess hydrological drought properties using univariate and bivariate drought distributions.

3.3. Univariate Drought Distribution Model. The VIC-simulated monthly streamflow time series were used to identify the hydrological drought events under the baseline (1961–1990) and three A1B (2011–2040) scenarios by the theory of runs. Following [25], three truncation levels of streamflow, Q_0, Q_1, and Q_2 ($Q_0 > Q_1 > Q_2$), were used to identify the hydrological drought events and relevant drought characteristics (Figure 2). As shown in Figure 2, four possible hydrological drought events (indicated as *a*, *b*, *c*, and *d*) are preliminarily identified during the period when the simulated monthly streamflow is below the truncation streamflow Q_1. For the events with one-month duration (*a* and *d* in Figure 2), only the event *a* is finally identified to be a drought event as its monthly streamflow is below the truncation streamflow Q_2, but the event *d* is rejected to be a hydrological drought with its monthly streamflow being above Q_2. For the two sequential events with the interval time of one month (*b* and *c* in Figure 2), the two events *b* and *c* are combined to be one drought event on the condition that the monthly streamflow at the interval is below the truncation streamflow Q_0; otherwise the events *b* and *c* are considered to be two independent drought events. For each identified drought event, the corresponding drought severity is the cumulative deviation below the truncation streamflow Q_1 during

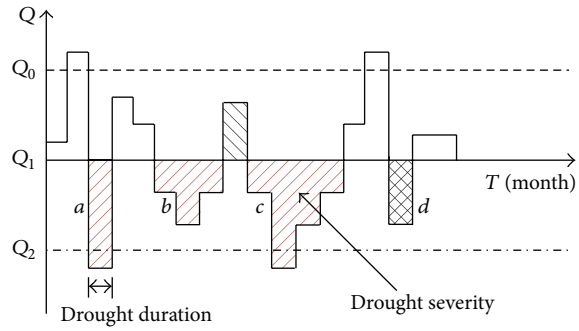

Figure 2: Diagram of drought identification using the theory of runs.

the drought duration (Figure 2). According to Standard for Information and Hydrological Forecasting of China [26], the truncation streamflow Q_0 in this study was defined to be the monthly mean of the simulated streamflow time series from 1961 to 1990 at Huaxian station, and Q_1 and Q_2 were assumed to be 10% and 20% below Q_0, respectively.

Using the drought identification scheme (Figure 2), the drought variables of duration and severity were derived for each drought event under the baseline and A1B PRECIS, A1B CSIRO, and A1B MPI scenarios. For the analysis using univariate drought distributions, the exponential and Weibull distributions were, respectively, used to fit the drought duration and severity samples under the baseline and three future scenarios, and the maximum likelihood method was used to estimate the distribution parameters. Additionally, the univariate return periods of drought events regarding only one variable (drought duration or severity) were also derived under the baseline and three A1B scenarios, which are shown as follows:

$$T_D = \frac{E(L)}{1 - F_D(d)}, \qquad T_S = \frac{E(L)}{1 - F_S(s)}, \tag{1}$$

where D and S denote drought duration and severity, respectively; T_D and T_S represent the univariate return period for droughts with $D \geq d$ and $S \geqslant s$, respectively; $E(L)$ is the mean interarrival time of droughts; $F_D(d)$ and $F_S(s)$ are the cumulative probability distribution functions of drought duration and severity, respectively.

3.4. Bivariate Drought Distribution Model. In reality, drought duration and severity are often significantly correlated. Therefore, the relevance between drought duration and severity should be carefully taken into account when using both drought variables for drought frequency analysis. Copulas are functions that link univariate distribution functions to form multivariate distributions [27, 28]. They are useful tools to effectively reflect the correlation features among multiple drought variables. With simple forms and good accuracies, the Archimedean copulas have been widely applied in drought studies [7, 13]. In this study, four Archimedean copulas were used to establish bivariate drought distribution that describes the joint probabilities of drought duration and severity. They are Gumbel-Hougaard, Clayton, Frank, and Ali-Mikhail-Haq copulas. Given the univariate distributions of drought duration and severity ($F_D(d)$ and $F_S(s)$), the joint distributions for drought duration and drought severity using the four Archimedean copulas can be, respectively, formulated as follows:

$$F_{D,S}(d,s) = \exp\left\{-\left[(-\ln F_D(d))^{\theta} + (-\ln F_S(s))^{\theta}\right]^{1/\theta}\right\}, \tag{2}$$

$$F_{D,S}(d,s) = \left(F_D(d)^{-\theta} + F_S(s)^{-\theta} - 1\right)^{-1/\theta}, \tag{3}$$

$$F_{D,S}(d,s) = -\frac{1}{\theta}\ln\left[1 + \frac{\left(e^{-\theta F_D(d)} - 1\right)\left(e^{-\theta F_S(s)} - 1\right)}{\left(e^{-\theta} - 1\right)}\right], \tag{4}$$

$$F_{D,S}(d,s) = \frac{(1-\theta)F_D(d)F_S(s)}{\{1-\theta[1-F_D(d)]\}\{1-\theta[1-F_D(d)]\} - \theta F_D(d)F_S(s)}, \tag{5}$$

where $F_{D,S}(d,s)$ is the joint probability distribution of drought duration and severity; θ is the copula parameter representing the degree of association between $F_D(d)$ and $F_S(s)$.

With the joint probability distribution of drought duration and severity, conditional probability can also be calculated. Given drought duration exceeding a certain threshold d, the probability of drought severity is defined as

$$P(S \leq s \mid D \geq d) = \frac{P(S \leqslant s, D \geqslant d)}{P(D \geqslant d)} = \frac{F_S(s) - F_{DS}(d,s)}{1 - F_D(d)}. \tag{6}$$

In addition, two types of bivariate return periods, defined as T_{DS}^{AND} and T_{DS}^{OR}, were calculated. T_{DS}^{AND} represents the return period when both drought duration and severity exceed their specific values:

$$T_{DS}^{AND} = \frac{E(L)}{P(D \geqslant d, S \geqslant s)} = \frac{E(L)}{1 - F_D(d) - F_S(s) + F_{DS}(d,s)}, \tag{7}$$

and T_{DS}^{OR} denotes the return period when drought duration is higher than a specific value or drought severity exceeds another specific value:

$$T_{DS}^{OR} = \frac{E(L)}{P(D \geqslant d \text{ or } S \geqslant s)} = \frac{E(L)}{1 - F_{DS}(d,s)}. \tag{8}$$

4. Results

4.1. Historical Hydrological Streamflow Simulations. Historical daily streamflow in the baseline period (1961–1990) at Huaxian station was simulated using the VIC model fed with the observed precipitation and air temperature data (baseline climate data set). The VIC model was calibrated by fitting the

Table 1: Performance of historical monthly streamflow simulations at Huaxian station.

Periods	Nash-Sutcliffe coefficient	Log-transformed Nash-Sutcliffe coefficient	Bias (%)
Calibration (1961–1980)	0.829	0.715	3.1
Validation (1981–1990)	0.902	0.809	7.3

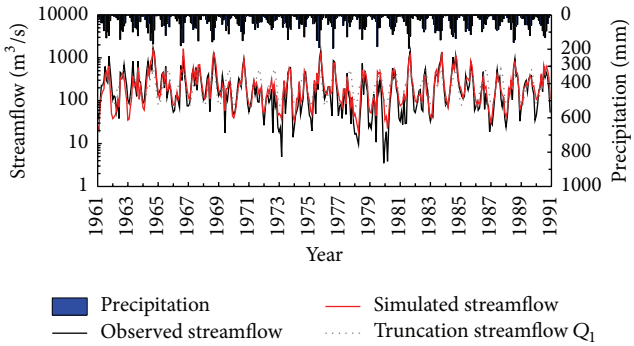

Figure 3: Observed and simulated monthly hydrographs at Huaxian station in the years 1961–1990.

Table 2: RMSE of fitting four copula functions to joint distributions for drought severity and duration under baseline and three A1B scenarios.

Scenarios	RMSE			
	Gumbel-Hougaard	Clayton	Frank	Ali-Mikhail-Haq
Baseline	0.2334	**0.0465**	0.1655	0.8975
A1B PRECIS	0.2368	**0.0536**	0.1746	0.2117
A1B CSIRO	0.2313	**0.0681**	0.1682	0.1569
A1B MPI	0.2309	**0.0703**	0.1425	1.6671

calculated daily streamflow against the observed streamflow at Huaxian station with the aid of the Shuffled Complex Evolution (SCE-UA) automatic optimization method. Table 1 and Figure 3 show that the VIC model can provide reasonable streamflow simulations in calibration and validation periods in terms of the log-transformed Nash-Sutcliffe model efficiency coefficient and the relative error (bias) between the simulated and the observed total runoff.

4.2. Validation of Historical Hydrological Droughts. According to the theory of runs, the simulated monthly streamflow time series at Huaxian station in the baseline period (1961–1990) were used to derive the historical hydrological drought characteristics for univariate and bivariate drought analysis. For univariate drought analysis, the exponential and Weibull distributions were adopted to fit the identified historical drought duration and severity samples, respectively. The two-sample Kolmogorov-Smirnov (K-S) test was used to test whether the selected theoretical distributions are able to effectively represent the distributions of drought duration and severity, respectively. Figure 4(a) shows that the Z-score of the K-S test statistics ($Z_{\text{K-S}}$) is much lower than the critical Z-score (Z_{cri}) at a 5% significance level, indicating that the historical drought duration and severity samples are in a good agreement with the exponential and Weibull distributions, respectively. To derive the joint distribution for the historical drought severity and duration, four copula functions were adopted. The root mean square error (RMSE) was used to calculate the biases between the empirical and theoretical joint distributions. Table 2 shows that the Clayton copula has the lowest RMSE among all the four copulas, and the Pearson correlation coefficient between the empirical probability and the Clayton-based theoretical joint probability is 0.991 in the baseline period (Figure 5(a)), implying that the Clayton copula is able to fit the joint duration-severity probability distribution for the historical drought events with very high accuracy.

Given that the records of historical hydrological droughts were not available in the WRB, the findings of [29] were used to validate the feasibility of the univariate and bivariate probabilistic models in identifying historical hydrological droughts. Reference [29] made survey of statistics on the historical droughts in provincial administrative regions in China in the years 1949–2000 and defined drought situations regarding the annual reduction rate of grain yield. For instance, a severe drought year refers to the time period when local annual grain yield reduces by 5~7%, and an extreme drought year with a reduction rate of over 7%. Figure 1 indicates that Shaanxi and Gansu provinces occupy the WRB predominantly. Therefore, the annual records with severe droughts or extreme droughts in Shaanxi or Gansu were used for historical hydrological drought validation. As shown in Table 3, severe droughts or/and extreme severe droughts occurred in Shaanxi or/and Gansu for twelve years in the baseline period (1961–1990), and the top ten most severe drought events in the baseline period (1961–1990) identified by the univariate and bivariate drought models were compared with the severe and extreme drought records in Shaanxi and Gansu. Table 3 shows that the univariate and bivariate drought models in this study are able to effectively identify most historical drought years with severe and extreme drought conditions in Shaanxi and Gansu provinces. Although the historical agricultural drought records from [29] are mostly consistent with the modeling results, it is still necessary to collect the hydrological drought records for model validation in future studies so as to improve the credibility of the drought models.

4.3. Projected Changes in Hydrometeorological Variables. The baseline mean monthly air temperature and precipitation were compared with the corresponding projected A1B values (Figures 6(a) and 6(b)). It is found that the three CMs project a considerable increase in air temperature under A1B throughout the whole year, with a rise of 1.0~2.0°C

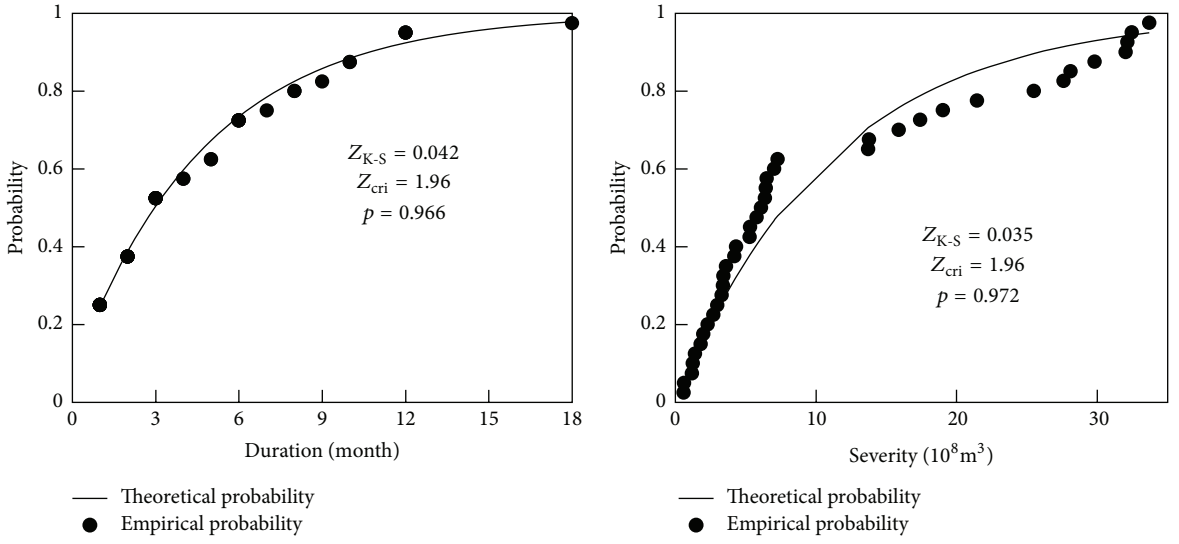

(a) Baseline

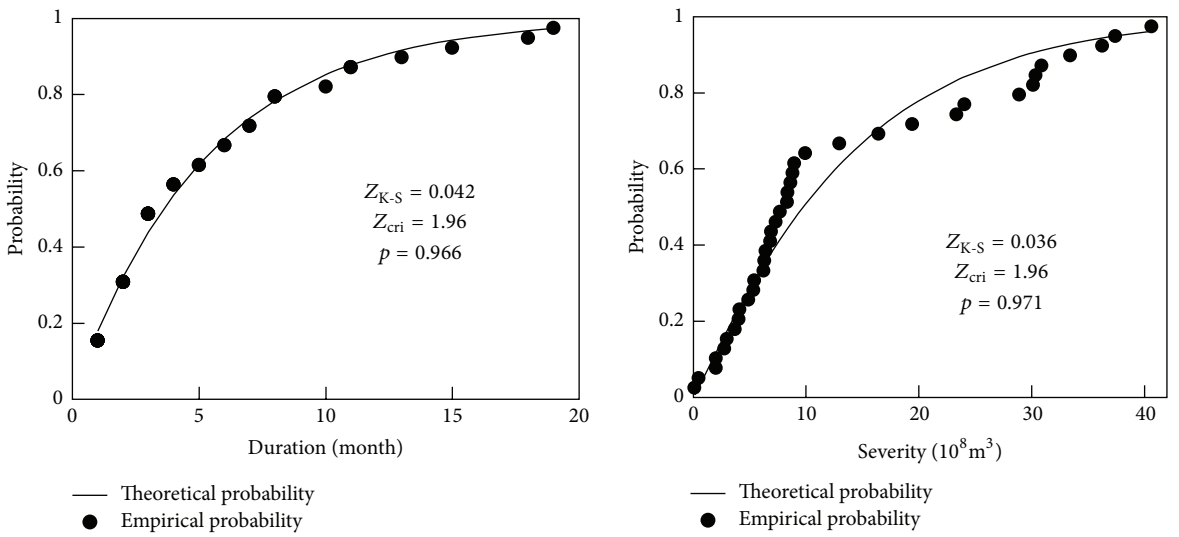

(b) A1B PRECIS

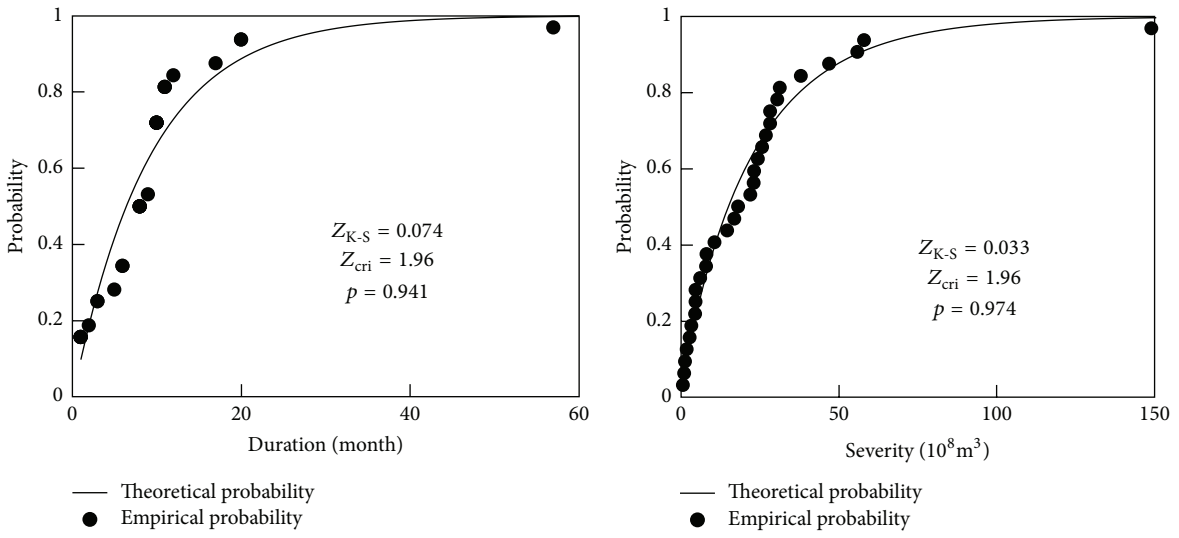

(c) A1B CSIRO

Figure 4: Continued.

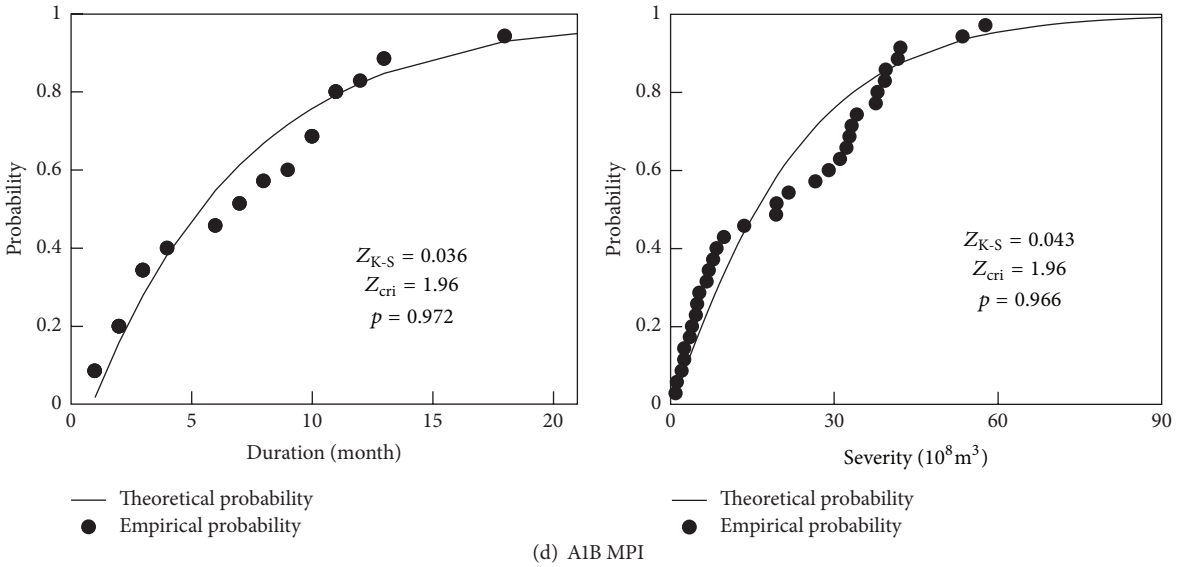

(d) A1B MPI

Figure 4: Theoretical distribution fitting for severity and duration under baseline and A1B scenarios with Z-score of two-sample Kolmogorov-Smirnov test statistics ($Z_{K\text{-}S}$ is the calculated Z-score of the K-S test statistics and Z_{cri} is the critical Z-score at a 5% significance level).

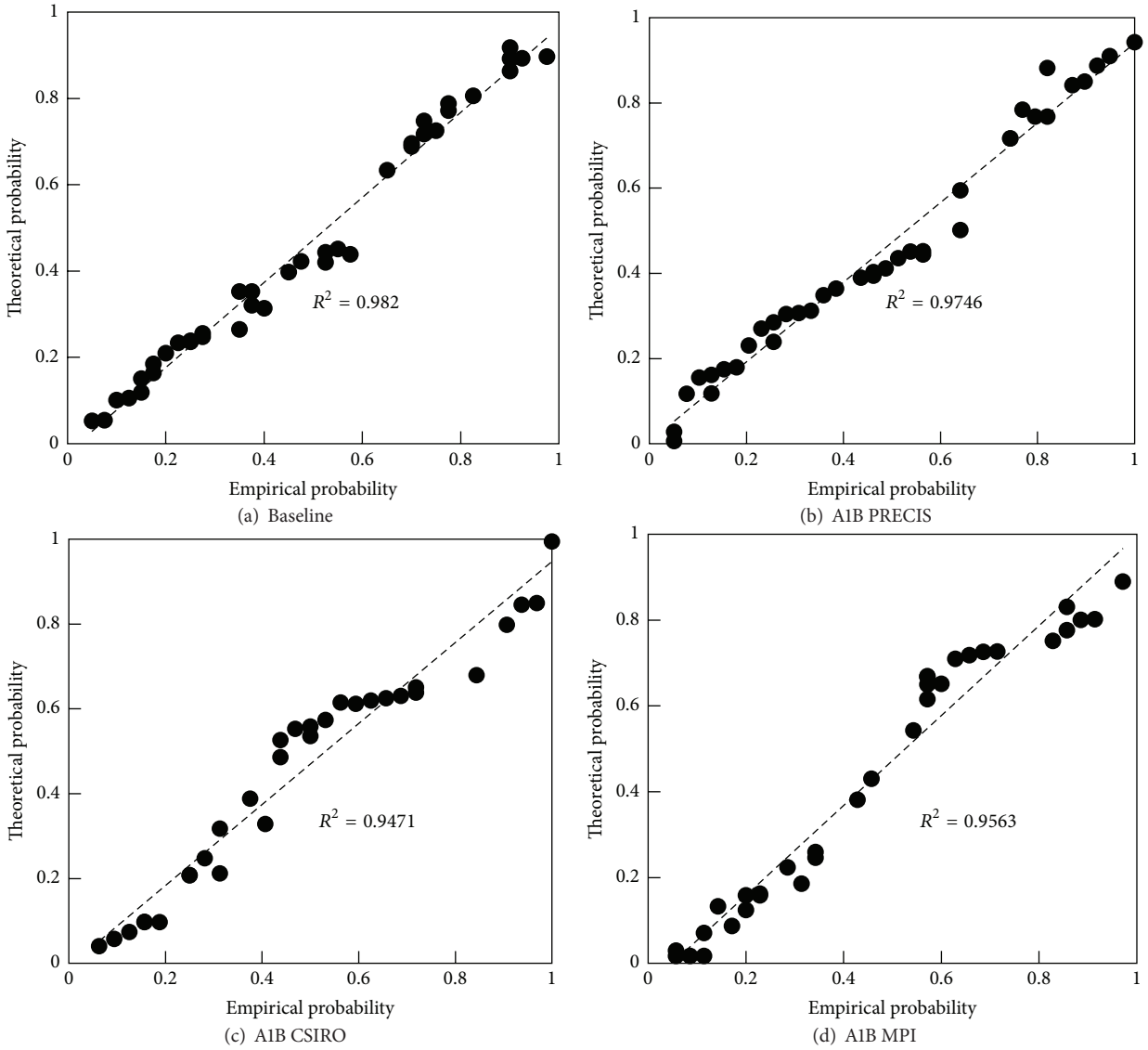

(a) Baseline
(b) A1B PRECIS
(c) A1B CSIRO
(d) A1B MPI

Figure 5: Empirical and theoretical joint probabilities of drought severity and duration under baseline and three A1B scenarios.

Table 3: Validation of univariate/bivariate model-based droughts against historical severe and extreme drought records in the baseline period (1961–1990).

Year	Historical drought conditions		Univariate model (Severity)	Univariate model (Duration)	Bivariate model (Duration-severity)
	Shaanxi	Gansu			
1962	*Severe*	*Extreme*	*Y*	*Y*	*Y*
1966	Moderate	*Severe*	*Y*	*Y*	*N*
1969	Mild	*Severe*	*Y*	*Y*	*Y*
1971	Moderate	*Extreme*	*Y*	*Y*	*Y*
1972	*Severe*	*Extreme*	*Y*	*Y*	*Y*
1973	Mild	*Extreme*	*Y*	*Y*	*Y*
1979	Mild	*Severe*	*N*	*Y*	*N*
1980	*Severe*	Moderate	*Y*	*Y*	*Y*
1981	Moderate	*Extreme*	*Y*	*Y*	*Y*
1982	Moderate	*Extreme*	*Y*	*Y*	*Y*
1986	*Severe*	Moderate	*Y*	*Y*	*Y*
1987	*Severe*	*Extreme*	*Y*	*Y*	*Y*

Note: symbol "*Y*" indicates that the univariate or bivariate drought model is able to effectively identify the historical severe or extreme drought years in Shaanxi or Gansu province; and symbol "*N*" denotes that the drought model fails to identify the historical drought records in Shaanxi or Gansu.

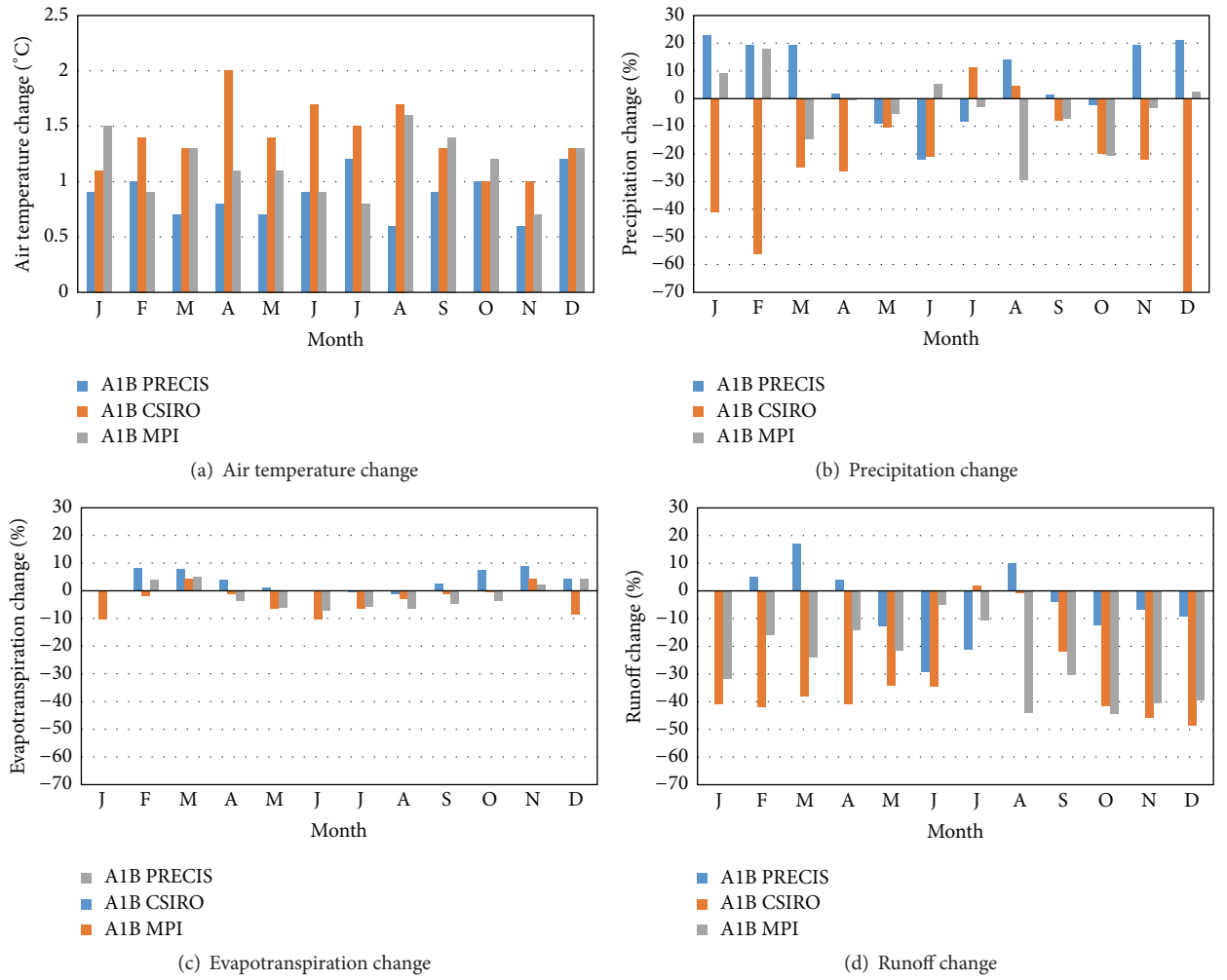

Figure 6: Projected changes in precipitation, air temperature, evapotranspiration, and runoff under A1B scenarios relative to baseline period.

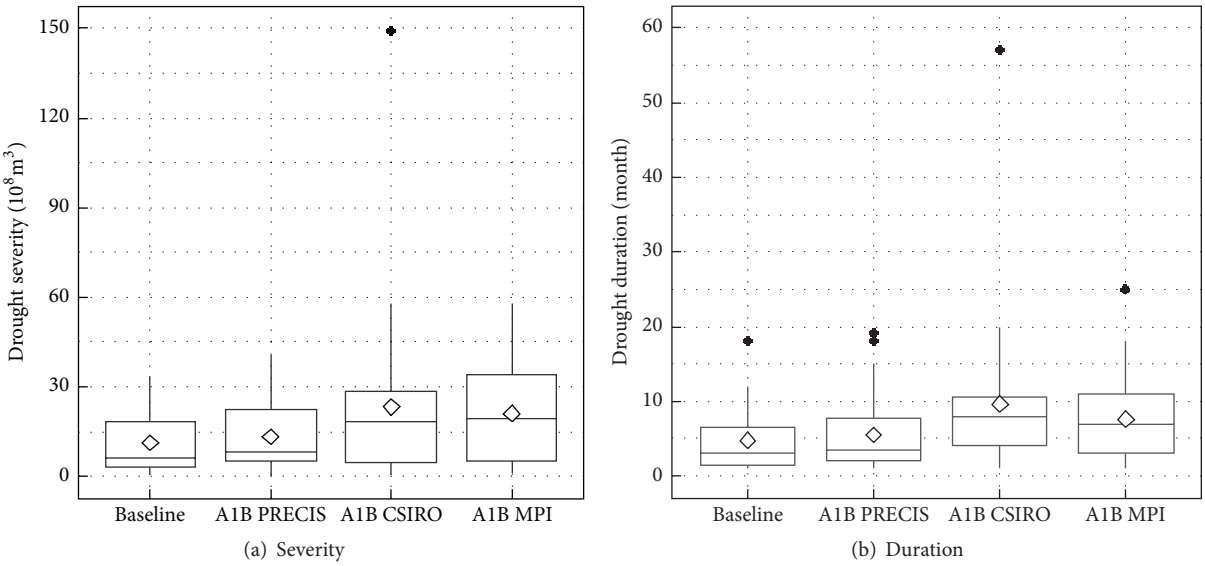

Figure 7: Boxplots for drought severity and duration samples under baseline and A1B scenarios (the diamond symbol indicates the means of drought severity or duration).

for A1B PRECIS, 1.0~2.0°C for A1B CSIRO, and 0.7~1.6°C for A1B MPI. PRECIS projects no distinct changes in mean annual precipitation under A1B scenario, with a minor drop of 1.4 mm relative to the baseline level (559.3 mm), while the CSIRO and MPI GCMs simulate a considerable reduction of 47.9 mm (8.6%) and 51.1 mm (9.1%) in mean annual precipitation under A1B. Meanwhile, all the three CMs project obvious changes in seasonal precipitation. As shown in Figure 6(b), precipitation would generally undergo a substantial decrease in most months. However, PRECIS projects a significant precipitation increase in August and November–March; CSIRO simulates a considerable remarkable rise of precipitation in July and August; MPI projects an obvious increase in precipitation in January and February.

Driven by the baseline and three future climate data sets, the VIC model was used to simulate and project hydrological processes under baseline and A1B scenarios. Although the obvious increase in air temperature potentially promotes the atmospheric demand for evapotranspiration, actual evapotranspiration would undergo a slight reduction almost throughout the year under A1B CSIRO and A1B MPI (Figure 6(c)). This is attributed to the phenomenon that both CSIRO and MPI project a considerable precipitation decrease in most months which is very likely to restrict the water supply for evapotranspiration. Using the A1B PRECIS climate data set as inputs, the VIC model projects a minor increase in evapotranspiration in spring and autumn and a slight decrease in summer. As shown in Figure 6(d), runoff would drop significantly in most months. Under A1B PRECIS, a substantial runoff increase would occur in February–April and August, mainly due to the projected remarkable precipitation rise in the same period. It is notable that although all the CMs generally project the WRB towards a drying trend in the future, the different magnitudes of air temperature and precipitation changes from different CMs are likely to lead to large uncertainties in the projected future runoff. This uncertainty may further largely impact the projections of hydrological drought events under future scenarios.

4.4. Projected Climate Change Impact on Hydrological Droughts. The simulated monthly streamflow at Huaxian station was used to derive the drought characteristics under baseline and A1B scenarios, and the identified properties of hydrological drought events were employed for univariate and copula-based bivariate drought analysis.

4.4.1. Univariate Drought Analysis. According to the theory of runs, 39 hydrological drought events were identified for the baseline period, together with 38, 31, and 34 events under A1B PRECIS, A1B CSIRO, and A1B MPI scenarios, respectively. Relative to the baseline level, fewer hydrological drought events would occur under A1B. However, the means and medians of drought variables under all three future scenarios are projected to increase considerably. Figure 7 shows that the mean drought severity and duration are 11.2×10^8 m^3 and 4.8 months for the baseline period, while the values of these drought variables would increase to be 12.9×10^8 m^3 and 5.5 months for A1B PRECIS, 18.5×10^8 m^3 and 9.6 months for A1B CSIRO, and 18.3×10^8 m^3 and 7.6 months for A1B MPI. Meanwhile, under A1B CSIRO and A1B MPI scenarios, much worse drought conditions are projected. In the baseline period, the most severe drought event was identified to be from November 1961 to April 1963, with the duration of 18 months and the severity of 29.8×10^8 m^3. However, under A1B CSIRO, a long-term extreme drought is projected from October 2020 to June 2025, with the duration and severity being up to 57 months and 149.0×10^8 m^3, respectively.

Table 4: Drought characteristics in different univariate return periods under baseline and A1B scenarios.

Return periods	Drought severity (10^8 m^3)				Drought duration (month)			
	Baseline	A1B PRECIS	A1B CSIRO	A1B MPI	Baseline	A1B PRECIS	A1B CSIRO	A1B MPI
50 years	44.2	48.0	98.2	73.9	18.4	20.5	35.8	26.1
20 years	33.8	37.6	73.5	58.3	13.9	15.7	27.4	20.1
10 years	25.9	29.5	55.2	46.1	10.7	12.0	21.1	15.7
5 years	18.1	21.2	37.4	33.4	7.3	8.4	17.4	11.2

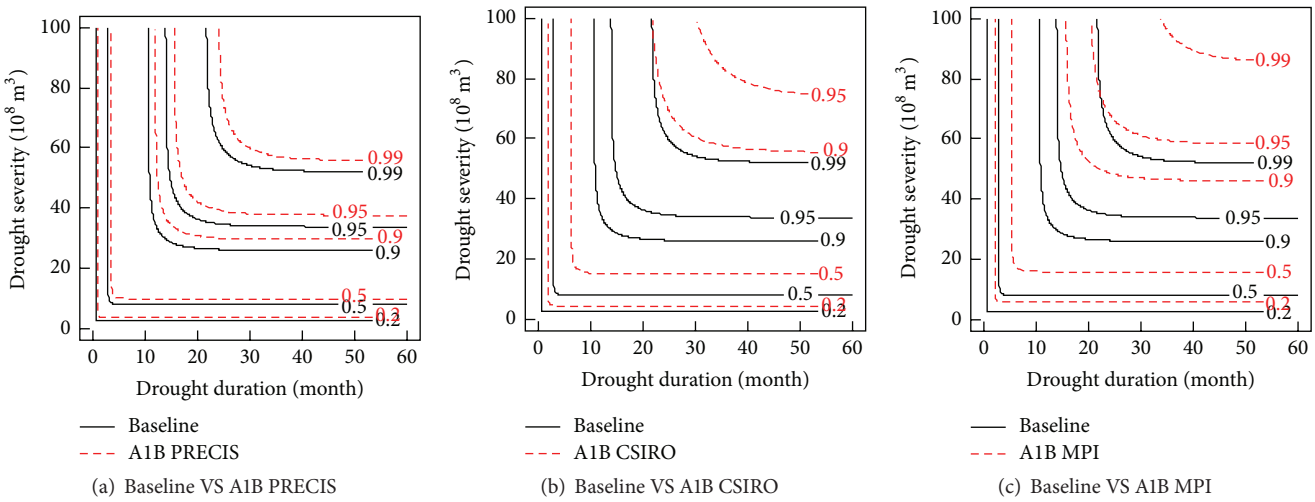

(a) Baseline VS A1B PRECIS (b) Baseline VS A1B CSIRO (c) Baseline VS A1B MPI

Figure 8: Bivariate joint probability of drought duration and severity under baseline and three A1B scenarios.

In the case of A1B MPI, the most extreme drought would occur from June 2023 to June 2025, with the duration of 25 months and the severity of 57.7 × 10^8 m^3; and a comparable extreme drought event is also projected under A1B PRECIS.

The exponential and Weibull distributions were adopted to fit the drought duration and severity samples under three future scenarios, respectively. Figures 4(b)–4(d) illustrate that the identified drought duration and severity samples preferably follow the exponential and Weibull distributions. With the univariate drought probabilistic models, drought severity and duration referring to different return periods were estimated. Table 4 shows that drought severity and duration in all return periods would increase remarkably under all three A1B scenarios, especially with the dramatic rise in the cases of A1B CSIRO and A1B MPI. Compared with the baseline situation, the 50-year drought severity would increase by 122.2% and 67.2% under A1B CSIRO and A1B MPI, and the 50-year drought duration is projected to rise by 17.4 and 7.7 months, respectively. This univariate drought analysis implies that future climate change under A1B would deteriorate the drought situation in the WRB, especially with increased frequencies of extreme hydrological drought events with higher severities and longer durations. It should be noted that the drought simulations as short as 30 years for both baseline and A1B scenarios may not sufficiently capture the changes in drought events at higher return period levels (such as 50 years) and a larger sample size of drought duration and severity data sets for both scenarios are required so as to reduce this uncertainty. In general, driven by the three CM data sets, the VIC hydrological model and the univariate probabilistic drought models project similar deteriorated drought conditions in the WRB under all three A1B scenarios, but with different magnitudes of changes in drought severity and duration. This uncertainty in drought projections might mainly result from the possible large uncertainties in climate data sets from different climate models.

4.4.2. Bivariate Drought Analysis. To derive the joint distributions of drought severity and duration under three A1B scenarios, four copula functions were adopted. Table 2 and Figures 5(b)–5(d) show that the Clayton copula is able to effectively characterize the joint duration-severity distributions under all A1B scenarios. To quantify possible future climate change impacts on drought conditions, the joint probability, conditional probability, and joint return period under all future scenarios were compared with those of the baseline period.

Figure 8 shows the contours of joint probability for drought duration and severity under baseline and future scenarios. It demonstrates that large distance exists between the contours for baseline and A1B drought events at the same probability levels. On the basis of those contours, if the same duration or severity is given for both baseline and future events, the corresponding severity or duration values under all A1B scenarios are found to be considerably larger than those of baseline drought events. In consequence,

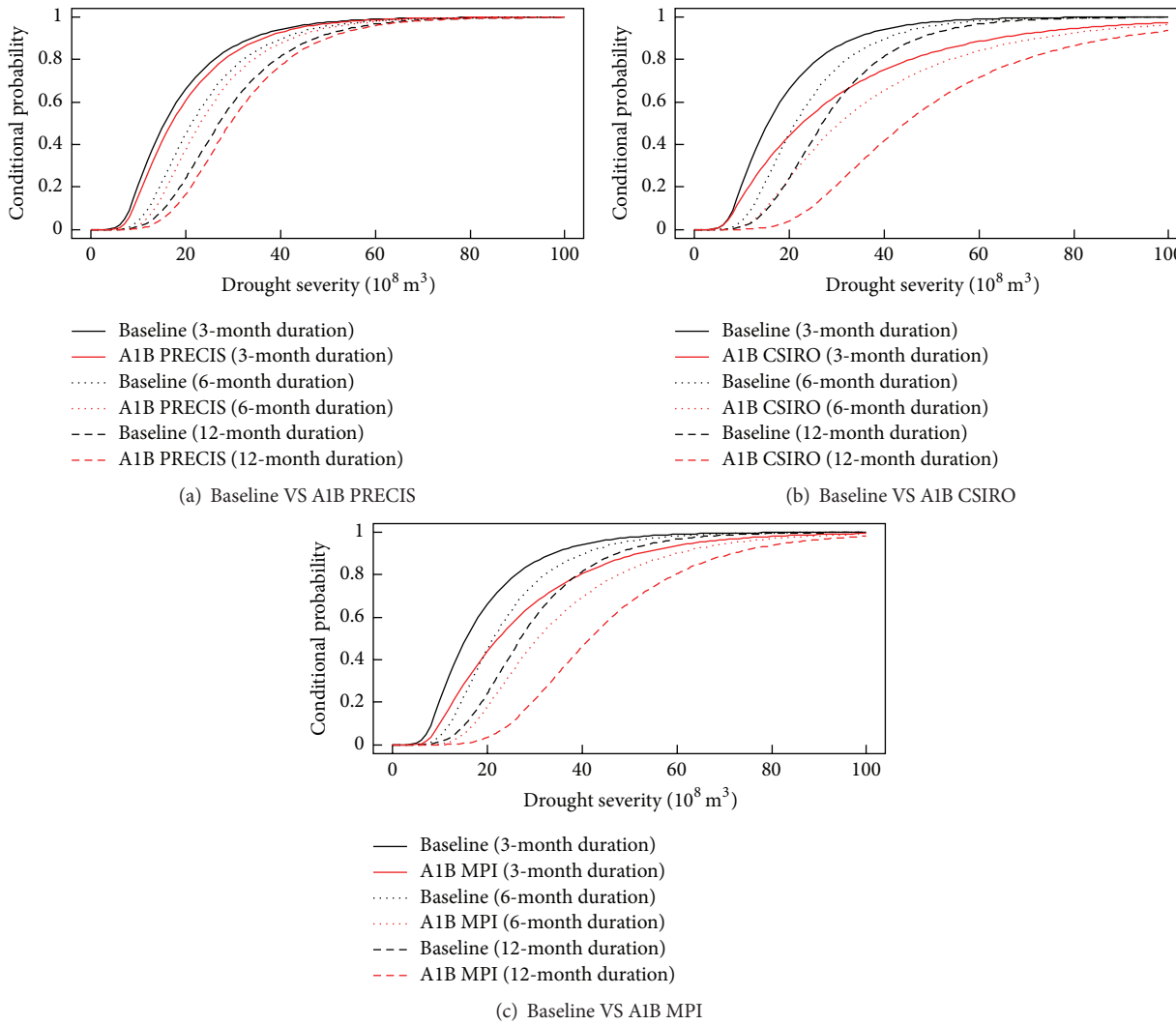

Figure 9: Conditional probability of drought severity distributions with given durations of 3, 6, and 12 months under baseline and three A1B scenarios.

more severe drought conditions are projected under three A1B scenarios, and the basin would experience the most serious hydrological drought situations under A1B CISRO and A1B MPI. This phenomenon can also be illustrated by the conditional distributions of drought severities given certain durations (Figure 9). For example, given a 6-month duration, the conditional probability of baseline drought events with severity less than or equal to 30.0×10^8 m^3 is approximately 0.758 (Figure 9(a)). However, the same probability corresponds to the A1B PRECIS drought event with severity less than or equal to 33.1×10^8 m^3 (Figure 9(a)), and such a probability is also in correspondence with the A1B CSIRO and A1B MPI drought events with severity less than or equal to 50.2×10^8 m^3 (Figure 9(b)) and 45.4×10^8 m^3 (Figure 9(c)), respectively.

Figure 10 shows the contour plots of joint severity-duration return periods of T_{DS}^{AND} and T_{DS}^{OR} under baseline and three A1B scenarios. In comparison with the baseline situation, more serious drying conditions under the three A1B scenarios are projected in terms of the calculated joint return periods. For instance, the drought event with a 10-month duration and a 40.0×10^8 m^3 severity leads to T_{DS}^{AND} of 41.3 years and T_{DS}^{OR} of 6.1 years in the baseline period. However, if the same drought event occurred under A1B PRECIS, such bivariate return periods would reduce to be 27.1 years and 5.0 years, respectively; T_{DS}^{AND} and T_{DS}^{OR} would further drop to be 7.7 years and 3.3 years under A1B MPI and to be 5.7 years and 2.8 years under A1B CSIRO.

5. Conclusions and Discussion

In this study, a modeling system for projecting the potential future climate change impacts on hydrological drought events in the WRB in North China is presented. This modeling system includes the VIC hydrological model driven by climate outputs from PRECIS RCM, CSIRO GCM, and MPI GCM for future streamflow projections, a univariate probabilistic model for drought severity and duration assessment, and a

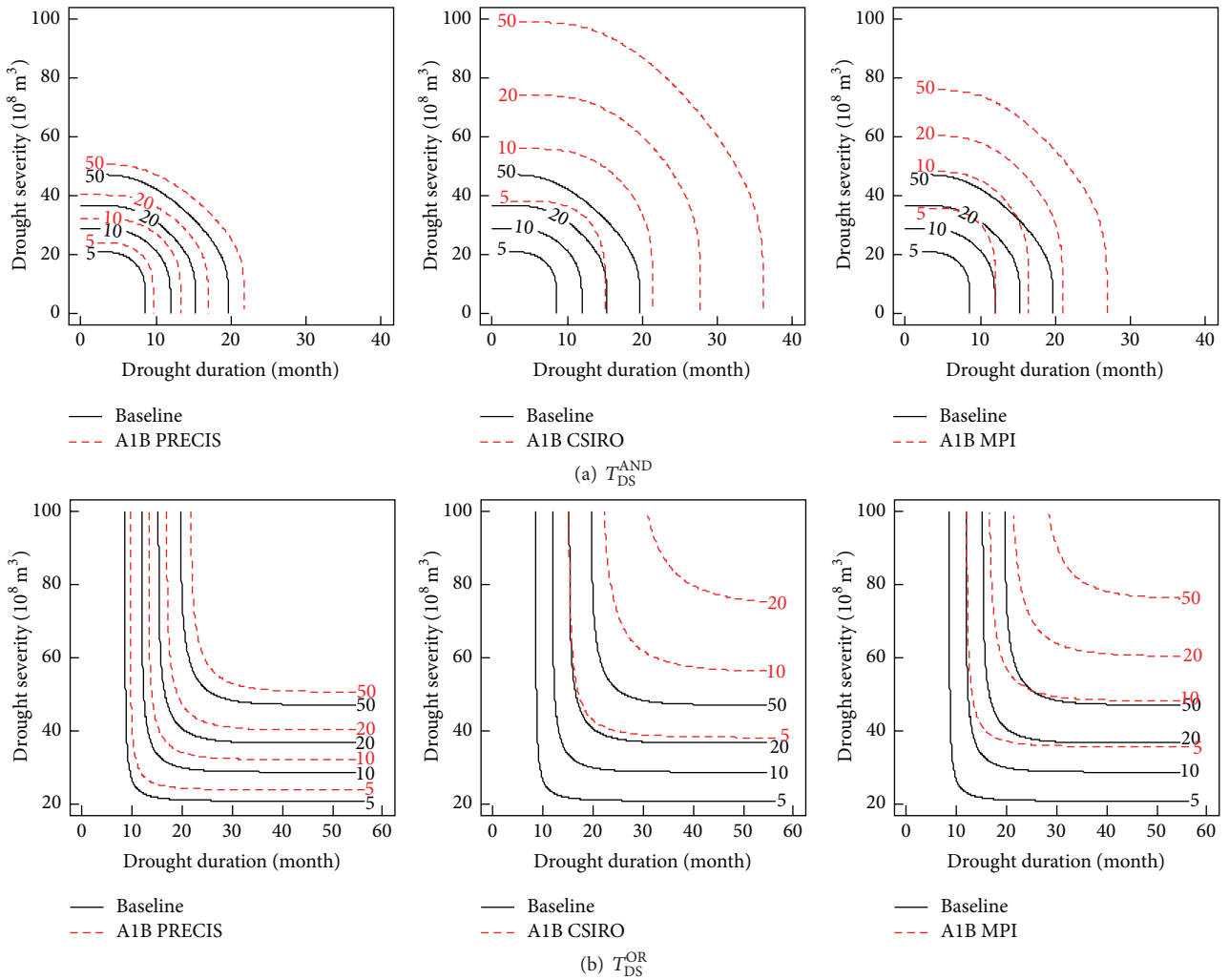

Figure 10: Bivariate joint return periods of drought duration and severity under baseline and A1B scenarios: (a) T_{DS}^{AND} defined by (7) and (b) T_{DS}^{OR} defined by (8).

copula-based model for bivariate drought assessment and joint frequency analysis under historical and future climates. Driven by the observed climate data, the modeling system is able to effectively identify most historical severe and extreme severe droughts in the WRB. The VIC model fed with three CM data sets, in general, projected a considerable runoff reduction under IPCC-SRES A1B scenario. This further triggers much worse drought conditions in the future. It is found in the univariate drought assessment that although fewer hydrological drought events would occur under A1B scenario, such drought variables as duration and severity were projected to increase considerably. The bivariate drought assessment using copula reveals that if historical droughts at a certain return period reoccurred under the future scenarios, the corresponding joint return periods would decrease remarkably. With these trends in the future, the hydrological drought situation in the WRB would be further deteriorated, and effective water saving techniques and rational water resources management strategies should be carried out for drought disaster mitigations.

It should be noted that, with the projected streamflow at Huaxian station being adopted for univariate and bivariate drought assessments, only the general drought conditions in the upstream area controlled by Huaxian hydrological station were projected in this study. To consider the spatiotemporal variations of drought conditions in the WRB, future work will be carried out to analyze the VIC-calculated runoff depth at each grid cell within the study area with the similar methodology in this study.

It is interesting to notice that although all modeling runs with different CM data sets consistently project future droughts to be deteriorated in the WRB, the projected drought conditions under A1B CSIRO and A1B MPI tend to be more serious than the case of A1B PRECIS. Several studies [30–32] found that CMs are the dominant uncertainty source, influencing future streamflow projections. Given that the VIC model is able to accurately reproduce the historical monthly streamflow at Huaxian station (Table 1 and Figure 3), the uncertainties of streamflow from CMs are very likely to predominantly further affect future hydrological drought

projections in this study. Consequently the uncertainty in drought projections might mainly originate from the uncertainties of CMs. Therefore, it is necessary to quantitatively evaluate the effects of the CM uncertainties on future drought projections. Furthermore, the PRECIS and CSIRO climate data sets under the IPCC-SRES B1 scenario were also adopted for future drought projections in this study (the results are not shown in this paper). It shows that the WRB would experience deteriorated drought conditions under B1, but the drying magnitude is less severe than that under A1B. This implies that the uncertainty from the adopted emission scenarios is nonignorable as well, which should be quantified in future studies. In addition, currently the new projected future climate data sets from the Coupled Model Intercomparison Project phase 5 (CMIP5) are available, which employed the latest generation of GCMs under the scenarios of Representative Concentration Pathways (RCPs) [33]. Therefore, it is encouraged to use this latest climate projection product for drought projections in future studies.

Conflict of Interests

The authors declare that there is no conflict of interests regarding the publication of this paper.

Acknowledgments

This study is sponsored by the National Key Technology R&D Program of Ministry of Sciences and Technology, China (Grant no. 2013BAC10B02), the Special Fund of State Key Laboratory of Hydrology-Water Resources and Hydraulic Engineering (Grant no. 20145031112), and the National Natural Science Foundation of China (Grant no. 41323001).

References

[1] M. Ma, L. Ren, V. P. Singh, X. Tu, S. Jiang, and Y. Liu, "Evaluation and application of the SPDI-JDI for droughts in Texas, USA," *Journal of Hydrology*, vol. 521, pp. 34–45, 2015.

[2] G. Yan, Z. Wu, and D. Li, "Comprehensive analysis of the persistent drought events in Southwest China," *Disaster Advances*, vol. 6, no. 3, pp. 306–315, 2013.

[3] F. K. Yu, X. H. Huang, Q. B. Liang et al., "Ecological water demand of regional vegetation: the example of the 2010 severe drought in Southwest China," *Plant Biosystems*, vol. 149, no. 1, pp. 100–110, 2015.

[4] G. Fu, S. Chen, C. Liu, and D. Shepard, "Hydro-climatic trends of the yellow river basin for the last 50 years," *Climatic Change*, vol. 65, no. 1-2, pp. 149–178, 2004.

[5] M. Ma, S. Song, L. Ren, S. Jiang, and J. Song, "Multivariate drought characteristics using trivariate Gaussian and student t copulas," *Hydrological Processes*, vol. 27, no. 8, pp. 1175–1190, 2013.

[6] B. Zhang, P. Wu, X. Zhao, Y. Wang, X. Gao, and X. Cao, "A drought hazard assessment index based on the VIC-PDSI model and its application on the Loess Plateau, China," *Theoretical and Applied Climatology*, vol. 114, no. 1-2, pp. 125–138, 2013.

[7] J.-T. Shiau, S. Feng, and S. Nadarajah, "Assessment of hydrological droughts for the Yellow River, China, using copulas," *Hydrological Processes*, vol. 21, no. 16, pp. 2157–2163, 2007.

[8] S. Song and V. P. Singh, "Frequency analysis of droughts using the Plackett copula and parameter estimation by genetic algorithm," *Stochastic Environmental Research and Risk Assessment*, vol. 24, no. 5, pp. 783–805, 2010.

[9] L. Cheng, Z. Xu, and Z. Liu, "Hydrological response to climate change in the weihe river basin," in *Proceedings of the 4th International Yellow River Forum on Ecological Civilization and River Ethics*, vol. 1, pp. 221–230, 2010.

[10] Q. Huang and J. Fan, "Detecting runoff variation of the mainstream in Weihe river," *Journal of Applied Mathematics*, vol. 2013, Article ID 356474, 8 pages, 2013.

[11] J. Du and C.-X. Shi, "Effects of climatic factors and human activities on runoff of the Weihe River in recent decades," *Quaternary International*, vol. 282, pp. 58–65, 2012.

[12] Y. Guo, Z. Li, M. Amo-Boateng, P. Deng, and P. Huang, "Quantitative assessment of the impact of climate variability and human activities on runoff changes for the upper reaches of Weihe River," *Stochastic Environmental Research and Risk Assessment*, vol. 28, no. 2, pp. 333–346, 2014.

[13] S. Madadgar and H. Moradkhani, "Drought analysis under climate change using copula," *Journal of Hydrologic Engineering*, vol. 18, no. 7, pp. 746–759, 2013.

[14] J. Liu, W. Kuang, Z. Zhang et al., "Spatiotemporal characteristics, patterns, and causes of land-use changes in China since the late 1980s," *Journal of Geographical Sciences*, vol. 24, no. 2, pp. 195–210, 2014.

[15] IPCC, *Climate Change 2001: The Scientific Basis, Contribution of Working Group I to the Third Assessment Report of the Intergovernmental Panel on Climate Change*, Cambridge University Press, Cambridge, UK, 2001.

[16] W. Chen, Z. Jiang, and L. Li, "Probabilistic projections of climate change over China under the SRES A1B scenario using 28 AOGCMs," *Journal of Climate*, vol. 24, no. 17, pp. 4741–4756, 2011.

[17] Y.-L. Song, D.-L. Chen, Y.-J. Liu, and Y. Xu, "The influence of climate change on winter wheat during 2012–2100 under A2 and A1B scenarios in China," *Advances in Climate Change Research*, vol. 3, no. 3, pp. 138–146, 2012.

[18] X. Liang, E. F. Wood, D. P. Lettenmaier, and S. J. Burges, "A simple hydrologically based model of land surface water and energy fluxes for general circulation models," *Journal of Geophysical Research*, vol. 99, no. 7, pp. 14415–14428, 1994.

[19] X. Liang, D. P. Lettenmaier, E. F. Wood, and S. J. Burges, "One-dimensional statistical dynamic representation of subgrid spatial variability of precipitation in the two-layer variable infiltration capacity model," *Journal of Geophysical Research D: Atmospheres*, vol. 101, no. 16, pp. 21403–21422, 1996.

[20] J. A. Cunge, "On the subject of a flood propagation computation method (Musklngum Method)," *Journal of Hydraulic Research*, vol. 7, no. 2, pp. 205–230, 1969.

[21] W. J. Rawls, L. R. Ahuja, D. L. Brakensiek, and A. Shirmohammadi, "Infiltration and soil water movement," in *Handbook of Hydrology*, D. R. Maidment, Ed., pp. 5.1–5.51, McGraw-Hill, New York, NY, USA, 1993.

[22] B. J. Cosby, G. M. Hornberger, R. B. Glapp, and T. R. Ginn, "A statistical exploration of the relationships of soil moisture characteristics to the physical properties of soils," *Water Resources Research*, vol. 20, no. 6, pp. 682–690, 1984.

[23] Z. Xie, F. Yuan, Q. Duan, J. Zheng, M. Liang, and F. Chen, "Regional parameter estimation of the VIC land surface model: methodology and application to river basins in China," *Journal of Hydrometeorology*, vol. 8, no. 3, pp. 447–468, 2007.

[24] Q. Duan, S. Sorooshian, and V. K. Gupta, "Optimal use of the SCE-UA global optimization method for calibrating watershed models," *Journal of Hydrology*, vol. 158, no. 3-4, pp. 265–284, 1994.

[25] A. K. Fleig, L. M. Tallaksen, H. Hisdal, and S. Demuth, "A global evaluation of streamflow drought characteristics," *Hydrology and Earth System Sciences*, vol. 10, no. 4, pp. 535–552, 2006.

[26] Ministry of Water Resources of the People's Republic of China, *Standard for Information and Hydrological Forecasting (GB/T 22482—2008)*, China Standard Press, Beijing, China, 2008.

[27] K. Sklar, "Fonctions de reparitition å n dimensions et leura marges," *Publications de l'Institut de statistique de l'Université de Paris*, vol. 8, pp. 229–231, 1959.

[28] R. B. Nelsen, *An Introduction to Copulas*, Springer, New York, NY, USA, 2006.

[29] S. Zhang, Y. Su, D. Song et al., *The Historical Droughts in China: 1949–2000*, Hohai University Press, Nanjing, China, 2008 (Chinese).

[30] T. Bosshard, M. Carambia, K. Goergen et al., "Quantifying uncertainty sources in an ensemble of hydrological climate-impact projections," *Water Resources Research*, vol. 49, no. 3, pp. 1523–1536, 2013.

[31] C. Dobler, S. Hagemann, R. L. Wilby, and J. Stötter, "Quantifying different sources of uncertainty in hydrological projections in an Alpine watershed," *Hydrology and Earth System Sciences*, vol. 16, no. 11, pp. 4343–4360, 2012.

[32] C. Prudhomme and H. Davies, "Assessing uncertainties in climate change impact analyses on the river flow regimes in the UK. Part 2: future climate," *Climatic Change*, vol. 93, no. 1-2, pp. 197–222, 2009.

[33] K. E. Taylor, R. J. Stouffer, and G. A. Meehl, "An overview of CMIP5 and the experiment design," *Bulletin of the American Meteorological Society*, vol. 93, no. 4, pp. 485–498, 2012.

Hindawi Publishing Corporation
Advances in Meteorology
Volume 2015, Article ID 248728, 8 pages
http://dx.doi.org/10.1155/2015/248728

Research Article

Drought Occurrence in Central European Mountainous Region (Tatra National Park, Slovakia) within the Period 1961–2010

Jaroslav Vido,[1] Tsegaye Tadesse,[2] Zbyšek Šustek,[3] Radoslav Kandrík,[1] Miriam Hanzelová,[1] Jaroslav Škvarenina,[1] Jana Škvareninová,[4] and Michael Hayes[2]

[1]*Department of Natural Environment, Faculty of Forestry, Technical University in Zvolen, T.G. Masaryka 24, 960 53 Zvolen, Slovakia*
[2]*The National Drought Mitigation Centre, University of Lincoln, 816 Hardin Hall, 3310 Holdrege Street, Lincoln, NE 68583-0988, USA*
[3]*Institute of Zoology, Slovak Academy of Sciences, Dúbravská cesta 9, 845 06 Bratislava, Slovakia*
[4]*Department of Applied Ecology, Faculty of Environmental Sciences, Technical University in Zvolen, T. G. Masaryka 24, 960 53 Zvolen, Slovakia*

Correspondence should be addressed to Jaroslav Vido; vido@tuzvo.sk

Received 29 May 2015; Revised 7 October 2015; Accepted 18 October 2015

Academic Editor: Mohsin Hafeez

Drought has recently become a significant topic in the Central European region. It has been observed that the drought phenomenon has severe impacts on the agriculture, hydrology, social, and economic sectors of lowland areas. This study focuses on how drought, defined as a precipitation shortage, occurs in higher altitudes of the Tatra National Park (Tatra Mts., Slovakia), which is a significant biological reserve of the Central European fauna and flora. The main goals of this research include identifying drought variability and its characteristics over the Tatra National Park in the West Carpathians (Slovakia), especially to characterizing drought variability and its spatial pattern across the Tatra National Park from 1961 to 2010 using the Standardized Precipitation Index (SPI) and standard Geographic Information System (GIS) methods. The results showed that frequency of drought occurrence has cyclic pattern with approximately 30-year period. The spatial analyses showed that precipitation shadow of the mountains influences the risk of drought occurrence. The drought-prone areas over the mountains are also identified.

1. Introduction

Drought, as a natural hazard resulting from precipitation deficits, causes various impacts in almost all types of ecosystem around the globe [1, 2]. The Central European region is no exception [3–5]. Crop yield failure in agricultural production [3, 6], hydrological droughts [7, 8], wildfires [9, 10], and bark beetle outbreaks [11, 12] are only few examples of drought-related impacts in Central European ecosystems. These impacts were observed during severe drought episodes that were previously relatively infrequent in the Central European region [13, 14]. However observed changes in precipitation patterns in the last few decades, as well as projected changes in future, imply an increase in number of drought episodes in the area [15, 16]. Despite this observed fact, there are local variabilities in the precipitation patterns and its severity. For example Škvarenina et al. [17] and Faško et al. [18] have found that an increase in drought frequency applies more across southern Slovakia as compared to the northern Slovakia (includes the Tatra National Park, a mountainous area), where significantly increasing trends of precipitation amounts were observed over the past 20 years.

However Niedźwiedź et al. [19] argued that this trend has a cyclic character with a period of about 30 years. In addition the author indicated that this wet climate feature has already begun to subside. The argument of the precipitation cyclic pattern has also been confirmed by Pekárová et al. [20] based on the long-term observations of water levels on the Central European rivers. Thus, this potentially anticipated change in precipitation patterns toward drier conditions in synergy with increasing temperature in the lower and middle altitudes over the Tatra National Park [21] could consequently exacerbate drought severity and its impacts.

Because of the controversial facts presented in the literature dealing with precipitation patterns in the area of northern Slovakia, where the Tatra National Park is located,

there is a more urgent need in understanding drought as a potential natural hazard and its spatial distribution features. This is very important because the Tatra National Park is unique by its high species diversity, high number of endemic animals (alpine marmot [*Marmota marmota latirostris*], Tatra chamois [*Rupicapra rupicapra tatrica*], Carabids [*Deltomerus tatricus*, *Nebria tatrica*]) and plants (*Cerinthe glabra subsp. tatrica*, *Primula halleri subsp. platyphylla*) [22–24] and specific cultural landscape structures. That is acknowledged by the membership of this park in the UNESCO world network of biosphere reserves since 1993.

However, in assessing the drought across the Tatra National Park, better understanding and consideration of the topographic impact on precipitation are needed including the strong effect created over the lee ward side of the Tatra mountain ridge, ridges of surrounding mountains, and local precipitation shadows in particular mountain valleys. These orographic features significantly influence spatial precipitation distribution that may exacerbate the drought impacts in the area [25]. In addition, it is necessary to consider the relatively higher precipitation amount compared to potential evapotranspiration in the mountain areas of the National Park [17]. For example, edificator tree species in the forest ecosystem such as spruce have normally more water (enough soil moisture) during the growing period, as characterized by the water balance method (i.e., precipitation minus evapotranspiration) calculated by Škvarenina et al. [17]. Therefore, a certain resistance level of ecosystems at higher altitudes due to short-lasting precipitation fluctuations is expected [26]. However, long-lasting subnormal precipitation periods have significant impacts on ecosystems in the Tatra National Park such as weakening of tree condition [12], increase of wild fire risk [27], changes in population dynamics of climate sensitive pests [28], and depletion of groundwater in the creeks watersheds [29] that causes significant impacts on qualitative and quantitative composition of benthic macrofauna [30]. Thus, better understanding of drought characteristics over the mountainous region is helpful for managing the Tatra National Park and preservation of its biodiversity. For instance, spatial information of drought prone areas could be used for improvement of the fire prevention plan. Other examples of usage are detection of biotopes with lower ecological stability under drought influence, because such localities could be source for future outbreaks of biotic pests [11].

The main goal of this study is to characterize drought variability and its characteristics across the Tatra National Park as an integral part of Tatra Mts. (Slovakia) in the period 1961–2010.

In this study the time series trend analysis of The Standardized Precipitation Index (SPI) [31] for 12 months at the stations in the area of the Tatra Mts. and the spatial patterns of drought episode occurrences across the Tatra National Park have been investigated. SPI has been used because of several advantages compared to other drought indices, for example, the requirement of fewer input variables, simplicity of calculation, and comparability of droughts considering the time and place (because the SPI is a dimensionless index) [32, 33]. The reason to use 12-month SPI for long-term drought

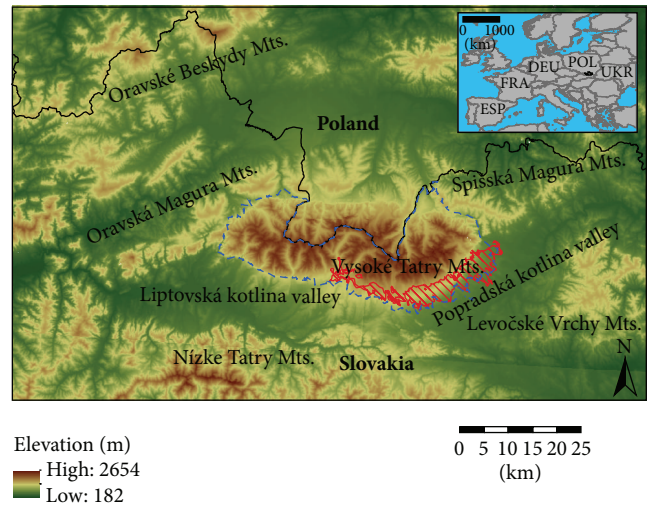

Figure 1: Geographical and geomorphological situation around the Tatra Mts. and Tatra National Park. Solid line represents state boundary between Slovakia and Poland. Dashed line represents border of the Tatra National Park. Area with left-hatching represents windstorm calamity in 2004. Black point in the index figure indicates location of the study area in European context.

assessment is based on results of Holko et al. [29], who found that one year of precipitation deficits leads to depletion of water basins in the Tatra Mountains, which had significant impact on ecosystems of the National Park.

2. Materials and Methods

2.1. The Area Specification. Tatra National Park is located in the Tatra Mountains (north Slovakia), the highest range in the Carpathian Mountains (the highest peak is Gerlachovský štít Mt., 2655 m a.s.l.). Two-thirds of the range belongs to Slovakia and one-third to Poland. Surrounding areas of mountains consist of the Oravské Beskydy Mts. (northwest) with highest peak Babia Hora, 1725 m a.s.l., Oravská Magura Mts. (west) reaching the height of 1394 m a.s.l. at Minčol peak, Nízke Tatry Mts. (south) with the maximum altitude at Ďumbier Peak (2043 m a.s.l.), and Spiššská Magura Mts. with Levočské Vrchy Mts. (east) reaching up to 1289 m a.s.l. at the Čierna Hora Peak. The massive of the Tatra Mts. is open only from north to northnorthwest, where a depression area is located—Subcarpathia (Poland). South of the Tatra Mts., the Liptovská Kotlina valley is located, which forms the southern border of the Tatra National Park and foothills of the Tatra Mts. (Figure 1).

The relief of the Tatra Mts. was created by glacial activity in the last ice age [35]. Subspecies endemic to the Tatra Mts. (e.g., Alpine marmot [*Marmota marmota latirostris*] and Tatra chamois [*Rupicapra rupicapra tatrica*], Carabids [*Deltomerus tatricus*, *Nebria tatrica*]) also date back to this era. Area of this unique species is located mostly over 1500 m a.s.l.

Geomorphologically, the mountains are divided into the West (Západné Tatry) and East Tatra Mts. (Východné Tatry). West Tatra Mountains are lower (highest peak is Bystrá,

Table 1: Meteorological stations used in this study with their selected parameters.

Station	ID number	North φ	East λ	Altitude (.)	Precipitation (mm/year)**	Potential ET (mm/year)***	Time period
Červený Kláštor	1	49° 23′	20° 25′	463	792	500	1961–2010
Lipt. Mikuláš*	2	49° 05′	19° 36′	569	657	550	1961–2007
Podolínec	3	49° 15′	20° 32′	573	720	525	1961–2010
Liptovský Hrádok	4	49° 2′	19° 43′	640	696	525	1961–2010
Liesek*	5	49° 21′	19° 40′	692	811	425	1961–2007
Poprad	6	49° 4′	20° 14′	694	599	575	1961–2010
Habovka*	7	49° 16′	19° 36′	745	936	425	1980–2002
Huty	8	49° 8′	19° 33′	808	918	375	1961–2010
Tatranská Lomnica	9	49° 9′	20° 17′	827	797	475	1961–2010
Podspády	10	49° 16′	20° 10′	913	1166	375	1961–2010
Podbanské	11	49° 8′	19° 54′	972	959	475	1961–2010
Tatranská Javorina	12	49° 15′	20° 8′	1007	1305	375	1961–2010
Starý Smokovec*	13	49° 8′	20° 13′	1010	857	475	1961–1990
Hrebienok*	14	49° 9′	20° 13′	1270	1024	425	1961–1990
Štrbské Pleso	15	49° 7′	20° 4′	1354	1026	425	1961–2010
Skalnaté Pleso	16	49° 11′	20° 14′	1778	1351	375	1961–2010
Lomnický Štít	17	49° 11′	20° 12′	2635	1498	325	1961–2010

*Station without calculated trend analysis. **Average precipitation amount calculated within the time period. ***Potential evapotranspiration totals calculated by Tomlain (2002) [34].

2248 m a.s.l.) than East Tatra Mts. with the highest peak Gerlachovský štít (2655 m a.s.l.). The East Tatra Mts. consist of the Vysoké Tatry Mts. and Belianske Tatry Mts. The southeast region of the study area was impacted by windstorms, especially in 2004 (Figure 1).

2.1.1. Climate of the Tatra Mountains. Geomorphology of the Mountains and surrounding areas influences the prevailing winds in the area [36]. Prevailing winds on the peak station (Lomnický Štít Peak 2655 m a.s.l., the second highest peak in the Tatra Mountains) blow from the north and northwest sector as well as on the lowland station Červený Kláštor (463 m a.s.l.) located northeast of the mountains beyond the lee effect of the Tatra Mountains massive (Figure 2). In contrast, a predominantly west wind direction is measured at stations located south of the mountains (Poprad, 694 m a.s.l., or Liptovský Hrádok, 640 m a.s.l.).

Precipitation amounts in the area vary from the 599 mm/year at the station Poprad in the Popradská kotlina valley to the maximum at the Lomnický štít peak (2635 m a.s.l.) with 1498 mm/year (Table 1). However, the effect of the mountain lee is visible in the precipitation amounts. While the precipitation amount at the lowest station Červený Kláštor (463 m a.s.l.) situated northeasterly of the mountain ridge is 792 mm/year, the stations Liptovský Mikuláš (569 m a.s.l.) and Liptovský Hrádok (640 m a.s.l.) situated in the Liptovská kotlina valley southerly of the mountain ridge vary from 657 to 696 mm/year. Localization of the mentioned stations is depicted in the Figure 2. The same effect is visible also at the station Poprad (694 m a.s.l.) located in the Popradská kotlina valley southeast of the mountain ridge.

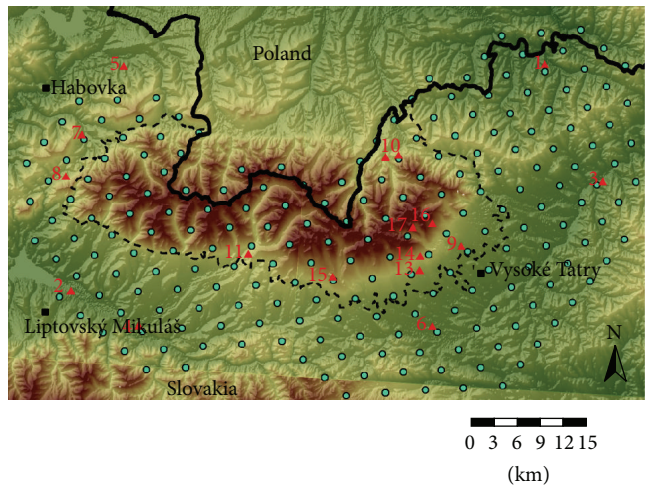

Figure 2: Localization of the used meteorological stations is depicted by triangles with number. Number near triangle corresponds to ID number of the station from Table 1. Circles represent grid points used in the GIS spatial analyses. Dashed line represents border of the Tatra National Park. Solid line depicts national boundary.

Potential evapotranspiration at all the stations around the Tatra Mountains ranges from 325 mm at the Lomnický štít peak (2635 m a.s.l.) to 550 mm per year at the Poprad station in the Popradská kotlina valley (694 m a.s.l.) [34]. As shown in the Table 1 at all the stations, the potential evapotranspiration is lower than precipitation totals. However, we see that at the stations situated southerly of the mountain ridge

(leeward) in the Popradská kotlina and Liptovská kotlina valleys (e.g., Liptovský Mikuláš and Poprad) the precipitation surplus is relatively low (e.g., at the station Poprad 24 mm and at the station Liptovský Mikuláš 107 mm).

2.2. Methods of Drought Analyses

2.2.1. The Standardized Precipitation Index (SPI). The Standardized Precipitation Index [31] is drought index calculated on the basis of the probability of the occurrence of certain amount of precipitation in given time period. The calculation requires a long-term monthly precipitation database with 30 years or more of data. The probability distribution function is derived from the long-term record by fitting a gamma function to the data. The cumulative distribution is then transformed using equal probability to a normal distribution with a mean of zero and standard deviation of one, so the values of the SPI are really in standard deviations [37]. Entire mathematical descriptions of the principles and calculation of the SPI are given in [37]. Positive SPI values indicate greater than median precipitation, while negative SPI values indicate less than median precipitation. The magnitude of departure from zero represents probability of occurrence, so decisions can be made based on this SPI value. Thus SPI values of less than −1.0 occur 16 times in 100 years, an SPI of less than −2.0 occurs two to three times in 100 years, and an SPI of less than −3.0 occurs once in approximately 200 years. The SPI can be calculated for a variety of timescales. This allows the SPI to monitor short-term water supplies (such as soil moisture) and longer-term water resources such as groundwater supplies or lake levels [38].

2.2.2. Data. Inputs for indices are monthly precipitation totals from 17 meteorological stations (Table 1) of the Slovak Hydrometeorological Institute (SHMI) in the period 1961–2010 situated in the area of the Tatra National Park. Precipitation data for stations with the shorter period (i.e., Habovka 1980–2002, Starý Smokovec, Hrebienok 1961–1990, Liesek 1961–2007, and Liptovský Mikuláš 1961–2007) were used as supplementary stations for spatial model improvement. For these stations long-term trend analyses were not prepared because of a shorter time period, which could have an impact on the SPI parameters.

2.2.3. Data Processing in SPI Analyses. Since all the data sets of the calculated SPI were normally distributed (normality was tested using Kolmogorov-Smirnov test) linear function and Student's t-test for trend analyses have been applied according to Yue and Pilon [39]. Trend analyses using linear trend were made for each station separately, except those stations with shorter observation periods as mentioned in Table 1. Trends were tested on significance by Student's t-test on the significance level $\alpha = 0.05$. This process has been carried out in order to get information of altitudinal variability of drought trends in the period 1961–2010.

To characterize the general overview of drought occurrence over the study region, an average SPI based on the stations SPI values (from Table 1) was constructed. In all the analyses in this paper, the 12-month SPI was used to evaluate a severe drought episodes in the area. The reason to use 12-month SPI for long-term drought assessment (as mentioned in introduction) is based on results of Holko et al. [29], who found that one year of precipitation deficits leads to depletion of water basins in the Tatra Mountains, which had significant impact on ecosystems of the National Park. In order to obtain information about alternation between wet and dry long-term episodes, curvilinear regression (fourth-order polynomial) has been constructed. The reason is that the curvilinear regression depicts periods or specific cycles (alternation between dry and wet episodes) more illustratively compared to another regression function (e.g., linear, moving average) as mentioned by Gulrado and Bermúdez [40].

2.2.4. Data Processing in Spatial Evaluations. To identify the geospatial pattern and distribution of drought within the seasons, 12-month SPI values were used and interpolated using the following GIS techniques based on the spatial average of two (modeled and observed) layers.

The first layer contains the spatial information of drought conditions provided by nodes (grid points) with appropriate SPI values. Here the SPI was calculated with precipitation data obtained by approximation between precipitation and altitude. The challenge was to find the best fit function able to identify the trend and effectively approximate the relationship between precipitation and altitude. However, we used the simple linear function to estimate the precipitation values. The results showed a strong correlation (i.e., $R^2 = 0.6977$ with $\alpha = 0.01$). Finally, the estimated values were plotted and interpolated using SPLINE function in GIS. Figure 2 shows the net of 220 nodes (grid points) used in GIS processing.

The second layer was obtained by spatial interpolation of the SPI station based data obtained by the meteorological stations around the Tatra Mountains (Figure 2 and Table 1). The spatial interpolation of the second layer was carried out using the SPLINE interpolation function.

Finally, the spatial average of the first and the second layer was processed (using raster calculator) and used as a drought spatial distribution model for the Tatra Mountains.

The spatial model was evaluated by comparing the observed and modeled precipitation totals for three different precipitation scenarios: above average, below average, and average precipitation. To represent these three scenarios, 2010, 2003, and 1997 were selected. Correlation of precipitation totals obtained using selected modeled grid points with the nearest totalizer rain gauge showed statistical significance evaluated by Pearson correlation ranging from 0.9583 to 0.9859. The spatial model and all trend analysis have been tested and approved using t-test at the significance level $\alpha = 0.05$.

3. Results and Discussion

3.1. General Overview of a Drought Occurrence in the Tatra Mountains Region. Niedźwiedź et al. [41], Labudová et al. [42], Büntgen et al. [4], and Konček et al. [25] indicated that the long-term variations in precipitation regime around the Tatra Mountains mostly depends on the atmospheric

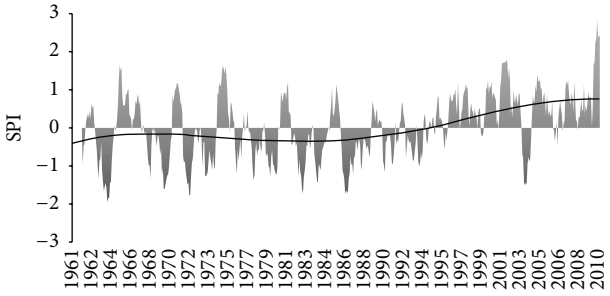

Figure 3: Average 12-month SPI for the Tatra Mountains region. The trend line is constructed by the curvilinear regression (fourth-order polynomial).

circulation, especially by westerly zonal circulation because of the mountains' orientation along a zonal air flow. Therefore, to understand the general conditions and occurrence of severe droughts over the region, we have used the average precipitation time-series pattern based on all station data (Table 1) except stations with shorter observations (i.e., Habovka, Starý Smokovec, Hrebienok, Liesek, and Liptovský Mikuláš). Figure 3 shows this temporal distribution of precipitation variations from 1961 to 2010 using the SPI for 12 months. The figure shows the occurrences of all drought episodes (negative values) during the 1961–2010 period. Thus, six severe drought episodes (SPI ≤ -1.5) using the 12-month SPI are identified. The 12-month SPI values indicated that an extreme drought episode was observed in the period from 1963 to 1965, which was the most intense drought during the record. Exceptional dry periods with frequent occurrences of drought situations persisted in 1962–1964, 1967–1969, 1971–1974, 1977–1980, 1982–1985, 1986–1989, and 2003 over the Tatra Mountains. A particularly long-lasting dry period also occurred from 1990 to 1995. These detected episodes correlate with results of Demeterová and Škoda [8]. The authors describe that hydrological drought over the study area persisted in 1963, 1972–1974, 1976, 1978, 1982–1985, 1987–1994, and 2003. An increase in wet episodes after 1995 (except pan-European drought of 2003) corresponds to results explained by Büntgen et al. [4] and Lapin and Faško [43] that the precipitation totals in the study area are mostly driven by western/northwestern zonal air flow. Niedźwiedź et al. [19] and Lapin and Tomlain [44] imply that the significant increase of the west cyclonal situation was recorded in this area after the first half of the 1990s. This correlates with an increase in wet situations shown by the SPI after 1993. However Niedźwiedź et al. [19] and Lapin and Faško [43] indicated that these changes in circulation patterns are cyclic, with an approximately 30-year period.

Our findings (based on approximate estimation of inflection points in the polynomial trend of the SPI) also showed that periodicity. Actually inflection points of the polynomial trend were detected in 1968 and 1998 (i.e., 29-year period). This result corresponds also with Pekárová et al. [20], which imply the same frequency based on analyzed long-term water levels of the central European rivers. Based on this we argue that the current "wet period" started from early nineties could be interrupted by a dry period in the future decade. This argument should be taken in the account in the National Park management plan for future decades. In addition, with the observed and anticipated regional temperature increase [15, 21], the drought severity could be worse in the future.

Table 2: Correlation coefficients of the SPI trends at the stations around the Tatra Mountains in context of altitude in the period 1961–2010.

Station	Altitude (m a.s.l.)	Coefficient of correlation R^2
Červený Kláštor	463	**0.2099**
Podolínec	573	0.0136
Liptovský Hrádok	640	0.0319
Poprad	694	0.0292
Huty	808	0.0314
Tatranská Lomnica	827	0.0108
Podspády	913	**0.1744**
Podbanské	972	**0.0604**
Tatranská Javorina	1007	**0.1991**
Štrbské pleso	1354	**0.1356**
Skalnaté pleso	1778	**0.1234**
Lomnický štít	2635	**0.4720**

Marked in bold indicates a statistically significant trend at the level of significance $\alpha = 0.05$.

3.2. Time Series Trend Analysis of SPI for 12 Months at the Stations in the Area of the Tatra Mountains. Analysis of the time series showed an increase in the number of wet episodes of SPI at all stations analyzed after 1995. However, this increasing trend is not significant (at the significance level $\alpha = 0.05$) for the stations located at lower altitudes, that is, Podolínec, Liptovský Hrádok, Poprad, Huty, and Tatranská Lomnica, except for one station Červený Kláštor (Table 2). This station is situated over the northeastern Tatra Mountains, where it is beyond the influence of rain shadow. Statistically, trends toward wet conditions over the higher altitudes over 900 m a.s.l. (i.e., Podspády, Podbanské, Tatranská Javorina, Štrbské Pleso, Skalnaté Pleso, and Lomnický štít) were found significant at the significance level $\alpha = 0.05$ (Table 2). Thus it seems that the habitats of the Tatra National Park including habitats of periglacial relict species are in "relatively drought-safer altitudinal zone," because the core area of the biosphere reserve, where habitats of this unique species are located, starts at 1500 m a.s.l. [22–24]. However, due to a relatively low precipitation surplus on stations in lower altitudes, what was shown in Table 1, and due to suggested cyclicity of the "wet" and "dry" periods in combination with observed temperature increase in Tatra Mountains [21], drought risk could increase in the future, especially during the prolonged drought episodes. This potential risk (based on ecological analyses) was outlined in results of Bitušík and Koppová [30], Konôpka and Konôpka [12], and Hlásny and Turčáni [28]. We have to consider that this could cause a potential ecological pressure, for example, by spreading of

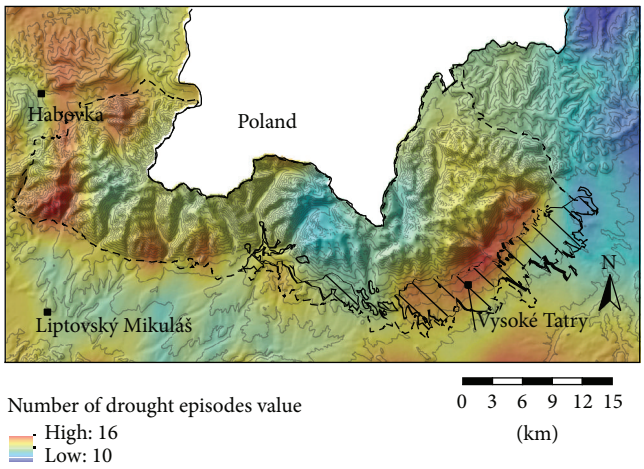

FIGURE 4: Number of all drought situations according to the 12-month SPI. Red color represents higher frequency of drought situations. Dashed line represents border of the National Park. Square represents city or settlement. Area with left-hatching represents calamity in 2004.

lowland xerophilous species to habitats of middle altitudes (buffer zones and transition areas of the park) because of their better adaptation to dry climatic conditions in contrast to mountain or even alpine stenobionts as shown in Šustek and Vido [45].

3.3. Spatial Patterns of Drought Episode Occurrences across the Tatra National Park. In general, precipitation totals relate proportionally to altitude [46]. However Konček et al. [25] argued that the orographic diversity of the Tatra Mountains modifies this dependence by local precipitation shadows. This fact could have a significant impact on precipitation totals and therefore number of drought situations in the lee ward areas. Spatial projection of areas with similar number of drought episodes (using the 12-month SPI) identifies a potential drought prone areas. These locations could be affected more often in contrast to other areas especially during the prolonged episodes with precipitation deficit. Spatial projection of the 12-month SPI depicts the prevalence of potentially severe drought episodes because of the previously mentioned impact of long-lasting precipitation deficits on water depletion in this area [29].

Figure 4 illustrates that the area with higher frequency of drought episodes can be divided into three main drought-prone subareas. The first is situated in west and northwest of the Tatra National Park. This area is influenced by precipitation shadow of the Oravská Magura and Oravské Beskydy Mountains located northwest of the Tatra National Park.

The second main drought-prone area is located on the lee side of the main mountain ridge of High Tatra, east of the Tatranská Kotlina village to Vyšné Hágy settlement. Secondary maximums of drought episode prevalence are recorded in the area of the valleys Jamnická dolina, Bystrá dolina, and Račková dolina in the West Tatra Mountains around the mouth of the valleys Tichá dolina and Kôprová dolina near the Podbanské village and in the valleys Zadné Med'odoly, Predné Med'odoly, Čierna javorová dolina, and Kolová dolina in the High Tatra. In contrast, locations with the lowest number of drought episodes are located outside of the influence of the rain shadow of the Tatra Mountains complex around the northeast headland of the mountains near meteorological station Červený Kláštor.

Finally the third area is the Popradská kotlina valley, southeast of the Tatra National Park. This area corresponds with the rain shadow in the Popradská kotlina and Spišská kotlina valleys, which is also noted by Konček et al. [25].

The most endangered (drought-prone) areas defined by number of drought episodes correspond in particular with the area of the massive windstorm of 2004 (spatial overlap reached 46%). This huge wind damage caused devastation of the spruce forests in the area [47]. Thus the ecosystems are in the process of secondary succession. Ecosystems in early succession stages in the area could be therefore more affected by drought because of their lower resistance level to natural disturbances [48].

These facts imply a potential of drought risk for the forest ecosystem during its succession process. Moreover, in synergy with the predicted temperature (evapotranspiration) increase at the middle altitudes [15, 21] and possible decline of "wet situations" in the following decades (because of the mentioned multidecadal cycle) [19, 20, 39] could be drought impact on this ecosystem worse in the future. So the restoration of the forests could be unpredictable and incalculable. Signals of such an ecological behavior were indicated by Šustek and Vido [45] (2013) in the structure of the sensitive ground beetle communities after the relatively hot and dry summer 2007 in the Tatra National Park.

4. Conclusions

This study showed that occurrence of drought has cyclic pattern with approximately 30-year period. Almost all years in the last two decades were relatively "wet" except the 2003, which was short but severe drought. Because of this cyclic pattern of precipitation regime over the Tatra Mountains, we expect "dry" period with numerous drought episodes in subsequent decades. However, in this study, it was found that core areas of the biosphere reserve of the Tatra National Park inhabited by the unique species (altitudes over 1500 m a.s.l.) are in relatively "drought-safer altitudinal zone" based on SPI station based trend analyses. Unfortunately, ecosystems of lower altitudes (up to 900 m a.s.l.) could be impacted by drought in anticipated dry period, due to presented low precipitation surplus and low significance of the SPI trend, respectively.

The SPI spatial analyses result in the fact that the occurrence of drought episodes is influenced by the precipitation shadow of the Tatra Mts. range and surrounding mountains situated north and to northwest of the Tatra Mts. Thus the occurrence of drought is more likely at the south and southeast regions of the mountains than at the north/northeast windward part of the Tatra Mountains. In addition, another drought prone area was also indicated in the West Tatra Mts. This area is influenced by the Oravské Beskydy and Oravská Magura Mts. located to the northwest.

On the other hand, the south and southeast part of the National Park was influenced by a severe windstorm in 2004. From the ecological point of view it is interesting that the area of the windstorm spatially correlates with identified drought-prone areas (spatial overlap is 46%). Therefore ecosystem restoration in this area could be affected by potential drought episodes in the future. We recommend that above presented information should be taken into account by decision makers responsible for forest restoration management within that affected area.

Conflict of Interests

The authors declare that there is no conflict of interests regarding the publication of this paper.

Acknowledgments

This contribution was supported by research grants of The Ministry of Education, Science, Research and Sport of the Slovak Republic: VEGA nos. 2/0101/14, 1/0463/14, 1/0589/15, and by grant of the Slovak Research and Development Agency no. APVV-0480-12 and no. APVV-0303-11.

References

[1] S. M. Vicente-Serrano, C. Gouveia, J. J. Camarero et al., "Response of vegetation to drought time-scales across global land biomes," *Proceedings of the National Academy of Sciences of the United States of America*, vol. 110, no. 1, pp. 52–57, 2013.

[2] C. D. Allen, A. K. Macalady, H. Chenchouni et al., "A global overview of drought and heat-induced tree mortality reveals emerging climate change risks for forests," *Forest Ecology and Management*, vol. 259, no. 4, pp. 660–684, 2010.

[3] M. Trnka, R. P. Rötter, M. Ruiz-Ramos et al., "Adverse weather conditions for European wheat production will become more frequent with climate change," *Nature Climate Change*, vol. 4, no. 7, pp. 637–643, 2014.

[4] U. Büntgen, R. Brázdil, D. Frank, and J. Esper, "Three centuries of Slovakian drought dynamics," *Climate Dynamics*, vol. 35, no. 2, pp. 315–329, 2010.

[5] P. Ciais, M. Reichstein, N. Viovy et al., "Europe-wide reduction in primary productivity caused by the heat and drought in 2003," *Nature*, vol. 437, no. 7058, pp. 529–533, 2005.

[6] P. Hlavinka, M. Trnka, D. Semerádová, M. Dubrovský, Z. Žalud, and M. Možný, "Effect of drought on yield variability of key crops in Czech Republic," *Agricultural and Forest Meteorology*, vol. 149, no. 3-4, pp. 431–442, 2009.

[7] J. Poórová, L. Blaškovičová, P. Škoda, and V. Šimor, "Trends of minimum annual and monthly flows in Slovakia," in *Zborník Abstraktov, Odborný Seminár Sucho a Jak mu Čelit*, pp. 20–23, Praha, Slovakia, 2013.

[8] B. Demeterová and P. Škoda, "Low flow in selected streams of Slovakia," *Journal of Hydrology and Hydromechanics*, vol. 57, no. 1, pp. 55–69, 2009.

[9] A. H. Fink, T. Brücher, A. Krüger, G. C. Leckebusch, J. G. Pinto, and U. Ulbrich, "The 2003 European summer heatwaves and drought-synoptic diagnosis and impacts," *Weather*, vol. 59, no. 8, pp. 209–216, 2003.

[10] J. Škvarenina, J. Miňďáš, J. Holécy, and J. Tuček, "Analysis of the natural and meteorological conditions during two largest forest fire events in the Slovak Paradise National Park," in *Proceedings of the International Bioclimatological Workshop*, p. 11, Bratislava, Slovakia, September 2003.

[11] M. J. Klapwijk, M. P. Ayres, A. Battisti, and S. Larsson, "Assessing the impact of climate change on outbreak potential," in *Insect Outbreaks Revisited*, pp. 429–450, Blackwell Publishing, Oxford, UK, 2012.

[12] J. Konôpka and B. Konôpka, "Influence of main kinds of abiotic harmful agents on forest ecosystems, research and practice," *Reports of Forestry Research*, vol. 47, no. 1, p. 40, 2002.

[13] M. Trnka, J. Kylselý, M. Možný, and M. Dubrovský, "Changes in Central European soil moisture availability and circulation patterns in 1881–2005," *International Journal of Climatology*, vol. 29, no. 5, pp. 655–672, 2009.

[14] B. Lloyd-Hughes and M. A. Saunders, "A drought climatology for Europe," *International Journal of Climatology*, vol. 22, no. 13, pp. 1571–1592, 2002.

[15] M. Lapin, M. Gera, J. HrvoĽ, M. Melo, and J. Tomlain, "Possible impacts of climate change on hydrologic cycle in Slovakia and results of observations in 1951–2007," *Biologia*, vol. 64, no. 3, pp. 454–459, 2009.

[16] M. Lapin and M. Melo, "Methods of climate change scenarios projection in Slovakia and selected results," *Journal of Hydrology and Hydromechanics*, vol. 52, no. 4, pp. 224–238, 2004.

[17] J. Škvarenina, J. Tomlain, J. Hrvol, J. Škvareninová, and P. Nejedlík, "Progress in dryness and wetness parameters in altitudinal vegetation stages of West Carpathians: time-series analysis 1951–2007," *Időjárás*, vol. 113, no. 1-2, pp. 47–54, 2009.

[18] P. Faško, M. Lapin, and J. Pecho, "20-Year extraordinary climatic period in Slovakia," *Meteorologický Časopis*, vol. 11, pp. 99–105, 2008.

[19] T. Niedźwiedź, R. Twardosz, and A. Walanus, "Long-term variability of precipitation series in east central Europe in relation to circulation patterns," *Theoretical and Applied Climatology*, vol. 98, no. 3-4, pp. 337–350, 2009.

[20] P. Pekárová, P. Miklanek, and J. Pekar, "Long-term trends and runoff fluctuations of European rivers," in *Climate Variability and Change: Hydrological Impacts, Proceedings of the Fifth FRIEND World Conference held at Havana, Cuba*, vol. 308, pp. 520–525, IAHS Publication, 2006.

[21] A. Pribullová, M. Chmelík, and J. Pecho, "Air temperature variability in the high tatra mountains," in *The Carpathians: Integrating Nature and Society Towards Sustainability*, Environmental Science and Engineering, pp. 111–130, Springer, Berlin, Germany, 2013.

[22] L. Vlček, "Geographical distribution of chamois (*Rupicapra rupicapra* L.) in the Western Carpathians territory during the last Glacial and the Holocene," *Acta Carsologica Slovaca*, vol. 48, no. 1, pp. 83–98, 2010.

[23] P. Bačkor, "Current distribution of the Alpine Marmot (*Marmota marmota*) in the Nízke Tatry Mts., Slovakia (Rodentia: Sciuridae)," *Lynx, Series Nova*, vol. 40, no. 1, pp. 5–13, 2009.

[24] J. Kliment, "Thoughts on recent phytogeographical regionalisation of Slovakia (notes to selected phytochorions)," *Bulletin Slovenskej Botanickej Spoločnosti*, vol. 25, pp. 199–224, 2003.

[25] M. Konček, I. Bohuš, V. Briedoň et al., *Climate of the Tatra Mountains, Veda, Bratislava*, Veda, Bratislava, Slovakia, 1974.

[26] M. Dubrovsky, M. D. Svoboda, M. Trnka et al., "Application of relative drought indices in assessing climate-change impacts

on drought conditions in Czechia," *Theoretical and Applied Climatology*, vol. 96, no. 1-2, pp. 155–171, 2009.

[27] SLS, *Climate of the High Tatra Mountains*, Scientia, Tatranská Lomnica, Slovakia, 2009.

[28] T. Hlásny and M. Turcáni, "Insect pests as climate change driven disturbances in forest ecosystems," in *Bioclimatology and Natural Hazards*, pp. 165–177, Springer, Dordrecht, The Netherlands, 2009.

[29] L. Holko, M. Dóša, and P. Škoda, "Depletion curves and hydrological reaction of mountain river basins," in *Hydrologie Malého Povodí*, K. Brych and M. Tesař, Eds., pp. 125–131, Ústav pro Hydrodynamiku AVČR & CHMI, Praha, Slovakia, 2014.

[30] P. Bitušík and K. Koppová, "Macrozoobenthos of the glacial lakes in the Low Tatras (West Carpathians)," *Biologia*, vol. 52, no. 2, pp. 227–232, 1997.

[31] T. B. McKee, J. N. Doeksen, and J. Kleist, "The relationship of drought frequency and duration to time scales," in *Proceedings of the 8th Conference on Applied Climatology*, pp. 179–184, American Meteorological Society, Anaheim, Calif, USA, 1993.

[32] Y. He, J. Ye, and X. Yang, "Analysis of the spatio-temporal patterns of dry and wet conditions in the Huai River Basin using the standardized precipitation index," *Atmospheric Research*, vol. 166, pp. 120–128, 2015.

[33] J. Bazrafshan, S. Hejabi, and J. Rahimi, "Drought monitoring using the multivariate standardized precipitation index (MSPI)," *Water Resources Management*, vol. 28, no. 4, pp. 1045–1060, 2014.

[34] J. Tomlain, "Mean annual actual and potential evapotranspiration totals," in *Landscape Atlas of the Slovak Republic*, p. 96, Ministerstvo Životného Prostredia Slovenskej Republiky, Slovenská Agentúra Životného Prostredia, Bratislava, Slovakia, 2002.

[35] M. Mišík, *Geological Excursions Around Slovakia*, vol. 276, SPN, Bratislava, Slovakia, 1979.

[36] M. Lapin and M. Tekušová, "Wind speed and direction, exposure of territory to inversion," in *Landscape Atlas of the Slovak Republic*, p. 100, Ministerstvo Životného Prostredia Slovenskej Republiky, Slovenská Agentúra Životného Prostredia, Bratislava, Slovakia, 2002.

[37] D. C. Edwards and T. B. McKee, "Characteristics of 20th century drought in the United States at multiple time scales," in *Climatology Report*, vol. 97, Colorado State University, Fort Collins, Colo, USA, 1997.

[38] M. J. Hayes, M. D. Svoboda, D. A. Wilhite, and O. V. Vanyarkho, "Monitoring the 1996 drought using the standardized precipitation index," *Bulletin of the American Meteorological Society*, vol. 80, no. 3, pp. 429–438, 1999.

[39] S. Yue and P. Pilon, "A comparison of the power of the t test, Mann-Kendall and bootstrap tests for trend detection," *Hydrological Sciences Journal*, vol. 49, no. 1, pp. 21–37, 2004.

[40] S. G. Gulrado and F. L. Bermúdez, "Trend of the rainfalls and temperatures in a small fluvial basin of peninsular semiarid south-east," *Boletín de la Asociación de Geógrafos Españoles*, vol. 56, pp. 473–478, 2011.

[41] T. Niedźwiedź, E. Łupikasza, I. Pińskwar, Z. W. Kundzewicz, M. Stoffel, and Ł. Małarzewski, "Variability of high rainfalls and related synoptic situations causing heavy floods at the northern foothills of the Tatra Mountains," *Theoretical and Applied Climatology*, vol. 119, pp. 273–284, 2014.

[42] L. Labudová, P. Šťastný, and M. Trizna, "The north atlantic oscillation and winter precipitation totals in Slovakia," *Moravian Geographical Reports*, vol. 21, no. 4, pp. 38–49, 2013.

[43] M. Lapin and P. Faško, "Precipitation and changes of the atmospheric circulation in the period 1874–1993 in Slovakia," *Meteorologické Zprávy*, vol. 49, pp. 1–11, 1996.

[44] M. Lapin and J. Tomlain, *General and Regional Climatology*, Vydavateľstvo UK, Bratislava, Slovakia, 2001.

[45] Z. Šustek and J. Vido, "Vegetation state and extreme drought as factors determining differentiation and succession of Carabidae communities in forests damaged by a windstorm in the High Tatra Mts," *Biologia*, vol. 68, no. 6, pp. 1198–1210, 2013.

[46] M. D. Eyre, S. P. Rushton, M. L. Luff, and M. G. Telfer, "Investigating the relationships between the distribution of British ground beetle species (Coleoptera, Carabidae) and temperature, precipitation and altitude," *Journal of Biogeography*, vol. 32, no. 6, pp. 973–983, 2005.

[47] P. Fleischer, "Windfall research and monitoring in the High Tatra Mts., objectives, principles, methods, and current status," *Contributions to Geophysics and Geodesy*, vol. 38, no. 3, pp. 233–248, 2008.

[48] R. Šoltés, J. Školek, Z. Homolová, and Z. Kyselová, "Early successional pathways in the Tatra Mountains (Slovakia) forest ecosystems following natural disturbances," *Biologia*, vol. 65, no. 6, pp. 958–964, 2010.